EU GRADUATE SCHOOL OF NATURAL AND APPLIED SCIENCE

EGE UNIVERSITY

PhD THESIS

THE DIAGNOSIS OF ALZHEIMER'S DISEASE BASED ON THE CLASSIFICATION OF FMRI DATA

Kaya OĞUZ

Supervisor: Assoc. Prof. Dr. Muhammet Gökhan CİNSDİKİCİ

Co-Supervisor: Prof. Dr. Tayfun DALBASTI

International Computer Department

Presentation Date: 15.08.2016

Bornova-İZMİR
2016

EGE UNIVERSITY GRADUATE SCHOOL OF NATURAL AND APPLIED SCIENCE

(PHD THESIS)

THE DIAGNOSIS OF ALZHEIMER'S DISEASE BASED ON THE CLASSIFICATION OF FMRI DATA

Kaya OĞUZ

Supervisor: Assoc. Prof. Dr. Muhammet Gökhan CİNSDİKİCİ

Co-Supervisor: Prof. Dr. Tayfun DALBASTI

International Computer Department

Presentation Date : 15.08.2016

Bornova-İZMİR
2016

Kaya OĞUZ tarafından Doktora tezi olarak sunulan “The Diagnosis of Alzheimer’s Disease Based on the Classification of fMRI Data” başlıklı bu çalışma EÜ Lisansüstü Eğitim ve Öğretim Yönetmeliği ile EÜ Fen Bilimleri Enstitüsü Eğitim ve Öğretim Yönergesi’nin ilgili hükümleri uyarınca tarafımızdan değerlendirilerek savunmaya değer bulunmuş ve 15.08.2016 tarihinde yapılan tez savunma sınavında aday oybirliği/oyçokluğu ile başarılı bulunmuştur.

Jüri Üyeleri : **İmza**

Jüri Başkanı **:** Doç. Dr. Muhammet Gökhan CİNSDİKİCİ .....

Raporter Üye **:** Prof. Dr. Ali Saffet GÖNÜL .....

Üye **:** Prof. Dr. Turhan TUNALI .....

Üye **:** Yrd. Doç. Dr. Haldun SARNEL .....

Üye **:** Yrd. Doç. Dr. Korhan KARABULUT .....

EGE ÜNİVERSİTESİ FEN BİLİMLERİ ENSTİTÜSÜ

ETİK KURALLARA UYGUNLUK BEYANI

EÜ Lisansüstü Eğitim ve Öğretim Yönetmeliğinin ilgili hükümleri uyarınca Doktora Tezi olarak sunduğum "The Diagnosis of Alzheimer's Disease Based on the Classification of fMRI Data" başlıklı bu tezin kendi çalışmam olduğunu, sunduğum tüm sonuç, doküman, bilgi ve belgeleri bizzat ve bu tez çalışması kapsamında elde ettiğimi, bu tez çalışmasıyla elde edilmeyen bütün bilgi ve yorumlara atıf yaptığımı ve bunları kaynaklar listesinde usulüne uygun olarak verdiğimi, tez çalışması ve yazımı sırasında patent ve telif haklarını ihlal edici bir davranışımın olmadığını, bu tezin herhangi bir bölümünü bu üniversite veya diğer bir üniversitede başka bir tez çalışması içinde sunmadığımı, bu tezin planlanmasından yazımına kadar bütün safhalarda bilimsel etik kurallarına uygun olarak davrandığımı ve aksinin ortaya çıkması durumunda her türlü yasal sonucu kabul edeceğimi beyan ederim.

15.08.2016

Kaya OĞUZ

ÖZET

ALZHEİMER HASTALIĞININ FMRI VERİSİNİN SINIFLANDIRILMASINA DAYALI TANISI

OĞUZ, Kaya

Doktora Tezi, Uluslararası Bilgisayar Anabilim Dalı
Tez Danışmanı: Doç. Dr. Muhammet Gökhan CİNSDİKİCİ
İkinci Danışmanı: Prof. Dr. Tayfun DALBASTI
Ağustos 2016, 88 sayfa

Alzheimer Hastalığı en sık rastlanan demans türlerinden biridir. Bu tezde hastalığın erken tespiti için, işlevsel manyetik rezonans görüntüleme verilerinin uygun olarak sınıflandırılması hedeflenmiştir. Alzheimer Hastalığının temelinde sinirlerdeki sinyal iletişiminin aksaması vardır. Bu aksamadan etkilenen beyin bölgelerini hedefleyen işlevsel görevler belirlenmiştir. İşlevsel çekimde görevi yapan farklı denek grupları arasında farklılıklar çıkması beklenmektedir. Etkinlikleri tespit edebilecek beş adet özgün yöntem önerilmiştir. Bu yöntemlerden üç tanesi anlık etkinlik tespiti yapmakta, diğer ikisi ise bütün deneyin verilerini kullanmaktadır. Yöntemlerde kararlı regresyon yöntemi kullanılarak dinlenme anındaki değerlerin regresyon doğrusu çıkartılmış ve bu doğruya olan uzaklıklar yeni bir metrik olarak kullanılmıştır. Etkinlik dışında, Alzheimer Hastalığını tespit etmede kullanılabilecek işlevsel bağlantısallık yöntemleri incelenmiştir. Varsayılan durum ağı, dinlenme anında beynin belirli bölgelerinin zamansal olarak korelasyon gösteren yerlerinden oluşur. Bu ağdaki bölgeler Alzheimer Hastalarında daha az korelasyon göstermektedir. Deneklere ait verilerin hem etkinlik, hem de işlevsel bağlantısallık bilgileri LVQ ve yapay sinir ağları ile sınıflandırılmıştır. Kullanılan üç veri setinde etkinlik verileri ile %98, fonksiyonel bağlantısallık ile de %90 başarı elde edilmiştir.

Anahtar sözcükler: İşlevsel manyetik rezonans görüntüleme, etkinlik tespiti, işlevsel bağlantısallık, varsayılan durum ağı, veri sınıflandırılması, Alzheimer Hastalığı

ABSTRACT

THE DIAGNOSIS OF ALZHEIMER'S DISEASE BASED ON THE CLASSIFICATION OF FMRI DATA

OĞUZ, Kaya

PhD in International Computer Department
Supervisor: Assoc. Prof. Dr. Muhammet Gökhan CİNSDİKİCİ
Co-Supervisor: Prof. Dr. Tayfun DALBASTI
August 2016, 88 pages

Alzheimer's Disease is the most common form of dementia. This thesis aims to use functional magnetic resonance imaging data classification to diagnose the disease. One of the main causes for Alzheimer's Disease is synaptic failure. An fMRI experiment that targets the brain regions that are affected by this failure has been developed. Differences are expected to emerge between the subjects in different groups. Five novel methods has been proposed to locate the activations. Three of these can detect an activation instantaneously, while the other two use the complete experiment data. The methods use robust regression to find the regression line for the resting state and use the distance to this line as a new metric. Besides activation information, functional connectivity methods has been researched which can be used to detect the Alzheimer's Disease. When the brain is at rest, the temporal correlations between specific regions form a network called the default mode network. There is a decrease in correlation in subjects with Alzheimer's Disease. The activations and functional connectivity features has been classified with LVQ and artificial neural networks. In the three data sets used, a success of 98% has been reached for the activation features, and 90% has been reached for functional connectivity.

Keywords: Functional magnetic resonance imaging, activation detection, functional connectivity, default mode network, data classification, Alzheimer's Disease

ACKNOWLEDGEMENT

I'm grateful to my advisor, Assoc. Prof. Dr. Muhammed CİNSDİKİCİ, for sharing his expertise and knowledge through his continuous support and guidance which permeates through the pages of this thesis. I sincerely thank Prof. Dr. Ali Saffet GÖNÜL for sharing his valuable contributions to the thesis, as well as accession of medical projects and data. I would like to thank my co-supervisor Prof. Dr. Tayfun DALBASTI for guiding the thesis with his valuable comments in thesis advisory committee meetings. I would like to thank Prof. Dr. Turhan TUNALI for his support and comments.

I would like to express my gratitude to all my colleagues, starting with Cemre CANDEMİR, Cihat ÇETİNKAYA, Elif HAYTAOĞLU, Gül BOZTOK ALGIN, Sercan DEMİRCİ, Serkan ERGUN, Sinem ASLAN and to all of the academic and administrative personnel at EU International Computer Institute for their continuous support and help. I would like to thank Burcu AKSOY for her great contributions in designing the fMRI task. I'm grateful to all my friends, colleagues and professors in the SoCAT research group and EU Radiology department for their help. I would like to thank Asst. Prof. Dr. Umut AVCI and Lecturer İlker KORKMAZ for their support and help.

I would like to thank Alzheimer's Disease Neuroimaging Initiative (ADNI) for funding data collection and sharing a large data set that is used in the classification process (National Institutes of Health Grant U01 AG024904). I would also like to thank TUBITAK for funding the Alzheimer's Project (214S029) developed at SoCAT.

I also would like to use this opportunity to thank all of the scientists all around world who work hard to increase human knowledge and share their work with us.

I would like to thank all of my family, starting with my mother Şükriye, my father Cengiz and my brother Özcan for supporting me in all of the decisions I've made through the years, whether those decisions turned out to be good or bad.

Finally, I would like to especially thank my wife Damla OĞUZ for supporting me in every aspect of my life. My work in this thesis is dedicated to her.

TABLE OF CONTENTS

TABLE OF CONTENTS (continued)

TABLE OF CONTENTS (continued)

TABLE OF CONTENTS (continued)

LIST OF FIGURES

LIST OF FIGURES (continued)

LIST OF FIGURES (continued)

LIST OF TABLES

LIST OF TABLES (continued)

LIST OF ABBREVIATIONS

Abbreviation	Explanation
AD	Alzheimer's Disease
ADNI	Alzheimer's Disease Neuroimaging Initiative
ANN	Artificial Neural Network
BOLD	Blood Level Oxygen Dependant
CDR	Clinical Dementia Rating
DICOM	Digital Imaging And Communications in Medicine
DMN	Default Mode Network
FCA	Fuzzy C-Means Analysis
fMRI	Functional Magnetic Resonance Imaging
FPR	False Positive Rate
FWE	Family-Wise Error
GLM	General Linear Model
GNB	Gaussian Naïve Bayes
HRF	Hemodynamic Response Function
IAM	Instantaneous Activation Method
IAMP	Instantaneous Activation Method Using Past Resting State Blocks
ICA	Independent Component Analysis
IRRD	Instantaneous Robust Regression Distance
LDC	Linear Discriminant Classifier
LVQ	Learning Vector Quantization
MCI	Mild Cognitive Impairement

LIST OF ABBREVIATIONS (continued)

Abbreviation	Explanation
MNI	Montreal Neurological Institute
mPFC	Medial Prefrontal Cortex
MRI	Magnetic Resonance Imaging
PCA	Principal Component Analysis
PCC	Posterior Cingulate Cortex
PET	Positron Emission Tomography
PSNR	Peak Signal Noise Ratio
ROC	Receiver Operating Characteristic
ROI	Region Of Interest
SNR	Signal Noise Ratio
SPM	Statistical Parametric Mapping
SVM	Support Vector Machine
TAM	Task Activation Method
TE	Echo Time
TPR	True Positive Rate
TR	Repetition Time
TRRD	Task Robust Regression Distance

1. INTRODUCTION

This interdisciplinary study presents a framework for classifying functional magnetic resonance imaging (fMRI) data among subjects with Alzheimer's Disease (AD), subjects with mild cognitive impairment (MCI) and healthy subjects. While the framework firmly rests on computational methods, the nature of the diseases, the data format and its acquisition plays a significant role. Therefore, it is imperative that they are briefly introduced before the discussion of the framework.

1.1 Alzheimer's Disease

Alzheimer's Disease is the most common form of dementia that slowly strips off the subject's mental capabilities due to synaptic dysfunctions (Weiner et al., 2015; Querfurth and LaFerla, 2010). The disease starts with loss of short term memory, and, as it progresses, leaves the subject unable to attend daily tasks as simple as eating in its final stages. According to the World Alzheimer Report 2015, published by Alzheimer's Disease International, there are over 45 million people living with AD, and this number is expected to reach 130 million by the year 2050 (Prince et al., 2015).

The main cause of AD is hypothesized to be the suppression of basic synaptic transmissions because of the accumulation of uncleared peptides in the synapses. Peptides are natural products of metabolism that are short chains of amino acid monomers with covalent bonds. The peptide of type Aβ_{42} is also known to be toxic to the cells, resulting in inflammation that leads to energy failure (Querfurth and LaFerla, 2010).

The synaptic failure can also be seen in patients with mild cognitive impairment. The studies report a 10 to 15 percent rate of conversion from MCI to AD which makes MCI a valid target for research, as it can be considered a precursor to AD (Janoutová et al., 2015; Brück et al., 2013).

The study by Querfurth and LaFerla (2010) lists the aforementioned hypothesis and others, such as mitochondrial dysfunction, and discusses the proposed treatments to each cause. Teipel et al. (2015) mention the usage of different modalities of medical imaging, such as magnetic resonance and positron emission tomography (PET), so that the accumulation of the peptides can be captured. On the other hand, a recent survey remarks that the research interest has turned to early diagnosis rather than treatment since the clinical trials on stopping the disease have failed, hence

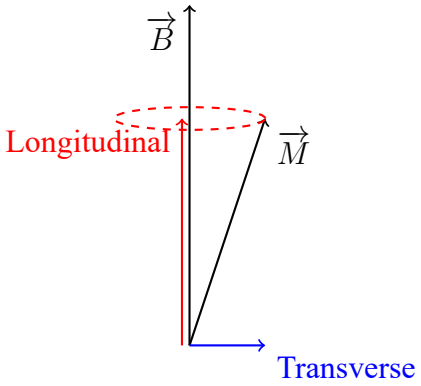

Figure 1.1. The net magnetization, $\overrightarrow{M}$, precessing around the magnetic field, $\overrightarrow{B}$, at Larmor Frequency, f. The net magnetization can be decomposed into the longitudinal and transverse vectors, shown in red and blue, respectively.

creating a "treatment versus prevention dilemma" (Deak et al., 2016).

The impact of the disease on both the subjects and the subjects' families creates an urgency to develop methods to diagnose, slow and stop the disease.

1.2 Magnetic Resonance Imaging

Magnetic resonance imaging (MRI) is a very common tool used in both research and clinical medical imaging. It works on the intrinsic angular momentum of atomic nuclei called the "spin". Spins behave like compass needles and have a magnetization of their own. While it is not possible to measure the magnetization of a single proton, it is possible to measure the net magnetization, $\overrightarrow{M}$, of all protons in a volume (Lindquist, 2014).

When there is no magnetic field, each spin has a different magnetic moment orientation, which in total sums up to a net magnetization of zero. Under the effect of a large magnetic field, $\overrightarrow{B}$, the spins align and create a net magnetization which can be decomposed into two vectors; one parallel and one orthogonal to the magnetic field. These components are called longitudinal and transverse vectors, as shown in Figure 1.1.

It is known in quantum mechanics that a spin in a magnetic field precesses in that field with Larmor Frequency, defined by the Equation 1.1, as follows (Brown et al., 2014).

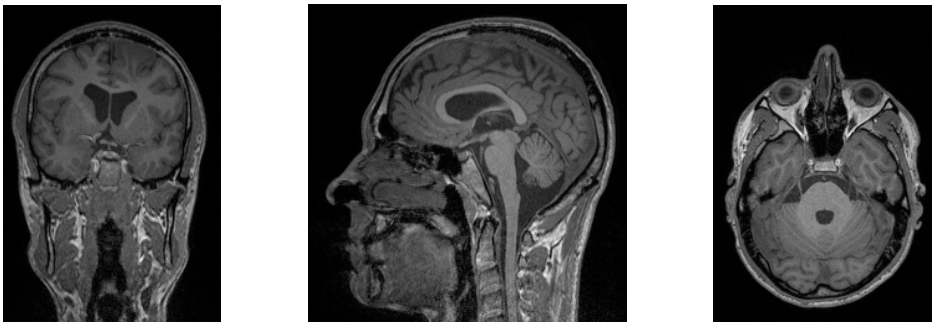

(a) Coronal slice of a subject (b) Sagittal slice of a subject (c) Axial slice of a subject

Figure 1.2. Slices from anatomical planes; coronal, sagittal and axial. The images are taken from Ege University MR Database.

$$f = \gamma B \tag{1.1}$$

The equation states that the frequency of the spin is proportional to the magnitude of the magnetic field and the gyromagnetic ratio, γ. This ratio is 42.58 MHz/T for hydrogen, hence, for a 3 Tesla MRI scanner, the frequency is around 127 MHz (Deichmann, 2009).

If an external pulse with the exact Larmor Frequency is sent when the spins are in alignment, they are tipped over and a transverse magnetization is created, while the longitudinal magnetization is lost. This process is called excitation. Once the external pulse is removed, the spins will try to return to equilibrium; transverse magnetization starts to disappear, while the longitudinal grows back to its original state (Lindquist, 2014). The precession of the spins produce a signal that can be captured by a receiver coil.

The time for the longitudinal magnetization to come to equilibrium is described by a time constant called T1. This constant is called T2 for the transversal magnetization. These values are the relaxation times. The time to excite the spins is called the repetition time, or TR for short. The time to start data acquisition after excitation is called echo time, and is shown as TE. The measured signal is approximately $M_0(1 - e^{-TR/T_1})e^{-TE/T_2}$ where it is possible to put emphasize of tissue properties T_1 and T_2 by changing the repetition time and the echo time (Lindquist, 2014).

The images acquired by T1 and T2 relaxation times are used for structural view of the tissues. For functional MRI, T2* is used. It is the combined effect of

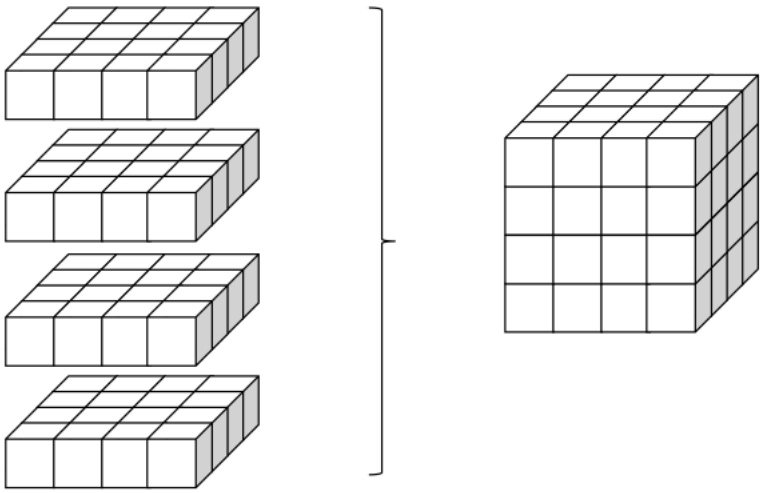

Figure 1.3. Voxels are acquired slice by slice and form the final volume, as shown in Lindquist (2014)

T2 and local inhomogeneities that are used to enable functional MRI.

These steps are the basic idea behind the magnetic resonance imaging. However, the important contribution has come from Lauterbur and Mansfield in 1973 when they proposed to vary the magnetic field spatially, hence generating signals with different Larmor Frequencies (Brown et al., 2014). In order to introduce the third dimension, this process is done within a slice of interest, and is repeated along the axis orthogonal to the slice. Naturally, the names for these axes come from the anatomical planes; axial, sagittal and coronal planes. The slices for each plane can be seen in Figure 1.2. While any plane can be used to acquire a series of slices, axial plane is a common preference.

The acquisition of the net magnetization is done in these varying magnetic fields of unit volumes. Each unit volume is called a voxel, short for volume element, akin to its two dimensional equivalent, pixel. The MRI acquisition is done slice by slice on the selected anatomical plane, and when it is done, these unit volumes form the three dimensional volume as can be seen in Figure 1.3 (Lindquist, 2014). Voxels enable the viewer to analyze the volume in other planes as well. For example, in Figure 1.3 the acquisition is done along the axial plane. However, if a sagittal slice is desired, the voxels along the coronal and axial slices for that sagittal slice can be viewed as a two dimensional image. The MRI viewers use the three anatomical planes to display the three dimensional data as in Figure 1.2.

1.3 Functional MRI

The nerve cells in the brain may or may not respond to a given stimulus according to the impulses that they receive. If they respond by firing an impulse, an electrical and chemical signal is transferred to a connecting neuron via their synapses. Sending this signal requires energy, and energy is generated at the mitochondria using the oxygen carried by the hemoglobin molecules in the blood.

The hemoglobin molecules with oxygen are called oxyhemoglobin, and those without oxygen are called deoxyhemoglobin. The absence or presence of oxygen in blood affects the magnetic field in the vicinity because oxyhemoglobin is diamagnetic, whereas deoxyhemoglobin is paramagnetic. These inhomogeneities can be captured by an MRI scanner using the T2* relaxation time, which form the basis for the functional MRI. This contrast in the MRI scanners used to capture the changes in oxygen levels is called blood level oxygen dependent (BOLD) (Deichmann, 2009).

1.3.1 Hemodynamic Response Function

When a stimulus is presented, oxygen is delivered by the blood flow to the regions responsible for handling it. This creates an increase in the BOLD signal. As the neurons use oxygen to fire, the oxygen concentration drops to previous levels, hence does the BOLD signal. This response to stimulus is called the hemodynamic response and its change in time is called the hemodynamic response function (HRF).

In order to capture the HRF, functional images have to be taken at regular time intervals. This brings physical constraints on the MRI device because the time for aligning spins with the magnetic field and their relaxation times limit the intervals that a new complete scan of the brain can be performed. A typical repetition time used in fMRI is two or three seconds.

Hemodynamic response function can be observed by empirical studies for voxels in well-studied regions such as primary visual and primary motor cortices (Glover, 1999; Handwerker et al., 2004). These studies show that the response function starts peaking after a few seconds of the stimulus and reaches its largest value around six seconds. This is followed by a decline where a post undershoot can be observed. The signal returns to its previous levels in about fifteen to twenty seconds. The latency to start peaking, the peak magnitude, the undershoot and other attributes may vary from subject to subject and even from region to region in a single subject because of the density of neurons in the voxels, as well as the structure of blood

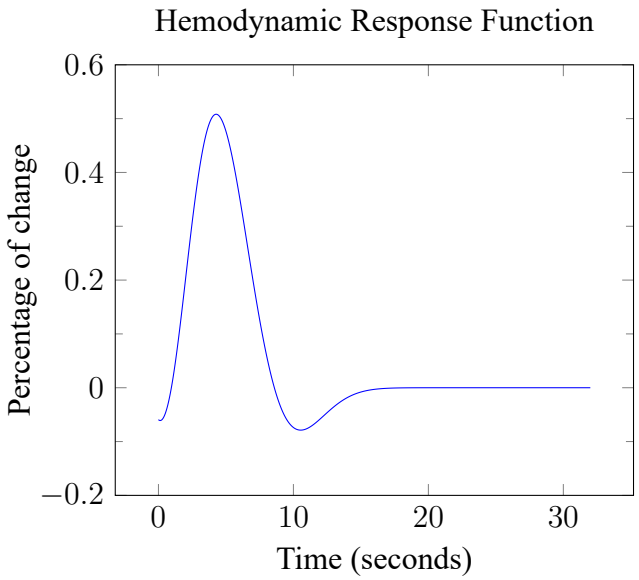

Figure 1.4. Hemodynamic response function as the difference of two gamma functions as defined in Equation 1.2 where $A_1 = 6$, $A_2 = 1$, $\tau_1 = 4$, $\tau_2 = 4$, $\delta_1 = 0$, $\delta_2 = 6$ and $C = 0$.

vessels. However, the shape of the response is consistent and is usually modeled as the difference of two parametrized gamma functions, as shown in Equation 1.2 where $x(t)$ is the gamma function, A_1 is the peak magnitude, A_2 is the depth of the undershoot, τ_1 and τ_2 are the width, and δ_1 and δ_2 are the latency values of the peak and undershoot, respectively (Handwerker et al., 2004). A sample HRF is plotted in Figure 1.4, where the peak and the post undershoot can be observed.

$$y(t) = A_1 \left(\frac{x(t) - \delta_1}{\tau_1} \right)^2 \frac{e^{-\left(\frac{x(t)-\delta_1}{\tau_1} \right)^2}}{\tau_1} - A_2 \left(\frac{x(t) - \delta_2}{\tau_2} \right)^2 \frac{e^{-\left(\frac{x(t)-\delta_2}{\tau_2} \right)^2}}{\tau_2} + C \quad (1.2)$$

1.3.2 fMRI Experiments

The challenge in fMRI is that the brain is always active and in order to bestow a function to a particular brain region, the functional images should be captured in a carefully crafted and executed experiment. These experiments contain tasks that the subjects are asked to perform. One of these tasks contains the sought brain function, usually called active task, whereas another one, usually called baseline, does not. Although it sounds simple, designing experiments that reveal the sought brain functions can be a daunting task.

As a simple example, consider locating the motor functions in the brain, as

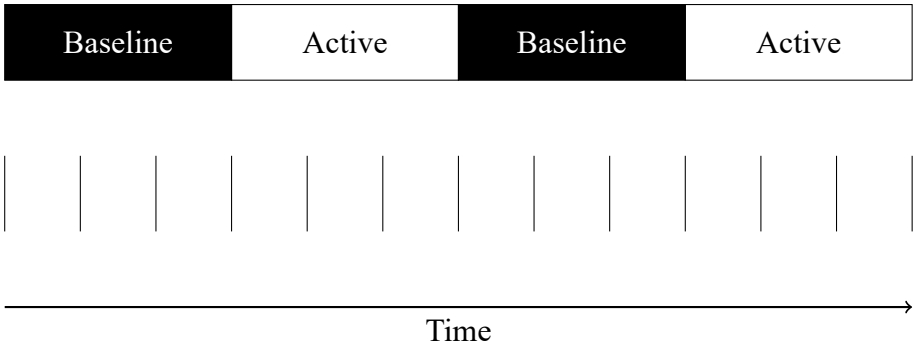

Figure 1.5. A simple fMRI experiment containing a baseline and an active task alternating. The bars under the tasks show the instances when a complete brain scan starts.

shown in Figure 1.5. The active task is tapping fingers for a period of time. For the baseline task, the user might just stay still. As these tasks alternate for two times as shown in Figure 1.5, a complete brain scan is done at instances defined by the repetition time, TR, shown by the bars under the tasks in the figure. These tasks are repeated until enough data is acquired for fMRI data analysis.

As a slightly harder example, consider locating the regions in the brain responsible when we see someone that we know. In this case, the active task requires the subject to look at photographs of very famous people. The baseline for this experiment should contain everything in the active task but the functions that work when we see someone that we know. So, the baseline can not be doing nothing, or it can not be looking at photos of random objects, but to photos of people that the subject does not know. Even for this slightly harder example, these photographs may not work because the faces in the photographs may resemble people that the subject knows.

These two experiments are examples of block design. Experiments with the block design contain tasks that have clearly defined durations that are run in succession, where each run is called a trial. The experiment may contain more than one task, but each trial contains the same tasks, repeating as many times as required. Another type of fMRI scan is the “resting state”, where the subject simply lies without doing any task. The data from this type of experiment is mostly the analysis of functional connectivity among different brain regions.

Block designs may cause habituation in the brain when the subject gets used to the task so much that the regions cease to respond to the stimuli. To overcome this problem, the task may be programmed to be event-driven, where the tasks may

have varying durations and the switching between tasks may also be random. These type of experiments require careful planning, logging, and analysis.

It should also be noted that the tasks should be carefully executed; that is, the time when the stimulus are shown has to be known, both for block and event-driven designs. For the simple experiment example above, where the motor functions are sought, the subject can be cued in to tap fingers by the MR operator. However, more complicated experiments have to be programmed so that they are synchronized with the functional MRI scans as the experiment runs. The software should also be aware of the MRI device and its pulses as it starts a new complete brain scan. It should also be able to log the stimuli presented to the subject and the subject's responses to the task, since they can be used in fMRI analysis once the experiment is complete.

In order to successfully execute such an experiment, both hardware and software requirements should be met. The MRI device is controlled by the operator using the MRI software on a computer. Using this software, the operator can set the modalities of the scan, as well as its duration. The fMRI experiments are run by another computer, which contains an extra set of synchronization hardware with the MRI device. The hardware set up includes goggles, headphones and controllers with buttons so that the user can view the experiment, hear commands and respond to the experiment using the buttons on the controllers. All of these devices are MRI compatible and does not produce noise and other artifacts around the scanned area. The main component of the synchronization hardware is the so-called SyncBox, which helps the synchronization with the MRI device. The software makes use of the synchronization hardware by checking its synchronization signals, using its goggles as an additional display and reading its input from the controllers during the execution of the experiment.

Figure 1.6 shows the hardware and software set up at the 3 Tesla MRI unit at Ege University. The unit is made up of two rooms. The MRI device is installed in one of the rooms. This is the room where the subjects are scanned. The MRI-compatible goggles, headphones and controllers are also in this room and they are used by the subject during the experiment execution. The goggles are mounted on the head coil and are adjustable to the subject's eye sight. The controllers have two buttons for each hand, one for thumbs, and one for the index fingers.

The other room is called the control room and it contains the main computer for controlling the MRI device, so that the modality of the scan and its parameters, such as repetition time, TR, and echo time, TE, can be set. Naturally, the MR device

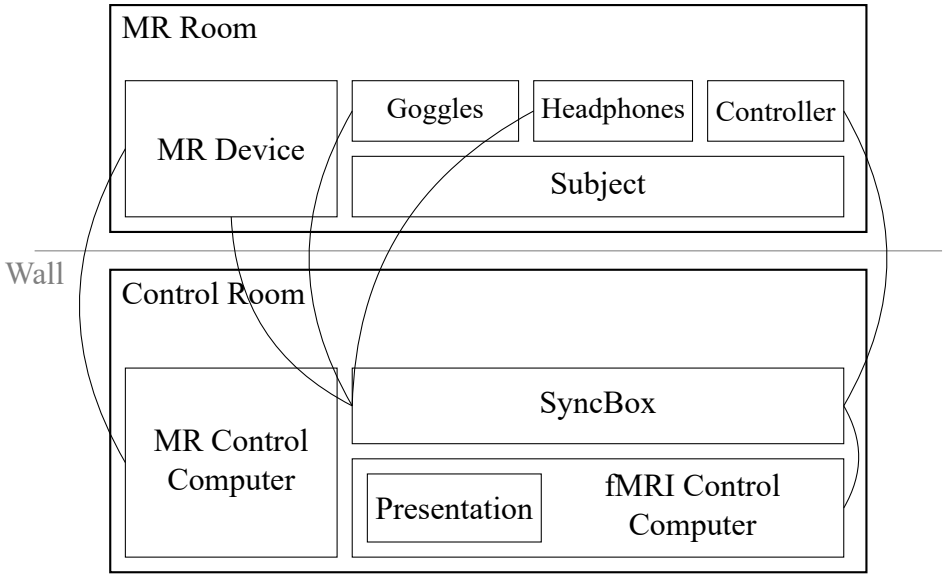

Figure 1.6. fMRI experiment execution setup at the 3 Tesla MR device in Ege University.

is connected to this computer. The device is also connected to the SyncBox, along with the goggles, headphones and the controllers. The SyncBox is connected to another computer, which is called the fMRI Control Computer, where the programmed experiment runs on the Presentation software.

The Presentation software is a commercial product developed at a company called NeuroBehavioral Systems (NBS) located in San Francisco, USA, for developing custom fMRI experiments (www.neurobs.com). It has built-in support for synchronizing with the MR device, a logging system and a programming language similar to JavaScript. It can present stimuli at a specific instant or at a specific pulse signal from the MRI device.

The experiments are executed as follows. The subject is first introduced to the task before going into the MR room and learns all that is required to complete the task. Once inside the scanner, the subject is scanned structurally before the fMRI task. This structural image is required for the analysis, but it also helps the operator and the radiologist to check for any pathological conditions of the subject. After the structural scan, the subject is informed that the fMRI task will start. The Presentation software is started from the fMRI Control Computer and the experiment is loaded. The execution code for the experiments always wait for the first MRI pulse to arrive, so the subject can see the “Ready” sign at the goggles. Once the subject confirms this, the scan is started from the MR Control Computer and as soon as the first MRI pulse is received, the Presentation software starts running the experiment.

Therefore, the scans and the experiment is always synchronized, and it is possible to know which stimuli is shown at any time.

Once the experiment is complete, a log file is also saved which contains the pulses, stimuli, subject responses and other events that occurred during the experiment. The scans are saved by the MR Control Computer in a standard data format, called DICOM (Digital Imaging and Communications in Medicine). The experiment data is now ready to be analyzed.

1.3.3 fMRI Analysis

An fMRI experiment consists of many brain volumes for a single subject. Usually, there are more than one group of subjects, so that the responses in the brain can be compared between these groups. Both of these requirements bring forth a set of challenges.

Subjects, being human, can not stay still for long periods of time. Even if they force themselves not to move, there would be involuntary movements because of their physiological functions, such as breathing. Therefore, the scanned head volumes must be spatially aligned before the analysis.

Another challenge is that every subject has a different head shape. If activations between two groups will be compared, a point in the three dimensional volume has to be the same point in all of the subject's data. A standard space is required to register all of these brain volumes.

All of these steps are called the preprocessing of fMRI data. Once it is complete, there are different approaches to analyze the data and locate the activations, which will be discussed in the upcoming chapters, since this dissertation also proposes new methods.

1.3.4 Preprocessing of fMRI Data

The preprocessing of the data is done using the SPM12 software, named after the Statistical Parametric Maps (SPM) approach that it uses. It is available from `http://www.fil.ion.ucl.ac.uk/spm/`.

Taking the first scan in the series as the reference volume, SPM12 realigns the remaining volumes of the subject using a least squares approach and a rigid

body transformation (Friston et al., 1995a). The SPM12 manual mentions the re-slicing of the volume so that every volume matches the reference volume voxel by voxel (Ashburner et al., 2014). This step also creates a mean image that contains the average value for each voxel, that will be used in the co-registration step.

Since the brain is scanned slice by slice as shown in Figure 1.3, the acquisition time for one slice is not the same with other slices. SPM12 adjusts the signals by shifting the sines that make them up to an earlier or a later moment in time (Ashburner et al., 2014).

Once the slices are spatially and temporally aligned and synchronized, SPM12 registers the structural scan of the subject to the mean image of the fMRI scans. Since both images use different modalities, a mutual information approach is used (Collignon et al., 1995).

An important part of preprocessing is segmentation, where the brain is separated from its surrounding tissues. SPM12 segments and saves the white and gray matter in the structural image of the subject using the tissue probability maps (Ashburner and Friston, 2005).

During segmentation, the structural image is also normalized to a global standard space. There are two standard spaces for locating brain regions independently from size and shape. One of them is Talairach coordinates (Talairach and Tournoux, 1988). Although still in use, Talairach standard space is largely replaced by the standard space originated at the Montreal Neurological Institute and Hospital, called MNI space (Evans et al., 1993). SPM12 normalizes the structural image to the MNI space and outputs a deformation field file, so that this normalization can be applied to functional images, as well (Ashburner et al., 2014).

The normalization of functional scans is done by using the deformation field created at the segmentation step. After this step, all of the functional images become registered to the MNI space. The final step in preprocessing is the smoothing of the volume. SPM12 convolves the image volumes with a Gaussian kernel in order to suppress noise and other effects due to residual differences during the previous steps (Ashburner et al., 2014).

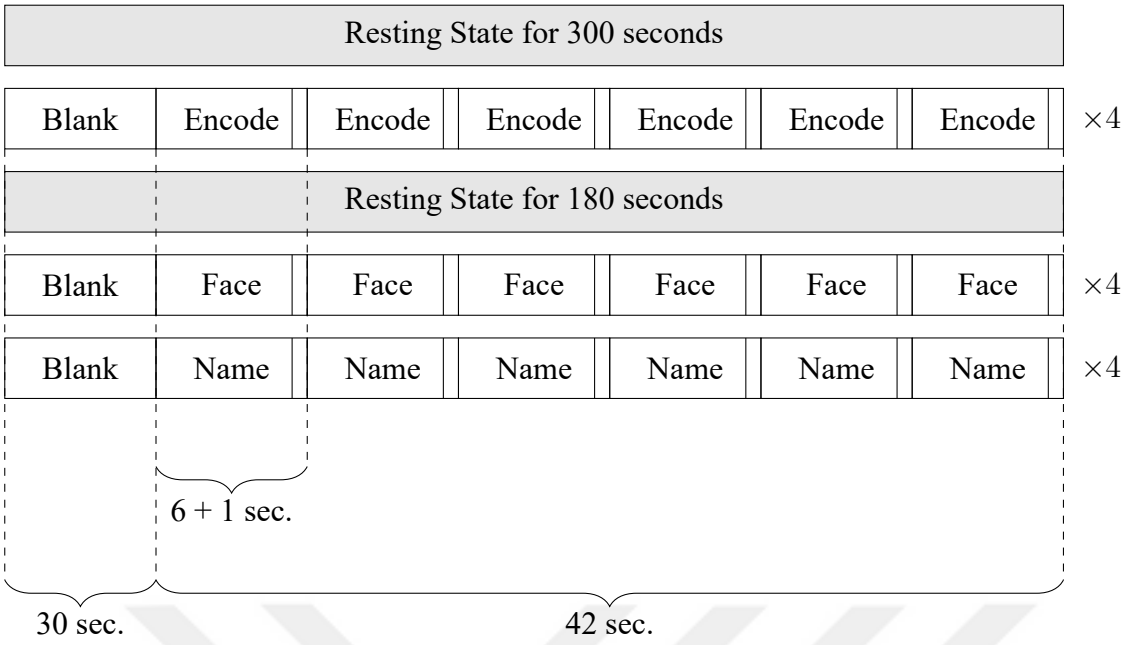

Figure 1.7. The fMRI Experiment Structure, developed by the Psychiatry Department. The experiment includes a resting state in the beginning and between the first and the second tasks. The experiment is 22 and a half minutes long, acquiring 448 full brain scans for each subject.

1.4 AD FMRI Experiment

The fMRI experiment is designed by the SoCAT research group in the Department of Psychiatry at the Ege University School of Medicine, in order to highlight the differences between the subject groups. The experiment contains three distinct tasks and two resting state scans.

In resting state scans, the subjects are not asked to do anything but to lay resting, similar to a structural scan. The subject is asked to just relax and not to think anything in particular. The resting state scans are used to correlate different brain regions. In their study, Raichle et al. (2001) show that certain brain regions work in correlation as the subject is in a resting state, and this correlation is weakened if the subject is asked to perform another task. In order to study the subjects further in other aspects such as connectivity, the resting state is also included in the experiment.

The faces used in the photographs are taken from the study by Ebner et al. (2010). The study contains 171 faces of young, middle-aged and older men and women, where each face has two sets of six facial expressions. From this set, 36 neutral faces are chosen and given Turkish names according to their age range, using the most commonly used names in Turkey, provided by the statistical study of

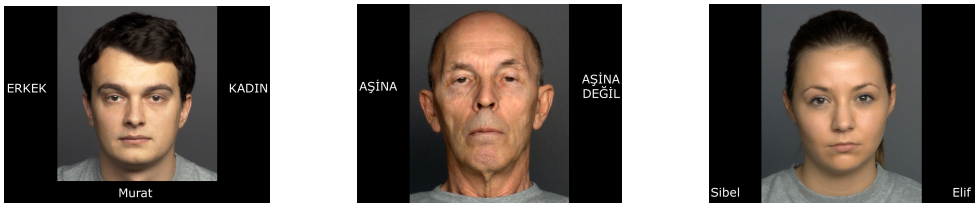

(a) The encoding task screen. The name of the face is shown at the bottom of the screen. The subject is asked the gender of the face and expected to push the button in the left or right hand, correctly.

(b) The face recognition task screen. The subject is expected to remember if the face was shown during the encoding task.

(c) The name recognition task screen. The subject is expected to remember the name of the face correctly.

Figure 1.8. Sample screens from encoding, face recognition and name recognition tasks in the AD fMRI Experiment.

General Directorate of Civil Registration and Nationality (Nüfus ve Vatandaşlık İşleri Genel Müdürlüğü, 2012). Among these 36 faces, 24 of them are used in the encoding task. They are shown in a random order for each subject, in sets of six faces, as the structure of the experiment implies.

As can be seen structurally in Figure 1.7, the experiment starts with the resting state scan for five minutes. As soon as it finishes, the first task begins. The structure for the tasks is the same for every task. They all start with thirty seconds of a blank screen, with a white plus sign (+) in the center, which helps the subject to focus. Then, the subject is shown a photograph for six seconds, and the task is performed here. It is followed by a one second of blank screen with a white plus sign in the center, again. The subject is shown six photographs in succession, then it is repeated four times in total.

The first task is called the “Encoding” task, and it is used to register faces to the subject’s memory, so that they can be queried in other tasks. During the six seconds where the subject is shown a photograph, the name of the person is shown at the bottom of the screen. Since six seconds is a lot of time to encode the name and the face, the subject is given another task during this six seconds: correct identification of the gender of the person in the photograph. If the person in the photograph is a man, they use the left hand button, or if the person is a woman, the right hand button is used. This simple task makes it more challenging for the subject to encode the photograph and the name. A sample screen can be seen in Figure 1.8.a.

After the encoding task, there is another resting state scan that takes three

minutes. This resting state is also used to better challenge the memory encoding of the subject.

The second task is called “Face Recognition.” The 12 remaining faces that were not used in the encoding tasks, and 12 faces from the encoding tasks are randomly queried with the phrases “Familiar” and “Not Familiar” on the left and right hand side of the photographs. The subject is expected to remember if the face was shown during the encoding task. A sample screen can be seen in Figure 1.8.b.

The final task is called “Name Recognition.” This task asks the subject the name of the face that was shown in the encoding task. An alternative name is displayed on either left or right hand side of the screen, and the subject is expected to remember the name. A sample screen can be seen in Figure 1.8.c.

The encoding, face recognition and name recognition takes $4\times(30+42) = 288$ seconds each. In total, the experiment takes $300 + (3 \times 288) + 180 = 1344$ seconds, which is roughly 22 minutes and a half. The TR time for the experiment is 3 seconds, which results in 448 full brain scans. Even though the tasks have random elements, they are still made up of blocks, and therefore are of block design.

1.5 Classification Framework

Now that the nature of the diseases and the data that will be used for classification are briefly introduced, the framework should be discussed concisely.

A broad view of the work flow can be seen in Figure 1.9. The work flow starts with the fMRI experiment. As aforementioned in section 1.3.2, fMRI experiments must be carefully designed to locate the activations responsible for brain functions. One of the first symptoms of both AD and MCI is the short term memory loss, as was discussed in section 1.1. The experiment is designed kindly by the Psychiatry Department as detailed in section 1.4 so that the brain regions responsible for short term memory can be compared among the three groups of subjects; the Alzheimer’s Disease (AD) group, the mild cognitive impairment (MCI) group, and healthy subjects (HS). In order to test the framework before the real data arrives, a set of synthetic data generation methods are implemented, as well.

Although classifiers can use the preprocessed subject data, the large size of the fMRI data, and the few number of samples compared to the size, enforces features to be extracted. These features are representations of the subject data, which are

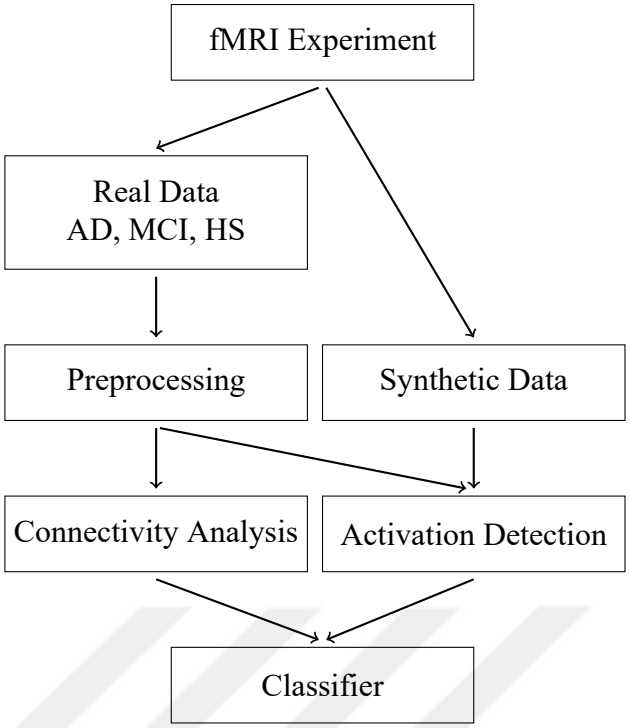

Figure 1.9. A broad view of the work flow. The data is either collected from an fMRI experiment, or generated synthetically simulating the experiment. The real data has to be preprocessed. Then the activation or functional connectivity features are extracted and they are passed to the supervised classifier.

smaller in size, while maintaining as much information as possible. The thesis uses both activations and functional connectivity analysis to extract features that will bring forth differences among the subject groups.

The real data can be a block design experiment, where activations are sought, or it can be a resting state scan, where the subject simply lies without doing anything. While the activations are sought in the first type, the second one requires a functional connectivity analysis. Both of these features are then fed into the classifier.

The synthetic data, on the other hand, is generated according to an experiment structure, and contains activations only. The results from this set is only evaluated with activation detection methods.

1.6 Organization Of The Thesis

The thesis continues with the literature review of activation detection methods, fMRI data classification methods, functional connectivity approaches, and the default mode network. The third chapter contains novel contributions to activation

analysis. The different approaches to synthetic data generation is also mentioned in this chapter. Chapter 4 discusses the classification of fMRI data using learning vector quantization and multilayer feedforward artificial neural networks. The thesis concludes with Chapter 5 where the evaluation and remarks about the methods, their results and the future work are discussed.

2. LITERATURE REVIEW

This section reviews the existing approaches to activation detection, fMRI data classification, and functional connectivity.

2.1 Activation Detection

The initial purpose in using the BOLD contrast to capture the hemodynamic response was to measure regional neural activity (Ogawa et al., 1990). As soon as it has become available, several approaches has been proposed to detect the activations. Some of these were already been in use with other medical imaging techniques, such as positron emission tomography (PET).

2.1.1 Early Approaches

One of the earliest approaches is the subtraction method which has been evaluated by a typical finger tapping experiment (Bandettini et al., 1993). The experiment consists of functional images taken at two second intervals where the subjects are asked to tap their right hand fingers to their thumbs for eight images and immediately asked switch to left hand fingers for the following eight images.

In the subtraction method the center voxels of the left and right motor cortices are chosen as reference points. The instance of the brain captured at the peak value of the left reference voxel is subtracted from the instance of the brain captured for the right reference voxel. In the resulting image, maximum negative values indicate the brain activity for the right hand tapping task, and the maximum positive values indicate the activity for the left hand task.

The second approach in the same study uses the mean value for each task, instead of the peak value of the reference points. The image quality improves, but both approaches suffer from an artifact in the sagittal sinus region of the brain.

The study also discusses the cross correlation approach. In order to correlate the signals with the experiment, the experiment is represented by a square wave function, also known as the boxcar function. In the boxcar function, the instances with the sought function is marked with the value of 1, whereas other instances are marked with 0. This reference signal has the same size as the voxel signals. For each voxel, the dot product of the voxel signal and the reference boxcar signal is computed. Higher correlation values produce brighter voxels in the resulting image,

which shows activity belonging to the sought brain function. The value 0.7, which corresponds to the cosine of $\alpha = 45$ degrees between two signals is chosen as a typical threshold to accept a voxel as active.

Another method proposed in the study uses the BOLD signal of an exemplar voxel from the expected activation area as a reference signal, instead of the boxcar signal. This method is extended by using the average BOLD signal of the expected area, as well.

The experiment data is also analyzed in the frequency domain. The spectral density versus frequency plots of the center voxels from both motor cortices of the brain reveals relatively similar constant frequency of the activity.

2.1.2 Statistical Parametric Maps

Statistical parametric maps (SPM) were previously developed to analyze PET images, but are introduced for analyzing fMRI data in Friston et al. (1994). The idea behind SPM is to obtain a series of values that will be thresholded via statistical methods with a predefined significance value, such as $p = 0.05$, to locate activated voxels.

In the initial study, Friston et al. (1994) use a similar technique to Bandettini et al. (1993) where statistical maps are produced by using cross-correlation between sensory input and hemodynamic responses. A more comprehensive approach that use the general linear model (GLM) to create the statistical parametric maps is proposed in their next study (Friston et al., 1995b).

The general linear model rests on the following equation,

$$Y = X\beta + e \tag{2.1}$$

where Y is a matrix that contains BOLD values of voxels in each of its columns, X contains variables that effect the experiment in each of its columns. The β matrix will be estimated by GLM and will show how much each of the variables affect the received signal. The e is used as an error, assumed to be independent and identically normally distributed.

The X matrix is also called a design matrix and is generally used to represent

the experiment structure. For a simple block design experiment, the effects are tasks, such as movement and visual tasks, and they are represented by the columns. The rows represent each scan in the experiment with regular intervals, such as TR=3. For the rows, or the scans, that are in the movement task, the related column is set as 1, and the remaining columns are set to 0. Similarly, for rows, or scans, that are in the visual task, the related column is set as 1, and the remaining columns are set to 0. A simple block experiment of six scans, where the first three are movement and the last three are visual tasks, the GLM Equation in 2.1 can be extended as follows for a single voxel, v;

$$\begin{bmatrix} v_1 \\ v_2 \\ v_3 \\ v_4 \\ v_5 \\ v_6 \end{bmatrix} = \begin{bmatrix} 1 & 0 \\ 1 & 0 \\ 1 & 0 \\ 0 & 1 \\ 0 & 1 \\ 0 & 1 \end{bmatrix} \begin{bmatrix} \beta_1 & \beta_2 \end{bmatrix} + \begin{bmatrix} e_1 \\ e_2 \\ e_3 \\ e_4 \\ e_5 \\ e_6 \end{bmatrix} \tag{2.2}$$

where $v_{1...6}$ represent the BOLD value for the voxel acquired at regular intervals, the first column of X matrix represents the movement task, and the second column represents the visual task.

Once the estimated $\hat{\beta}$ matrix is computed by the ordinary least squares method, a contrast vector c, such as $c^T = \begin{bmatrix} 1 & -1 \end{bmatrix}$ can be used to get results for different effects. A value of 1 is positive activation, a value of -1 is negative activation, and a value of 0 completely removes the effect from the results. Table 2.1 shows a set of contrast vectors that can be used to query the results for the simple block experiment designed above, and gives a possible list of queries that can be answered (Woolrich et al., 2009).

The `t` statistic in Equation 2.3 is computed for each voxel in the brain.

$$\texttt{t} = \frac{c^T \hat{\beta}}{\sqrt{\text{var}(c^T \hat{\beta})}} \tag{2.3}$$

To get a statistically significant result, this value is compared to a previously defined p value. In cases where there are too many results, such as this, the possibil-

Table 2.1. The questions that can be answered by the simple block design experiment where a movement and a visual task is involved (Woolrich et al., 2009).

Contrast	Meaning
$[1\ 0]$	Where is there significant movement activation?
$[0\ 1]$	Where is there significant visual activation?
$[-1\ 0]$	Where is there significant negative movement activation?
$[0\ -1]$	Where is there significant negative visual activation?
$[1\ -1]$	Where is there movement activation significantly greater than visual activation?
$[-1\ 1]$	Where is there visual activation significantly greater than movement activation?
$[1\ 1]$	Where is there significant activation averaged across both conditions?

ity to get a greater `t` value than expected increases. To overcome this problem, the values are corrected by family-wise error (FWE). To do so, the expected p value is divided by the number of voxels and the result is used to get the t distribution value.

Figure 2.1 shows the SPM results for an early version of the Alzheimer experiment, where the resting states were not yet included. The middle right shows the design matrix as a gray/white graphic where the thirty seconds of blank screens followed by photographs for each task, encoding, face recognition and name recognition can be seen. On top of the design matrix, the selected contrast $[-1\ 1]$ is shown as a bar chart, which asks the question "Where is there encoding activation significantly greater than the blank screen?" On the left of the design matrix and the contrast chart, the activation results are displayed in anatomical cross sections in gray-level. The darker tones shows statistically more significant activations. In order to improve visual inspection, the results can be rendered on the MNI standard template, as can be seen in the colored images on the right. The significance value is $p = 0.05$ with FWE correction.

The general linear model in statistical parametric maps approach is implemented in the software with the same name, SPM, and is the most commonly used solution in detecting activations in both research and clinical analysis.

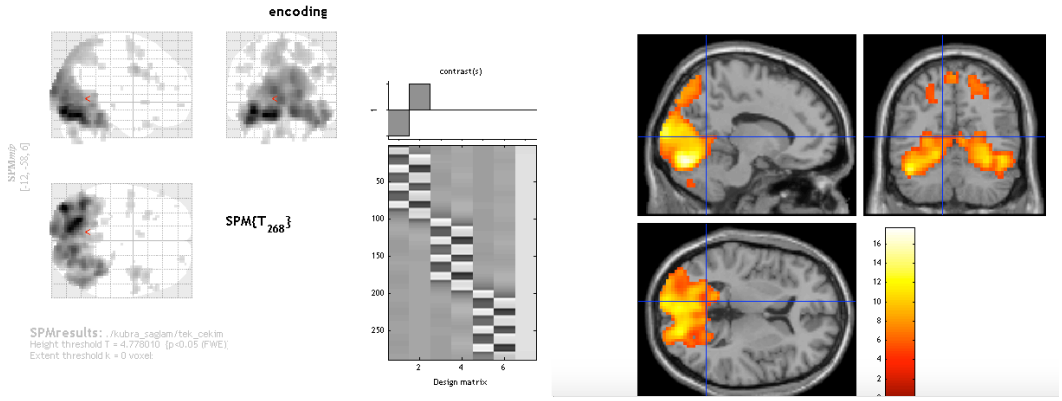

Figure 2.1. The SPM results for one of the early Alzheimer experiment tests. The results are shown in top left anatomical cross sections. The contrast vector bar chart and the design matrix graphic can be seen in middle right. The results are also rendered on the MNI standard template to improve visual inspection.

2.1.3 Other Approaches

Xiong et al. (1996) evaluates several techniques for fMRI activations. Using synthetic images, both parametric and non-parametric statistical tests are assessed. As a result, independent t-test and cross correlation coefficient comes out on top of other tests such as Mann-Whitney and Wilcoxon signed rank test.

Descombes et al. (1998) use Markov Random Fields as a preprocessing step of SPM analysis where the noise in functional MR images are reduced with an edge preserving approach. Ardekani et al. (1999) claim that Fourier series of a boxcar function should contain a secondary harmonic component besides the odd harmonics, so, the system should not be modeled with linear time-invariant (LTI) system models. They assume that a periodic input signal should output a periodic response and they further assume that the system is low pass in which the system can be modeled as a truncated Fourier series with unknown Fourier coefficients. The voxels are assumed to be activated if their value is above the significant threshold in an F statistic.

Singh et al. (1999) propose a technique that can handle not just “on” and “off” but multiple conditions. The authors emphasize that SPM also supports multiple conditions since the underlying GLM approach is a general solution. However, they argue that the computational complexity of GLM reduces the possibility of a real-time approach. The study includes an experiment with three conditions that are left hand movement, right hand movement and no movement that produce their respective images. A logic based true-false analysis is applied to these images.

Feilner et al. (2000) use t-tests in the wavelet domain to find the activated voxels. Since the temporal information is lost in the frequency domain processing, von Tscharner and Thulborn (2001) propose a method in which analysis of non-orthogonal wavelets are used.

In another approach, Sanguineti et al. (2000) use mixtures of Gaussians to find the activations instead of boxcar function which does not require the explicit model of the activation model.

Lukic et al. (2001) model the activations using circular spatial basis functions and then use reversible-jump Markov-chain Monte-Carlo procedures to estimate activated regions. Thirion and Faugeras (2001) focus on the causality between the given stimuli and the voxel responses where the BOLD signal is modeled by Markov chain. They use t-test as an activation measure.

Thompson et al. (2002) use Space-time Adaptive Processing (STAP) algorithm to find the activations. STAP is an algorithm that is designed for sensor array processing. Since the algorithm handles spatial and temporal data as a spatiotemporal set, the activations can be found both in spatial and frequency domains, similar to the study by Noh and Solo (2006).

Hossein-Zadeh et al. (2003) propose a filter that increases the activation signal whereas reduces noise and nuisance components. The problem is solved as an eigenproblem and the authors use the largest eigenvalues in the statistical tests which will define the activated regions. The authors report that finding the optimum size of the filter requires further investigation.

Deshmukh et al. (2004) find activations by searching periodicity in the BOLD signal of experiments with two state designs. Roche et al. (2004) use the extended Kalman filter to fit the BOLD signals of fMRI experiments to a general linear model. Being an incremental algorithm they propose a method to compute activations for each scan. The implementation is kept at the prototype level and authors report that more engineering is required for real-time conditions.

Other studies can be briefly summarized as follows. Tzikas et al. (2004) present a method to find activations in a two-state experiment with a Bayesian approach based on the Relevance Vector Machine. Noh and Solo (2006) detect activations spatiotemporally, based on a noise model which is spatially and temporally correlated. In another study, Akhbari et al. (2010) first compute the sources of func-

tional MR images using independent component analysis (ICA). In order to select the most meaningful sources, they use criterion based on the entropy of the BOLD values. In a more recent attempt to detect the activations, Lian et al. (2014) emphasize the difference in temporal activation patterns in different parts of the brain. To handle different patterns in various regions they develop a Bayesian magnitude change point model around cortical landmarks.

2.2 Classification Of FMRI Data

Classification is the process of finding the correct values for the parameters of a function that will map an input data set to its true class. This function is usually called a classifier. Using a set of correctly labeled data, called the training set, the parameters of the function are updated until the change becomes as small as a predefined ε value, or until the set is exhausted.

Classification of fMRI data has been applied in many scenarios with various methods. Although this section will bring forth the approaches used in Alzheimer's Disease, other influential papers are also discussed.

The idea that the BOLD signals of the voxels can yield information about different states of brain, or can be used as a mind reader (Cox and Savoy, 2003), or a lie detector (Haynes and Rees, 2006) comes a bit later than the activation analysis studies.

One of the earliest studies is done by Haxby et al. (2001), where the authors wanted to find out if the voxels in the ventral temporal cortex respond differently to different objects. To do so, they have studied six subjects as they viewed pictures of faces, cats, houses, chairs, scissors, shoes, bottles and non-sense control images. These categories had two sets, called evens and odds, which are used for within-category and between-category correlations. They have found out that they could match the data that belong to the same category. In a follow up study, Hanson et al. (2004) used an artificial neural network (ANN) and achieved a success rate of 82.5%.

In their initial study, Pereira et al. (2001), work on a set of sentences that are either ambiguous or unambiguous. First, the activated voxels are determined using a voxel-wise t-test comparison, then the data that belongs to these voxels are categorized using an artificial neural network with a single sigmoidal hidden unit, and a linear kernel support vector machine (SVM). The data is represented as the BOLD

values for each sentence, captured for 16 scans during and after the sentence is presented to the subject. The results yielded a 82% success for NN and, 77% success for SVM. The analysis is extended in a follow study, this time using Gaussian naïve Bayes classifier (GNB) (Mitchell et al., 2003).

Cox and Savoy (2003) use linear discriminant analysis and support vector machines to classify fMRI data coming from several sessions where pictures of different categories were shown to four subjects. In order to select a subset of voxels, they have used two approaches; one set is chosen by analysis of variance (ANOVA) methods, where voxels that vary significantly across other categories, and another set is chosen by correlation analysis with a single boxcar predictor. To classify the data, a standard linear discriminant classifier (LDC), a support vector machine classifier for linear classification, and $k(k-1)/2$ pairwise binary classifiers for multi-class classification, where k represents the number of classes, are used. The results show that voxels chosen with analysis of variance perform better, with values from 58% to 97% for different subjects, whereas the classification with voxels chosen by correlation scored at most %55. Among the classifiers, linear SVM outperforms others, whereas LDC has the worst performance.

Tripoliti et al. (2008) use Random Forests algorithm on selected features of fMRI data and other subject features such as demographics, head motion, behavioral data, volumetric measures, activation patterns and hemodynamic modeling to classify Alzheimer's Disease. The prediction is done by the votes of many decision trees that make up the Random Forest. They have used modifications from other studies to improve the Random Forest algorithm and achieved an accuracy rate of 88%.

Random Forests is one of many ensemble methods that works on subsets of a large data set and makes the prediction according to the votes of these sub-classifiers. Kuncheva and Rodríguez (2010) compares 18 classifiers that contain both individual and ensemble methods using the data set in the study by Haxby et al. (2001). The individual methods in the comparison are linear discriminant classifier, logistic classifier, support vector machines, decision trees, Naïve Bayes, nearest neighbor and multilayer perceptron or neural networks. The ensemble methods include bagging, AdaBoost, random subspace, random forest, rotation forest and random oracle. Methods such as bagging, AdaBoost and Random Subspace are implemented both as a decision tree ensemble and an SVM ensemble. The authors remark that ensemble classifiers are not universally better than SVM. They also mention that complexity of ensemble classifiers are more complex, but not by much compared

to single classifiers. Another study by Yu et al. (2015) where they propose a hybrid adaptive ensemble classifier argues that different subspaces in the ensemble have varying degrees of importance which may affect the result.

Similar studies where decoding of brain activity has been applied successfully outside of AD classification are as follows. Haynes and Rees (2005) use linear discriminant analysis, Kamitani and Tong (2005) use support vector machines to decode the orientation of the stimulus. Thirion et al. (2006) use support vector machines to infer the visual content of images from brain activation patterns. Mourão-Miranda et al. (2005) use support vector machines to classify brain states and compare it to Fisher Linear Discriminant classifier. Douglas et al. (2011) compare classification methods such as K-Star, Naïve Bayes, support vector machines, C4.5 decision trees, AdaBoost and Random Forests to decode fMRI data where subjects were shown statements with different categories. Although the authors remark that there is no single classifier that is universally best, Random Forest classifier has the highest overall correct classification, closely followed by AdaBoost.

2.3 Functional Connectivity

The brain is a complex structure and activation detection is not the only information that can be extracted from the fMRI data. Even though a region can be bound to a function with activation detection, complicated tasks require spatially remote regions to work together without an anatomical connection. The temporal correlation between the signals of two or more such regions is called “functional connectivity” (Friston et al., 1993). The recent studies have started to concentrate on the networks that are formed by the functional connectivity in the brain.

There are several approaches to extract the functional connectivity and Li et al. (2009) has summarized them in a fairly recent survey. Figure 2.2 is based on their categorization with new studies added under the clustering and independent component analysis branches. The survey discriminates the methods under two categories; Model-based and Data-driven. Model-based approaches require knowledge about the fMRI task, or brain regions to analyze. The data-driven methods do not assume anything about the data and try to deduce information either by decomposing the data or clustering it.

The most common approach to detect the temporal correlations is the cross correlation analysis. It is popular because it is simple, computationally fast and easy to implement. Being a model-based approach, this method requires a predefined

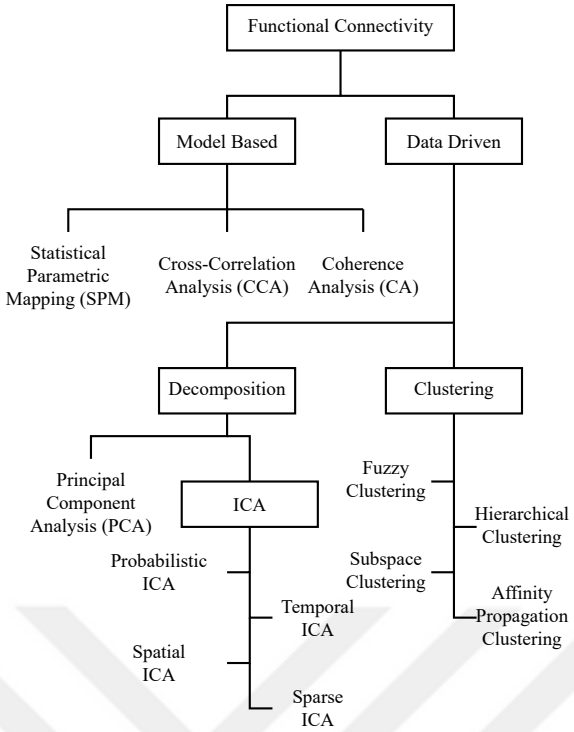

Figure 2.2. Functional connectivity methods. This categorization is extended from Li et al. (2009).

region of interest that is called a seed. Since this region will contain many voxels, the average BOLD signal is computed and it is used as one of the signals in the correlation equation given in Equation 2.4 for two signals X and Y where Cov is the covariance of two signals and σ_X and σ_Y are the standard deviations of named signals.

$$\text{Corr}(X, Y) = \frac{\text{Cov}(X, Y)}{\sigma_X \sigma_Y} \tag{2.4}$$

The other signal that will be correlated can be the BOLD signal for any voxel in the brain, where a functional connectivity is sought. In this case it is called region-to-voxel analysis. The signal can also be cross correlated against the average of another region, which in this case it is called region-to-region analysis.

The technique has been applied to fMRI data for the first time in the study by Cao and Worsley (1999), where they take correlations of the signals at various lags, shown in Equation 2.4 as μ. Since computing at every lag would be computationally expensive, the analysis is almost always done with zero lag.

The result of the correlation analysis will always result in a value between

$[-1, 1]$, so a certain threshold value is defined. Two BOLD signals are considered functionally connected if the correlation is above this threshold value.

Other model-based methods include the coherence analysis and the statistical parametric mapping. Coherence analysis is cross correlation in the frequency domain, introduced by Sun et al. (2004). Although the purpose of SPM is to find activations using a design matrix, it is abused by setting an average of a seed as a covariate of interest to find regions similar to the seed (Greicius et al., 2003).

Data-driven methods are branched into decomposition and clustering algorithms. Both of these approaches contain popular methods that have been in use for other problems.

Principal component analysis (PCA) is a widely used decomposition method. For a signal in R^n space, PCA extracts n components that are orthogonal, and an eigenvalue for each component which shows how much it contributes to the overall information of the data. In PCA, it is common to discard components with low contributions, and reduce the data while maintaining the information. Friston et al. (1993) were first to apply PCA in functional connectivity analysis.

While PCA tries to find orthogonal components, independent component analysis tries to find components with statistical independence (Hyvärinen and Oja, 2000). It is possible to decompose the data spatially or temporally, which are named sICA and tICA, respectively. In addition to both of these approaches, Beckmann and Smith (2004) introduced probabilistic ICA, where they assume that BOLD signals are generated by statistically independent non-Gaussian sources. Recently, Wang et al. (2013) introduced sparse approximation coefficients to ICA.

The other data-driven set of methods is the clustering of fMRI data. Clustering algorithms separate the data into a set of clusters according to some similarity criteria. Golay et al. (1998) applied the fuzzy c-means (FCA) analysis to fMRI data with two distance metrics based on Pearson's correlation coefficient. Cordes et al. (2002) used hierarchical clustering with a distance metric based on the combination of correlation analysis and frequency decomposition. Ren et al. (2014) proposed an approach where they combine sparsity with affinity propagation clustering. Recently, sub-space clustering methods have been applied to fMRI data as well (Liu et al., 2015; Tang et al., 2015).

2.4 Medical Imaging And Alzheimer's Disease

The main purpose of the thesis is the diagnosis of AD using the data coming from an fMRI scan. Although the activation detection, classification and functional connectivity methods have been reviewed so far, they would not help if there is no difference in the BOLD signals of healthy subjects and subjects with AD. For that regard, the literature review would be incomplete without mentioning the following valuable research.

As mentioned earlier, the main cause for AD is suppression of synaptic transmission (Querfurth and LaFerla, 2010; Selkoe, 2002). Scheff et al. (2007) studied the postmortem autopsy brain tissues from hippocampal CA1 subfield of mild AD, MCI and healthy subjects. The study has found out that subjects with mild AD had %55 percent fewer synapses than the two other groups, whereas subjects with MCI had %18 percent fewer synapses. Wenk (2006) lists the following regions as affected from synaptic failure; the temporal and parietal lobes, restricted regions within frontal cortex and hippocampus. The study also mentions reduction of activity in cerebral cortex and hippocampus.

Raichle et al. (2001) has investigated the decreases in regional brain activity even when the subject is lying quietly and found out that during resting, some regions of the brain start to work in correlation. This network of regions has been named as the "default mode network" (DMN). Further studies showed that, as the subject rests, the BOLD signals from the regions Posterior cingulate cortex (PCC) and medial prefrontal cortex (mPFC) show increased functional correlation (Greicius et al., 2003). If a task is given, the correlations start to decrease, and a network dedicated to the given task starts to emerge.

After its inception, the DMN has become a popular research topic. Buckner et al. (2008) lists the regions and their brain areas in Broadmann numbering (Brodmann, 1909) in Table 2.2 as the core regions associated with the default mode network. The study also states that the medial prefrontal cortex and posterior cingulate/retosplenial cortex have the highest correlation in resting state default mode network activity.

The study by Greicius et al. (2004) showed that default mode network activity can distinguish subjects with AD from healthy subjects, because the functional connectivity of the default mode network is disrupted when AD is present, followed by other studies claiming the similar outcomes (Rombouts et al., 2005; Wang et al.,

Table 2.2. The table is from Buckner et al. (2008) and lists the core regions in the default mode network. The Lateral temporal cortex is not listed because the paper lists it as the most tentative region for humans. The Hippocampal formation includes the entorhinal cortex (EC) and surrounding cortex, such as parahippocampal cortex. The brain area labels correspond to the original numbering by Broadmann (1909).

Region	**Included Brain Areas**
Ventral medial prefrontal cortex	24, 10 m/10 r/10 p, 32ac
Posterior cingulate/retosplenial cortex	29/30, 23/31
Inferior parietal lobule	39, 40
Dorsal medial prefrontal cortex	24, 32ac, 10p, 9
Hippocampal formation	Hippocampus proper, EC, PH

2007; Sorg et al., 2007).

3. ROBUST ACTIVATION DETECTION METHODS

This chapter discusses the novel approaches developed for detecting activations in a block design fMRI experiment. These methods are developed using a two-state block design experiment as a test-bed with synthetic and real fMRI data.

The data generation and the proposed methods are all implemented in MATLAB (MATLAB Student version 2016a, http://www.mathworks.com).

3.1 Definitions Of An FMRI Experiment

Let an fMRI experiment take T time to complete. At every time instance t_i of T, a volume V_i of the brain is acquired by the MRI device. This volume is made up of voxels denoted by $v_{(a,s,c)_i}$ where a stands for axial, s stands for sagittal and c stands for coronal planes.

Since these volumes are acquired at regular time intervals, r, let there will be $n = T/r$ number of instances, $V_{1...n}$. Each voxel will have n number of BOLD signal values, b_i, which make up the BOLD signal as indicated in Equation 3.1.

$$v_{a,s,c} = (b_1, \ldots, b_i, \ldots, b_n) \tag{3.1}$$

In Equation 3.1 i is the time index captured at r intervals. This shows that a voxel $v_{(a,s,c)_i}$ for an instance i has the BOLD intensity value b_i and these b values make up the whole volume V_i.

The resulting data set is denoted by $\mathcal{F}$ and is defined as in Equation 3.2.

$$\mathcal{F} = \{V_1, V_2, \ldots, V_n\} \tag{3.2}$$

3.1.1 Experiment Structure

The proposed methods are tested with the data coming from a two-state block experiment acquired by the 3 Tesla MR device in Ege University. One of the states is always “no activity”, also called “resting”, while the other state is an activity that is either “finger tapping” or “word generation”. The former task is related to motor regions of the brain, while the latter makes the speech center active. Although the

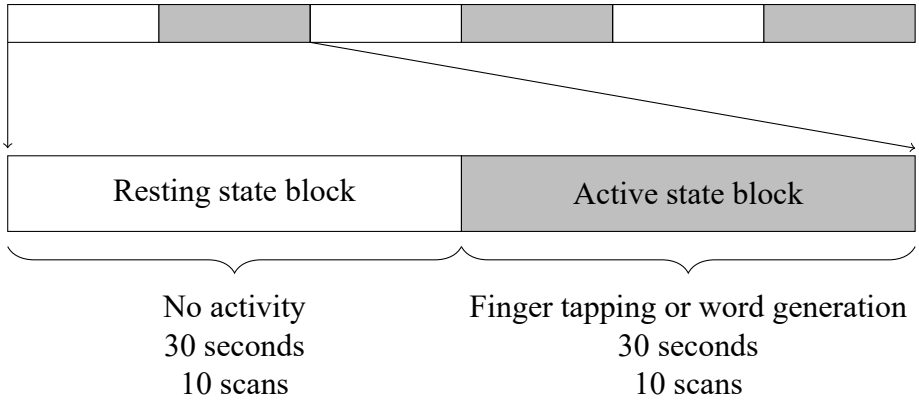

Figure 3.1. The experiment consists of two alternating states; no activity, which acts as a baseline; and activity, which is either finger tapping or word generation. Both states are 30 seconds long, which is captured in 10 scans where the scan interval is $r = 3$. These states are repeated three times which results in $T = 180$ seconds or $n = 60$ scans per subject.

activities change, the structure of the experiments is always the same.

As can be seen in Figure 3.1, experiment is divided into 30 seconds of blocks. It starts with the resting state block, followed by active state block. The complete experiment is composed of three runs of resting followed by active state blocks, which adds up to $T = 180$ seconds.

The images are acquired in $r = 3$ seconds of intervals. During each of these intervals, a complete brain volume V_i is acquired, resulting in $n = 60$ continuous BOLD values for each voxel in the brain. The final data set $\mathcal{F}$ contains volumes $V_{1...60}$.

In the finger tapping experiment the subjects are asked to tap their index fingers and thumbs rapidly. The tapping is self-paced. The subjects are cued to start or to stop tapping their fingers by the operator.

In the word generation experiment, the subjects are shown a letter and are asked to generate words that start with that letter. For each activity block, three different letters are shown where each letter stays on the screen for 10 seconds. The subject will be shown 9 different letters in total. The experiment is programmed in the Presentation software (Version 16, www.neurobs.com).

3.2 Synthetic FMRI Data

Besides the real fMRI data, a set of synthetic fMRI data is also generated to test the proposed methods. The advantage of using artificial functional images is that the activated voxels are known beforehand, which green-lights a method to test it with real functional data on the condition that it can successfully detect the activations.

When synthetic data is selected for preliminary evaluation, a new problem arises about how the artificial signals are generated to successfully simulate real life data. It is vital to learn the nature of the fMRI signals to create almost identical synthetic samples. A real fMRI data contains the BOLD signal and noises generated by the MRI device and the subject's physiological functions such as breathing and cardiac fluctuations.

The generation of HRF has been discussed in detail in Section 1.3.1. The shape of the HRF is modeled as the difference of two gamma functions as given in Equation 1.2. Using the magnitude, width and latency parameters, it is possible to generate varying hemodynamic responses that can emulate different subjects and regions.

The noise is going to be discussed in Section 3.2.1. How synthetic data is generated will be given in Section 3.2.2. Hybridizing the real data with synthetic activations is going to be discussed in Section 3.2.3.

3.2.1 Noise

Functional images contain noise from both the device and the subject. This proves to be a challenge for both acquisition, where the tasks have to be repeated, and the analysis (Ou et al., 2010). The noise coming from the device can be estimated using the voxels that does not contain any living tissue. The only signal received from these empty voxels are the noise that is coming from the MRI device. If this signal is inspected in the frequency domain, the spectral information about the noise can be obtained. The noise can be removed from the functional data by spectral subtraction, or can be added to synthetic data.

One of the most important features of functional imaging is that it captures living tissues without any harm to the subject. However, living organisms cause physiological noise by cardiac and respiratory fluctuations. It is possible to generate similar noise for cardiac and respiratory fluctuations (Handwerker et al., 2004).

Table 3.1. HRF generated by different parameters. HRF varies from subject to subject and from region to region for a single subject. In order to include a wide range of types, the listed HRFs are generated with parameters as indicated.

HRF	A_1	A_2	τ_1	τ_2	δ_1	δ_2	C
HRF 1	6	1	4	4	0	6	0
HRF 2	6	3	3	4	0	6	0
HRF 3	2	1	12	14	0	6	0
HRF 4	8	3	3	4	0	6	0
HRF 5	6	1	9	12	0	6	0
HRF 6	6	1	7	15	0	6	0
HRF 7	3	1	8	12	3	10	0
HRF 8	6	1	8	12	4	14	0
HRF 9	12	1	2	4	0	6	0
HRF 10	5	3	4	7	0	6	0

3.2.2 Approach 1: Generating Synthetic Data

The synthetic data uses the identical two-state experiment structure as the real fMRI data. Both states are 30 seconds long, which is supposed to be captured in 10 scans where the scan interval is $r = 3$ seconds. These states are repeated 3 times which results in $T = 180$ seconds or $n = 60$ scans. The initial state is a "no activity" or "resting" state where it is assumed that there is no neural activity. This state is followed by the "active" state where neural activity is expected.

The HRF varies from subject to subject and from region to region for a single subject as aforementioned. In order to include a wide range of types, 10 HRFs are generated with parameters as indicated Table 3.1.

The studies, specially (Glover, 1999) and (Handwerker et al., 2004), try to find out the parameters of the canonical HRF using the subject's observed responses. In this process, the parameters of the canonical HRF model fit to the sum of two gamma functions with the largest and smallest residuals across subjects and regions.

The generated HRFs can be seen in Figure 3.2 and in more detail in Appendix 1. Some of these HRFs have higher magnitudes, some have higher latency values and some have a larger width for the peak.

Figure 3.3 shows the synthetic data generation for one of the ten HRFs. The

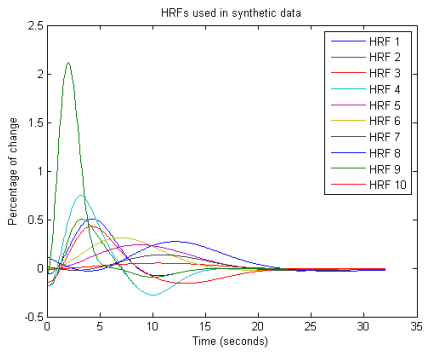

(a) HRFs with a 0.1 seconds sampling rate.

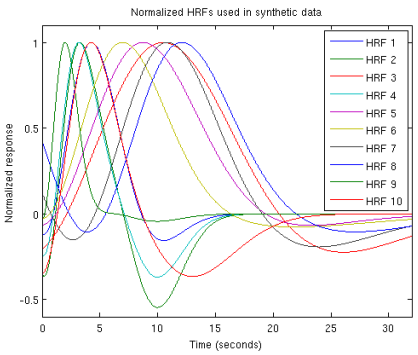

(b) The normalized HRFs with a 0.1 seconds sampling rate.

Figure 3.2. The resulting HRFs from Table 3.1, sampled at 0.1 seconds.

first step is to obtain a single mid-axial slice from one of the real fMRI experiments. This slice serves as a base for the synthetic data. It is duplicated as many as the number of acquisitions in $T = 180$ seconds, which in this case is $n = 60$, which can be seen in Figure 3.3.a. For each voxel in the slice, the BOLD values are constant and equal to the initial value.

Figure 3.3.b shows the selection of a set of 16 voxels and their 8-connected neighbors as synthetic active voxels. The selected voxel coordinates are also saved in a variable so that they can be used in receiver operating characteristics (ROC) analysis. These selected voxels are shown as black squares in the figure. For each of these voxels, a boxcar function is generated as in Equation 3.3 where t shows the instance in the experiment, active set contains the instances for the active state and resting set contains the instances for the resting state.

$$s(t) = \begin{cases} 1 & \text{if } t \in \text{active} \\ 0 & \text{if } t \in \text{resting} \end{cases} \tag{3.3}$$

This signal is called s and it is convolved with the selected HRF signal, h, in Figure 3.3.c. The convolution operation gives an expected activation signal g that can be seen in Figure 3.3.d.

$$g = (s * h)(t) = \int_0^t s(\tau)h(t-\tau)d\tau \tag{3.4}$$

If the voxel is not an active voxel, its values are not changed.

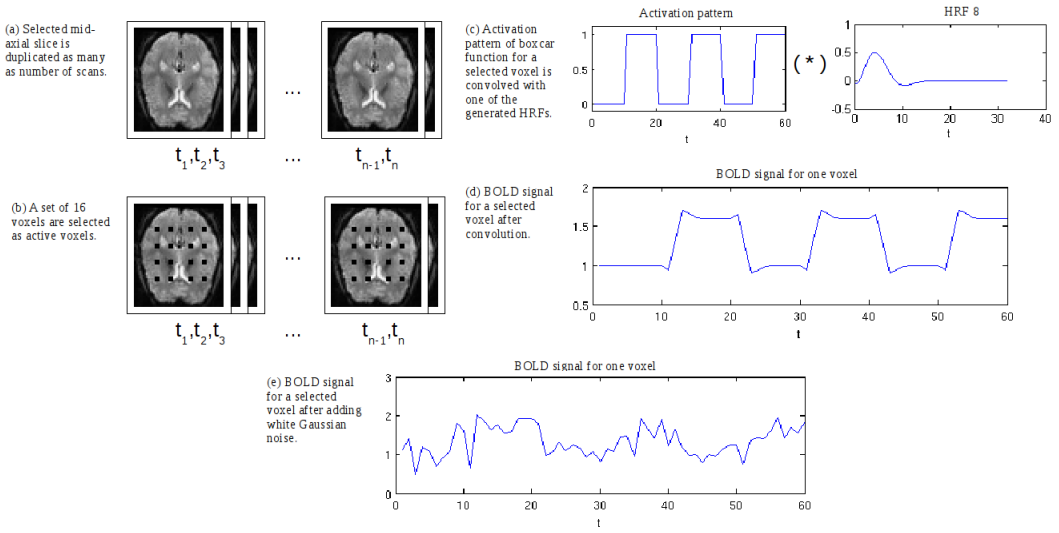

Figure 3.3. (a) shows the mid-axial slice in time instances t_1 to t_n. (b) shows the selected activated voxels and their 8-connected neighbours in black. For each of the selected active voxels, a box-car function is created and this function is convolved with HRF 8, as can be seen in (c). The result of the convolution is shown in (d) and finally, noise is added to the voxel values, as can be seen in (e).

The final step is to add noise to all voxels in the data set. As mentioned earlier, the noise in the fMRI data comes from the equipment and the subject. The reported values for signal noise ratio (SNR) values range from 0.35 to 203.6 (Welvaert and Rosseel, 2013). In their study, (Parrish et al., 2000), report the SNR as 14 for a 1.5 Tesla MR device. The SNR is expected to be higher for a 3 Tesla MR device. In our study, we projected our efforts to lower SNR values so that the proposed method could detect activations even in more challenging data sets. Therefore noise is added to the synthetic data so that the resulting data sets would have the chosen SNR values of 3, 5, 10, 15 and 20.

The important aspect of adding noise to existing signal is to set the SNR correctly in the synthetic data. SNR values are expressed in decibels and as the name suggests, they are the ratio of the power of the signal, P_{signal}, to the power of the noise, P_{noise} as shown in

$$\mathrm{SNR}_{dB} = 10 \log_{10} \left(\frac{P_{signal}}{P_{noise}} \right) \tag{3.5}$$

The noise in the fMRI is generally modeled as a Gaussian (Welvaert and Rosseel, 2014). When adding noise to the synthetic data that will match the targeted SNR value, the power of the random Gaussian noise can be computed with Equation 3.5, since the SNR is known and the power of the signal can be computed

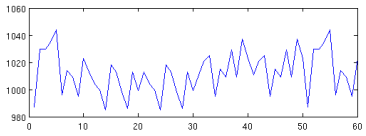

(a) Time versus voxel intensity plot of real BOLD signal of a voxel.

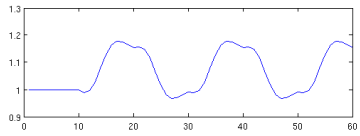

(b) Time versus percentage change plot of the expected signal g, convolved with HRF 3.

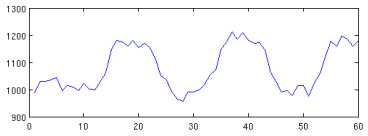

(c) Time versus voxel intensity plot of the signal for real BOLD signal after applying the changes in g

Figure 3.4. The synthetic activations are formed by applying the percentage of changes in the expected signal g to the real BOLD signal.

using the existing signal. This power value of the noise is used as a magnitude to the randomly generated numbers from the standard Gaussian distribution. A resulting sample signal with noise can be seen in Figure 3.3.e.

This procedure is repeated with a new unaltered slice for each of the HRFs.

3.2.3 Approach 2: Synthetic Activations on Real Data

This approach creates synthetic activations using the resting state signals of the real fMRI data. The experiment structure is used identically in Approach 2; the resting state blocks are followed by active state blocks. The synthetic activations on the active state blocks are generated using the data from the resting state blocks and the HRFs given in the Table 3.1. In order not to affect the statistical results, the base signal for an active state block is chosen as the following resting state block, rather than the preceding one.

Instead of mid-axial slice duplication used in Approach 1, this approach saves mid-axial slices from each resting state of the real fMRI instances. The boxcar signal s is once again convolved with one of the HRFs, h, with the Equation 3.4 to form the signal g that denotes the expected change. The same voxels in Approach 1 and their 8-connected neighbors are once again selected and the expected changes in g are applied to their BOLD signals to form the synthetic activations, as can be seen in Figure 3.4. Remaining voxels retain their original real BOLD signals.

This approach removes the need to generate artificial noise since it is already

embedded in the real BOLD signal.

3.3 Proposed Methods

The experiment data, whether real or synthetic (Approach 1 and 2), contains n number of brain volumes, denoted by V, acquired in regular r intervals in time, where each volume is made up of unit volumes called voxels. The voxel BOLD values, b_i, captured at each instance i, form the signal v as shown in Equation 3.6.

$$v = (b_1, ..., b_i, ..., b_n) \tag{3.6}$$

The experiment data contains two states; resting and active. These states alternate in blocks during acquisitions as mentioned earlier.

For each voxel, the states can be denoted separately in two sequences. The b values belonging to resting state are a sequence called R and b values belonging to active state are another sequence called A. Clearly, because of the structure of the experiment, both of these sequences have $n/2$ elements. It should also be noted that each sequence contains three blocks of a state, where each block has $n/6$ elements.

Let k denote the index value of the sequence blocks. For instance, $R^{k=3}$ indicates third resting state block in resting state sequence, R. In the same manner, $A^{k=2}$ indicates the second active state block in the active state sequence, A.

3.3.1 Instantaneous Activation Method

Activation analyses are almost always done offline, over the complete set of images. However, there may be cases where activation information needs to be queried at a specific instant, t_i. The goal in the instantaneous activation method (IAM) is to estimate if there is an activation at time t_i using the values in its preceding resting state block.

Let the queried time t_i belong to the block k of the sequence A, and let the preceding resting block be denoted by R^k. The IAM method asserts that the BOLD value at t_i should have the same statistical characteristics of R^k if it is not activated. The similarity is based on the confidence interval (CI) estimate for the mean of the values in sequence R^k. The accepted definition of the confidence interval equation is computed by the Equation 3.7;

$$\text{CI} = E \pm \frac{\mathtt{t}_{(p/2,n-1)} S}{\sqrt{(n/6)}} \tag{3.7}$$

where E is the mean and S is the sample standard deviation of values in sequence R^k (Montgomery and Runger, 2011). The variable $\mathtt{t}$ denotes the t-statistic for a given significance level in this equation. The half of the p significance value and the degrees of freedom $(n-1)$ are used for the $\mathtt{t}$ value lookup table.

Equation 3.7 yields an upper, CI_u, and a lower boundary, CI_l for the mean estimate. The BOLD signal is expected to increase if there is an activation, therefore for any value b acquired in a specific time t_i in an active state block, the activation is decided by the following function;

$$f_{\text{activation}}(b) = \begin{cases} \text{true} & \text{if } b > \text{CI}_u, \\ \text{false} & \text{if } b \leq \text{CI}_u \end{cases} \tag{3.8}$$

The reliability of the confidence interval rests on the significance value p. Therefore, it is advised to apply a family wise error correction before the $\mathtt{t}$ value table lookup is performed, to improve the reliability of the results.

IAM is a novel approach that introduces the application of confidence intervals to instantaneous activation analysis.

3.3.2 Instantaneous Activation Method using Past Resting Blocks

The number of samples in the IAM method affects the confidence interval estimate and the method can further be improved by including samples from previous resting state blocks. In Instantaneous Activation Method using Past Resting Blocks (IAMP), all the previous resting state blocks are used to estimate the activation for a voxel at time t_i.

Let the activation sought for t_i belong to the active state block k in sequence A. For a voxel, let BOLD values from the beginning to the preceding resting state block be denoted by R^k.

Similar to IAM method, the IAMP method asserts that the BOLD value at t_i should have the same statistical characteristics of R^k if it is not activated. The similarity is based on the confidence interval (CI) estimate for the mean of the values in

sequence R^k. The number of elements for R^k increases for IAMP method, therefore the equation is updated as follows;

$$\text{CI} = E \pm \frac{\mathtt{t}_{(p/2,n-1)}S}{\sqrt{kn/6}} \tag{3.9}$$

The rest of the steps are identical with the IAM method, where the upper CI boundary, CI_u, is used with the $f_{\text{activation}}(b)$ function in Equation 3.8 to decide if a voxel is activated at an instant or not.

As in IAM, IAMP has the contribution of confidence interval application to instantaneous activation analysis. Since it makes use of the confidence intervals, the reliability of the interval depends on the significance value p and a family wise error correction is advised before the t value table lookup.

3.3.3 Task Activation Method

The Task Activation Method (TAM) uses the R sequence values and A sequence values to find the activated voxels in the experiment. Two sequences of a voxel are compared using a two-sample t-test, similar to the study by (Constable et al., 1993). The null hypothesis is that both of these sequences come from the same distribution and if it can be rejected for a predefined significance level, the voxel in question is considered active.

The t-statistic value can be calculated by the following equation;

$$\mathtt{t} = \frac{\mu_0 - \mu_1}{\sqrt{\frac{\sigma_0^2}{n/2} + \frac{\sigma_1^2}{n/2}}} \tag{3.10}$$

where μ_0 is the mean for the values in R sequence and μ_1 is the mean for the values in A sequence. Similarly σ_0^2 and σ_1^2 are the variances for the values in R sequence and A sequence, respectively. Both of the time series have the same number of elements, $n/2$ and this value is used for each of them in the equation. The probability level of the t-statistic is denoted by t in this equation and it is compared with the significance value, p. The voxel is considered active if the t-statistic probability is smaller. Hence, the function to decide activation is as follows;

$$f_{\text{activation}}(t) = \begin{cases} \text{true} & \text{if } \mathtt{t} \leq p, \\ \text{false} & \text{if } \mathtt{t} > p \end{cases} \tag{3.11}$$

3.3.4 Instantaneous Robust Regression Distance Method

A novel approach is proposed in the Instantaneous Robust Regression Distance Method (IRRD) to estimate activations by using robust regression on the resting state block.

Consider Figure 3.5 where the preceding resting state block values are shown in red and the active state values are shown in blue for a voxel from sample real fMRI data. Let $f_{\text{line}}(t) = X\beta + \varepsilon$ denote the regression line for the resting state block where β denotes the slope and ε denotes the y-intercept of the line. The values β and ε is computed by the iteratively re-weighted least squares method with bi-square weighting function, so that the influence of the outliers are minimized (Fritsch et al., 2012). The resulting line is shown in green in Figure 3.5.

At instance t_i, the basic unit that IRRD works on is the vertical distance between the voxel BOLD value, b_i and its projection on the robust regression line, $f_{\text{line}}(t_i)$. The distances for the resting state block compose the Dist_R vector, while the distances for the active state block form the Dist_A vector. IRRD decides on the activation of the voxel for instance t_i with the values in these vectors, instead of the BOLD values as in IAM.

The IRRD method asserts that the distance to the regression line at time t_i should be similar to the distances in sequence Dist_R, if the voxel is not activated. The similarity is based on the confidence interval estimate for the mean distance in the sequence. Equation 3.7 yields two boundaries, CI_u and CI_l for the mean estimate. The distance to the robust regression line, d, is expected to increase if there is an activation, as defined by the following function;

$$f_{\text{activation}}(d) = \begin{cases} \text{true} & \text{if } d > \text{CI}_u, \\ \text{false} & \text{if } d \leq \text{CI}_u \end{cases} \tag{3.12}$$

This novel approach introduces a new metric that is not bound by the voxel intensities.

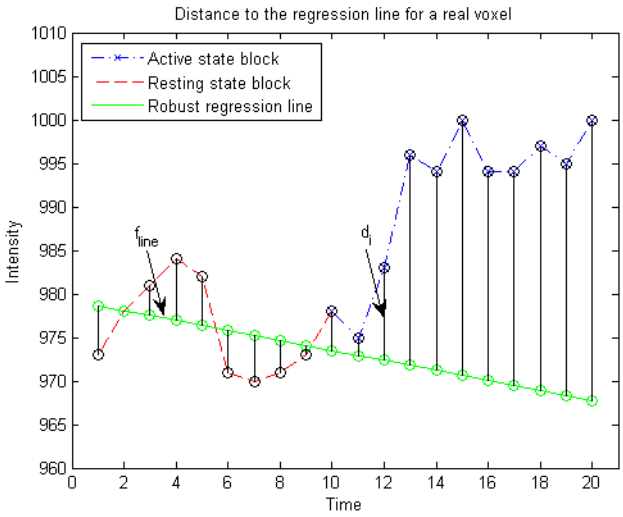

Figure 3.5. This figure shows the first resting state block in red, followed by the immediate active block in blue for a voxel from real fMRI data. The green regression line is computed by the resting state block values. Instead of using voxel intensities, the distance to this regression line, shown in black, is used for the IRRD and TRRD methods.

3.3.5 Task Robust Regression Distance Method

The Task Linear Regression Distance Method (TRRD) makes use of the IRRD approach to compare the distances in resting and active states, similar to the TAM.

Let the regression line for all of the values in sequence R be defined by the function $f_{\text{line}}(x) = X\beta + \varepsilon$. The slope β and the y-intercept ε is computed by the iteratively re-weighted least squares method with bi-square weighting function, minimizing the influence of the outliers.

For each BOLD value in both sequences R and A, the distance to the robust regression line in the y-direction is calculated, similar to the IRRD method. These distances, denoted by variable d, are saved in sequences Dist_R and Dist_A, respectively. TRRD method compares these two sequences using a two-sample t-test where the t-statistic is calculated with Equation 3.10. The null hypothesis is that both of these sequences come from the same distribution and if the hypothesis can be rejected for a predefined significance level, p, the voxel is considered active. Hence, the function to decide activation is the same as $f_{\text{activation}}(t)$ in Equation 3.11.

Similar to the IRRD, this novel approach introduces a new metric that is not bound by the voxel intensities.

3.3.6 Correlation Method

As previously stated, correlation has been used earlier to find the activated voxels in an fMRI experiment (Bandettini et al., 1993; Friston et al., 1994; Xiong et al., 1996; Singh et al., 1999). One of the earliest approaches to find the activations are done by correlating the fMRI signal for a voxel with a box-car function. While the box-car proves to be adequate, it can be improved by convolving it with the canonical HRF.

As in synthetic data generation, a boxcar function is generated as follows;

$$s(t) = \begin{cases} 1 & \text{if } t \in \text{active} \\ 0 & \text{if } t \in \text{resting} \end{cases} \tag{3.13}$$

where t shows the instances acquired in time. The function returns 1 for instances that belong to active state and 0 for the instances that belong to resting state. This s vector is convolved with the canonical HRF signal, h. The convolution operation gives an expected activation signal g;

$$g = (s * h)(t) = \int_0^t s(\tau)h(t-\tau)d\tau \tag{3.14}$$

If the BOLD signal of a voxel is similar to this vector, then it is considered active. The similarity is based on the correlation between the expected vector, and the voxel BOLD signal. It is computed by the following equation;

$$c = \frac{\text{cov}(g, s)}{\sigma_g \sigma_s} \tag{3.15}$$

where g represents the expected vector, s represents the voxel BOLD signal, σ_g and σ_s represent the standard deviations of these signals. The cov is the covariance function. The activated voxels are expected to have values close to 1. The voxel is considered active if its c value is above a selected threshold value. A common value of 0.7 has been chosen for this threshold as practiced in the study by (Bandettini et al., 1993).

3.4 Results

For the synthetic data sets generated by Approaches 1 and 2, as discussed in sections 3.2.2 and 3.2.3, the coordinates and the activation information of the selected voxels and their neighbors are known. Therefore it is possible to compare the activation coordinates with the fully automatic activation results of the proposed methods.

Basically, the estimation performance of the proposed methods can be unveiled with the help of a binary classifier. Thus, receiver operating characteristic (ROC) analysis is utilized as such for this study. In the light of the ROC curve analysis results, the results for which methods perform best under which conditions are discussed in detail in the following sections.

The results are further discussed using peak signal-to-noise ratio (PSNR) measurements for perceptual visual quality. To compute PSNR, two images are created; one from the original fMRI images that has been used to generate the synthetic data in Approaches 1 and 2, the other one is from each instance of the active block of the synthetic data. The maximum PSNR values from the active state instances are used to represent the method.

Following the synthetic experiment results, the methods are executed for real fMRI experiment data, and are compared against the commonly used SPM method.

3.4.1 Receiver Operating Characteristics

The ROC analysis is used to evaluate the performance of methods with the synthetic datasets where the activations are known beforehand. The analysis is done using a ROC curve which plots the true positive rate (TPR) of the results against the false positive rate (FPR) (Zou et al., 2007; Lasko et al., 2005).

The true positive rate is the rate of correctly identified active voxels. This value is also called sensitivity. The false positive rate is the rate of voxels erroneously identified as active. It is also referred as $1 -$ specificity. Both of these values are in the range [0,1].

The true positive and false positive rates are computed gradually for the whole range of the threshold variables. Since the *p-value* represents the probability, its range is taken between [0,1] and incremented with a step-size of 0.01. The c value

stands for the correlation between two signals, therefore its range is between [-1,1] with intervals of 0.01.

The plotted ROC curves show the accuracy of the methods for classifying the voxels as active or inactive. A good classifier gets a high true positive rate and a low false positive rate, which results in values close to the point (0,1). If the ROC curve is the sensitivity $= 1 -$ specificity, or the $y = x$ line, it means that the classifier decides on the activations with random chance (Zou et al., 2007). Any curve above this line are considered successful classifiers, which can decide on the activations better than random chance.

Although the position of the curve relative to the sensitivity $= 1 -$ specificity line is a common measure, every problem has its own sensitivity and specificity expectations (Lasko et al., 2005). In the following sections, the results of the methods with combinations of SNR values and different HRFs are given as ROC curve plots and ROC area under the curve (AUC) tables. The difficulties in methods, errors and performance evaluations are also discussed in detail for real fMRI data and the synthetic data generated by Approach 1 and 2.

3.4.2 ROC Curve Construction for Instantaneous Methods

The instantaneous methods, IAM, IAMP and IRRD, use the confidence interval for the mean of the resting state blocks, prior to the active state blocks. The threshold value for the confidence interval is the *p-value*, which in return affects the t-statistic, denoted by `t` value, as shown in Equation 3.7.

As the name suggests, the confidence interval returns a range about the mean value, which is bound to the t-statistic. However, in our methods, we only mark the voxels that have a greater value than the upper confidence bound, CI_u, as shown in Equation 3.8. Thus, even in the case when $p = 1$ where all voxels should be considered active, there remains voxels that are not marked so.

The other approach is to mark voxels that are not within the confidence interval as active, including the voxel values where the value is less than the lower confidence bound ($b < \text{CI}_l$). Clearly, this contradicts with the canonical HRF where the voxel intensity value is expected to increase when there is an activation. Therefore, the ROC curves for these methods have low false positive rates, even in the high *p-values*. To make the visual and numerical comparison easier, the values (0, 0) and (1, 1) are included when plotting these curves. Theoretically, when $p = 0$, none of

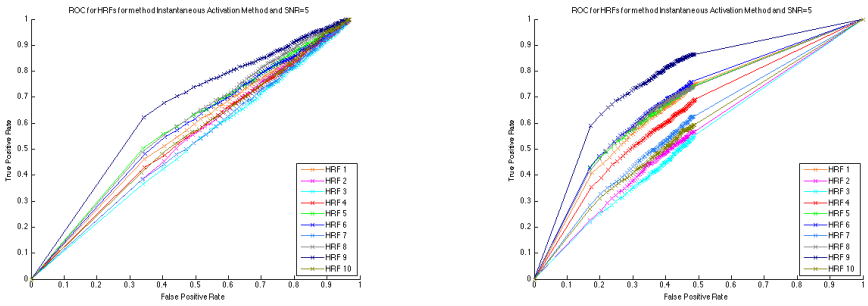

(a) ROC Curves for IAM at SNR=5, using the both confidence bounds.

(b) ROC Curves for IAM at SNR=5, using only the upper confidence bound.

Figure 3.6. ROC Curves with both confidence bounds and only the upper confidence bound when SNR=5.

the voxels should be considered active, therefore the point (0, 0) is included. Similarly, when $p = 1$, all of the voxels should be considered active, so the point (1,1) is also included. The area under the curve values tables 3.2, 3.3, 3.5 and those in the Appendix are also computed with these points included.

In order to supply a visual comparison, the ROC curves for IAM method when SNR=5 are given in Figure 3.6. If both boundaries are used, and the BOLD values outside these boundaries are considered active, the ROC curves are plotted as expected, as can be seen in Figure 3.6.a. As mentioned, this approach causes a contradiction with the HRF, so the approach in Figure 3.6.b is used, where the results with only the upper confidence interval bound are drawn with the points (0,0) and (1,1) included.

3.4.3 On the Results for the Correlation Method

For synthetic data generated by Approaches 1 and 2, combinations of SNR values and different HRFs are evaluated for the complete range of threshold values. The ROC curve plots and AUC tables are given in tables and figures in the following sub-sections. Also, the PSNR values for each method with varying SNR values and different HRFs are detailed in the tables. The following is an important remark when considering and evaluating the given tables.

The correlation method uses the expected signal, g, generated by convolving the canonical HRF with the square wave function of experiment design as in Equation 3.4. In other words, the BOLD signal, such as in Figure 3.3.d, and the synthetically generated activations, such as in Figure 3.3.e depend on the same activation pattern. Therefore the results for the correlation method produce higher values which are not used for comparison but for evaluating relative performance

Table 3.2. Area Under the ROC Curve for Synthetic Data Created by Approach 1

HRFS	IAM(*)	IAMP(*)	TAM	IRRD (*)	TRRD	Correlation(**)
HRF 1	0,8652	0,7972	0,9687	0,8566	0,9674	0,969
HRF 2	0,6421	0,6684	0,9603	0,6383	0,9605	0,9686
HRF 3	0,7233	0,6482	0,918	0,7129	0,9177	0,9671
HRF 4	0,8451	0,7912	0,9671	0,8332	0,9671	0,969
HRF 5	0,8301	0,716	0,9674	0,8202	0,9671	0,969
HRF 6	0,8502	0,7576	0,9674	0,8307	0,9674	0,969
HRF 7	0,7927	0,7012	0,966	0,7859	0,9666	0,969
HRF 8	0,8526	0,6831	0,9658	0,8402	0,9655	0,969
HRF 9	0,8717	0,8019	0,9668	0,8643	0,9668	0,969
HRF 10	0,754	0,7568	0,9662	0,7432	0,9659	0,969
(*)	Please refer to Section 3.4.2 for details on instantaneous methods.					
(**)	Please refer to Section 3.4.3 for details on Correlation method.					

of other methods.

3.4.4 Results on the Synthetic Data Generated by Approach 1

The following analyses are done on the synthetic data generated in the Section 3.2.2 using combinations of varying SNR values and different HRFs. The results are given in the tables and figures that follow. The importance of sections 3.4.2 and 3.4.3 for the subtle but vital details on the generation of these tables should once again be emphasized.

The areas under the curves are computed for each HRF and SNR combination and given in the table in Appendix 2, showing the maximum values in bold text for each HRF. A brief version of this table, where only the maximum values are listed for an HRF, is given in Figure 3.2. As it can be deduced from this brief table, the results are consistent with the HRF variations. The task based methods, TAM and TRRD, perform better compared to the instantaneous methods, even though the instantaneous methods are capable of finding the activations. This shows that they are not as good as other methods to locate activations. However, it should be emphasized that, the purpose in instantaneous methods is to locate activations to stimuli at specific instants, rather than taking the complete experiment into account. Therefore, the instantaneous methods show their worth in yielding results that show us how the activations in brain regions change temporally as the experiment is being executed.

Table 3.3. Area Under the ROC Curve for All HRFs in Synthetic Data Created by Approach 1

Method	SNR 3	SNR 5	SNR 10	SNR 15	SNR 20
IAM(*)	0,6124	0,634	0,7017	0,7615	0,8019
IAMP(*)	0,5963	0,6128	0,6721	0,711	0,732
TAM	**0,7127**	**0,7719**	0,8794	**0,9368**	0,9609
IRRD(*)	0,6072	0,6289	0,6951	0,7534	0,7926
TRRD	**0,7127**	**0,7719**	**0,8795**	**0,9368**	**0,9608**
Correlation(**)	0,8515	0,8822	0,9403	0,9619	0,9688
(*)	Please refer to Section 3.4.2 for details.				
(**)	Please refer to Section 3.4.3 for details.				

The figures in Appendix 4 show the ROC plots for the instantaneous methods IAM, IAMP and IRRD, and the figures in Appendix 5 show the ROC plots for TAM, TRRD and Correlation. The figures include plots for the lowest SNR value, SNR=3, and highest SNR=20 for comparison. The mid-ranges, where SNR is 5, 10 and 15 are left out to save space, but their results are available in the table in Appendix 2. The plots show that as the SNR increases, the data contains less noise, which results in better results, as expected. If the proposed methods can identify active voxels even when SNR is as low as 3, then they can be considered successful. Indeed, the plots show that instantaneous methods are able to locate these activations, since they are above the sensitivity $= 1 -$ specificity line.

The table 3.3 shows the combined results of all HRFs for AUC values. In the table, bold text shows the highest value among the methods. As mentioned earlier, HRFs can change from subject to subject, and even from region to region in a single subject. The combined results give another perspective to evaluate these methods, as if all of these HRFs happen at different regions in a single subject. The table shows that the methods TAM and TRRD have fairly close results, confirming the conclusion that these methods are good alternatives to find activations in fMRI experiments. The table also reflects the expected increase in the results as the SNR increases, as it was in the HRF-wise analysis.

While the ROC curve plots for all methods when SNR=3 and SNR=20 are given in Appendices 4 and 5, Figure 3.7 shows all methods in one plot, at the same SNR values. The plot when SNR=3 shows that, even when there is a lot of noise, the methods are capable of finding activations.

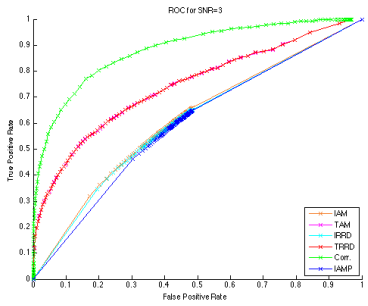

(a) ROC Curves of all methods at SNR=3

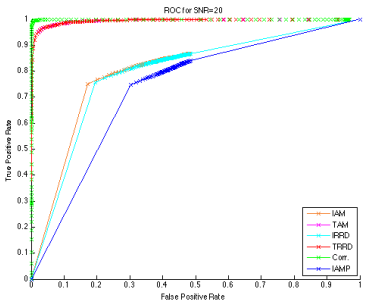

(b) ROC Curves of all methods at SNR=20

Figure 3.7. ROC Curves with all HRFs for SNR=3 and SNR=20

Table 3.4. PSNR Values for All HRFs in Synthetic Data Created by Approach 1

Method	SNR 3	SNR 5	SNR 10	SNR 15	SNR 20
IAM	8.5723	8.7958	9.3488	9.7625	10.0847
IAMP	6.3018	6.5557	6.9775	7.1528	8.0015
TAM	**20.0818**	19.8751	19.3489	**20.6003**	**23.321**
IRRD	8.2224	8.2825	8.595	8.9654	9.3583
TRRD	20.0757	**19.8589**	**19.3729**	20.5623	23.3153
Correlation(*)	23.6819	23.7353	26.5129	27.883	29.5002
(*)	Please refer to Section 3.4.3 for details.				

In the table in Appendix 3, the maximum PSNR values are given for every combination of SNR values and different HRFs. The maximum PSNR value for each HRF is shown in bold text. The PSNR values show how much of the activations are successfully identified; the higher the PSNR value, the more activations are found.

As with ROC curves, Table 3.4 shows the combined results of all HRFs for PSNR values. Similar to the HRF-based table, the methods TAM and TRRD have high PSNR values as they do have high AUC values. These methods can be regarded as successful methods that can be alternatives to established methods such as SPM.

3.4.5 Results on the Synthetic Data Generated by Approach 2

The following analyses are done on the synthetic activations on real data, which were generated in the Section 3.2.3. Since the subjects are anonymous, their data has been identified with codes KAMUEGE205, KAMUEGE305, KAMUEGE320 and KAMUEGE505. As the data includes synthetic activations on real data, there

Table 3.5. Area Under the ROC Curve for All HRFs in Synthetic Data Created by Approach 2

Method	Subject 1	Subject 2	Subject 3	Subject 4
IAM(*)	0,851	0,8072	0,8292	0,8373
IAMP(*)	0,7339	0,7001	0,7129	0,6816
TAM	**0,928**	**0,9637**	0,9186	**0,9449**
IRRD(*)	0,8348	0,7964	0,8161	0,8181
TRRD	0,9117	0,9596	**0,9189**	0,9302
Correlation(**)	0,9677	0,9942	0,9908	0,9849
(*)	Please refer to Section 3.4.2 for details.			
(**)	Please refer to Section 3.4.3 for details.			

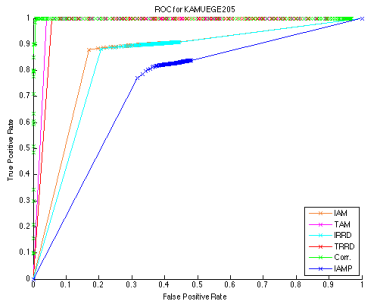

(a) ROC Curves of all methods for Subject KAMUEGE205

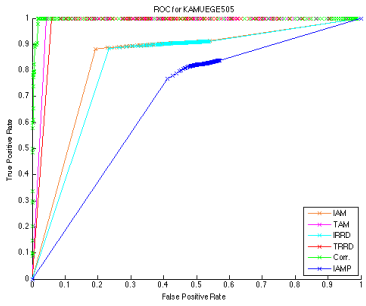

(b) ROC Curves of all methods for Subject KAMUEGE505

Figure 3.8. ROC Curves with all HRFs for KAMUEGE205, KAMUEGE505

are no different SNR levels. Therefore, results for different subjects are provided for comparison and evaluation. The importance of sections 3.4.2 and 3.4.3 should once again be reminded for the subtle but vital details on the generation of the tables that are given.

The area under the curves are computed for each combination and are given in the table in Appendix 6, showing the maximum values in bold text for each Subject. Since the data does not have different SNR levels, the results are fairly close to each other, showing the consistency in the methods. The task related methods, TAM and TRRD, perform better. However in this data set, they perform considerably better than the synthetic data generated by Approach 1. This is likely because the noise in the data generated by Approach 2 only has the original noise from the real fMRI data. The results for all HRFs are given in Table 3.5. Similar to the first approach TAM and TRRD fair very close to each other.

The ROC plots for these combined results is shown in Figure 3.8. The in-

Table 3.6. PSNR Values for All HRFs in Synthetic Data Created by Approach 2

Method	Subject 1	Subject 2	Subject 3	Subject 4
IAM	11.107	10.7141	9.5908	11.0631
IAMP	8.1117	8.4917	8.2989	8.1247
TAM	**17.1575**	**16.9513**	14.5624	**15.9465**
IRRD	9.893	9.8263	9.0945	9.4809
TRRD	15.32	16.9105	**14.5764**	15.0163
Correlation (*)	27.137	22.3865	22.666	22.8744
(*)	Please refer to Section 3.4.3 for details.			

stantaneous methods, similar to the results in Approach 1, are able to identify active voxels in all of the subjects, as they are above the sensitivity $= 1 -$ specificity line. The ROC plots of HRFs for all methods are given in Appendix 8.

In the table in Appendix 7, the maximum PSNR values are given for every combination of SNR values and different HRFs. Table 3.6 show the combined results for all HRFs of PSNR values. In these tables the maximum PSNR value for each subject is shown in bold text. The PSNR values show how much of the activations are successfully identified; the higher the PSNR value, the more activations are found. Similar to the results for the data set generated by Approach 1, the methods TAM and TRRD have high PSNR values and high AUC values as can be seen in the tables. These methods can be regarded as successful methods that can be alternatives to established methods such as SPM.

As both the tables and the figure show for both approaches, the methods TAM and TRRD perform very close to each other, once again confirming our conclusion in the previous tables that, these methods are good alternatives for finding activations in fMRI experiments.

3.4.6 Results on the Real fMRI Data

The results for the real experiments are compared visually with the SPM method which is implemented in the SPM12 software (`http://www.fil.ion.ucl.ac.uk/spm/software/spm12/`). The results for the SPM are thresholded with a FWE corrected *p-value* of 0.05. The voxels that are classified as active by the SPM are compared visually with all of the methods as in (Faisan et al., 2005).

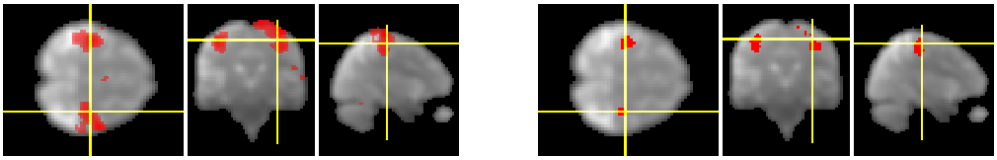

(a) Results for SPM with a FWE corrected $p = 0.05$

(b) Results for TRRD with a FWE corrected $p = 0.05$

Figure 3.9. Comparison of SPM and TRRD for subject KAMUEGE305 with a FWE corrected $p = 0.05$.

Proposed methods that use the statistical p value for thresholding are executed with the same FWE corrected value as SPM, $p = 0.05$. For the correlation method in this study, a threshold of $c = 0.7$ is used.

The activations detected by SPM and the proposed methods for the subject KAMUEGE305 can be seen in the figures in Appendix 9. The instantaneous methods, such as IAM, IAMP and IRRD, have an activation map for each of the scans for the active state block. The third instance in the active state block is chosen to be shown in the Figure, since the BOLD value is expected to increase.

In the instantaneous methods, the activations at each instance of the active state block are identified. The relevant information extracted with the instantaneous methods will not be accessible to methods such as SPM, TAM and TRDD where the complete experiment data is used. Even though the area under the curves for instantaneous methods in ROC analysis are less than other methods, they provide an opportunity to observe the activations in the various brain regions instantly. Another contribution of these methods is to causally represent the active brain regions in consequent instances.

The results show that TAM and TRRD yield similar but more scrutinized results compared to SPM, as can be seen in Figure 3.9. When the methods are compared among themselves, the ones that use the distance to robust regression line, such as IRRD and TRRD, have results closer to the SPM than their counterparts IAM, IAMP and TAM. These better results are possibly caused by the new distance metric introduced by these methods. Finally, the results for the correlation method are also consistent with SPM, despite correlation being a much simpler approach.

3.5 Conclusion

The ROC analyses show that the instantaneous methods are capable of finding the activations, but are not as good as other methods where the complete experiment

data is used. However, instantaneous methods are good for locating activations to a stimulus at a specific instant, rather than the complete experiment. These activations, which may include relevant and important information may otherwise be statistically lost when the complete experiment is taken into account. The instantaneous methods provide the temporal flow of the activations which may yield more information. The relevant information extracted with the instantaneous methods will not be accessible to methods such as SPM, TAM and TRDD where the complete experiment data is used. Another contribution of these methods is to causally represent the active brain regions in consequent instances.

All of the methods are good at finding locations even at low SNR values. As the SNR value gets higher, the noise levels decrease and the methods perform better. It is also important to note that all of the methods are sensitive to the magnitude of the HRF. The instantaneous methods are sensitive to latency, since they try to find the activations at every instance of the active state and a late peak decreases their performance. The methods do as well as SPM on real data. The results, as can be seen in the figures in Appendix 9, are consistent with the activations detected by SPM.

The instantaneous methods have the advantage over current methods by keeping the temporal activation information and paving a new way for real-time analyses of fMRI data. The new metric introduced by the IRRD and TRRD methods produce slightly more activations than their counterparts which highlights the improvement over them.

4. CLASSIFICATION OF FMRI DATA

This chapter discusses the data sets, feature extraction from these data sets, data representation, classification methods, their application and the results.

The classification is done among three groups of subjects. The first group is made up of the subjects with Alzheimer's Disease. The second group contains the subjects with mild cognitive impairment. The final group is formed by the healthy subjects.

4.1 Data Sets

The data is still being collected at Ege University, so in order to develop and test the methods three data sets have been used. The first set is totally synthetic, similar to the data in activation detection methods. The second set comes from the National fMRI Data Center (http://www.fmridc.org/). The final set comes from the The Alzheimer's Disease Neuroimaging Initiative (ADNI) database. While the first and the second data sets have activations of a simple task, the third data set contains resting state fMRI data.

It should be noted that the data sets from the Ege University will have both activations and the resting state data, therefore they can be used by both of the feature extraction methods that will be discussed in this chapter.

4.1.1 Data Set 1: Synthetic Data

Synthetic data is generated by using the same steps in the "Approach 1" which is detailed in section 3.2.2, with three distinct differences.

The first distinction is the number of HRFs. Instead of 10, the HRFs 1, 2, 4, 9 and 10 has been chosen from Table 3.1. The second distinction is using the complete brain volume instead of a single slice for each HRF. The volume is the first complete brain scan from one of the real data discussed in Section 3.1.1. For this set of data, each voxel has been assigned to a random HRF, within the complete brain volume. This also leads up to 26-connected voxels, instead of 8-connected voxels for a single slice.

Finally, the voxel coordinates are not set as fixed. Instead, three volumes have been defined for three different groups. The volume boundaries are given in Table

Table 4.1. Volume boundaries for three different groups. The synthetic data is generated by choosing random voxels among these defined boundaries. Each group contains 10 from its own region, random number of 1 to 6 voxels from each of two other groups, and 5 random voxels from the whole brain.

	Sagittal	Axial	Coronal
AD	$8-17, 38-47$	$23-38$	$23-38$
MCI	$18-32$	$43-58$	$23-38$
Healthy	$16-38$	$13-28$	$13-28$

4.1. Random voxels has been chosen from these volumes to form a list of random activated voxels for each subject. They are selected as follows. For a subject that belongs to a particular group, 10 voxels are randomly selected from the volume defined for that group. From the two other groups, a random number of voxels, between 1 to 6, are chosen for each. Finally, 5 voxels are selected randomly from the complete brain volume. These steps create synthetic fMRI data that have a degree of similarity between the synthetic subjects within the group, but they also have similarity with other groups, which will challenge the classification methods.

For each group, 500 randomly generated synthetic data is generated, which sums up to a total of 1500 subjects.

4.1.2 Data Set 2: Motor Task Data Set

Buckner et al. (2000) recruited 41 participants, of which 14 were young adults, 14 were non-demented older adults and 13 were demented older adults to qualify the age-related changes in hemodynamic responses. The subjects underwent an fMRI task which was based on an earlier study (Dale and Buckner, 1997). The experiment involves the simple motor task of pushing a button when a visual stimulus is given.

The data has been submitted to National fMRI Data Center with accession number 2-2000-1118w. Thanks to the submission, it has been used as real data for many studies such as the study by Greicius et al. (2004) where they have found out that the DMN activity distinguishes AD. More recently, it has been used with ensemble classifiers by Armananzas et al. (2016), where the authors left out 14 young adults to avoid bias in the results due to age differences. Following the same flow of thought, the young adults were left out in this thesis study as well.

The female / male ratio in the non-demented group is 9/5. The mean age for this group is 74.9. The demented group has a female / male ratio of 7/6 and a

mean age of 77.2. The subjects are evaluated with the recruitment and assessment procedures of Washington University Alzheimer's Disease Research Center (Berg et al., 1998). A Clinical Demential Rating (CDR) rating of 0 indicates no dementia, where a value of 0.5 and 1 indicate very mild and mild dementia (Morris, 1993). The demented group contains subjects with a CDR value of 0.5 or 1, and the non-demented group contains subjects with a CDR value of 0.

The data includes four sessions of the experiment for each subject, except there are three for subject 36. The TR value is 2.68 and the visual stimulus events are saved in a separate text file. A session takes 15 runs of the task, where each run has 8 complete volume scans. The complete session includes 128 scans. However, the first and last 4 are non-task stabilization scans and are discarded in the analysis.

The sensory-motor task in the data set has minimum cognitive requirements and Greicius et al. (2004) claims that the default mode network connectivity would not be disrupted. Therefore, this set can also be used for functional connectivity analysis of the DMN.

4.1.3 Data Set 3: ADNI Resting State Data Set

This data set were obtained from the Alzheimer's Disease Neuroimaging Initiative (ADNI) database (adni.loni.usc.edu). The ADNI was launched in 2003 as a public-private partnership, led by Principal Investigator Michael W. Weiner, MD. The primary goal of ADNI has been to test whether serial magnetic resonance imaging (MRI), positron emission tomography (PET), other biological markers, and clinical and neuropsychological assessment can be combined to measure the progression of mild cognitive impairment (MCI) and early Alzheimer's disease (AD). The database grows and is used by many researchers around the world (Weiner et al., 2013). For the interest of this thesis study, the data set contains structural and resting state functional MR images.

To comply with the group definitions, a set of healthy subjects, another set of subjects with late MCI and a final set of subjects with AD has been downloaded with both fMRI and structural data. The subject information can be seen in Table 4.2. The subjects have been attending sessions for more than once in bi-annual to annual intervals.

The data includes resting state fMRI session, where the subjects are resting with their eyes open for seven minutes with a TR value of 3, resulting in 140 brain

Table 4.2. ADNI database subject information; the unique number of subjects, the total number of sessions, female / male ratio, mean and standard deviation of age.

	Unique Subjects	F/M	Sessions	Mean Age	Age Std. Dev.
AD	34	18/16	118	74.7	7.47
MCI	46	18/28	170	72.3	7.74
Healthy	52	30/22	195	75.09	6.37

volume scans. Some of the resting state sessions are doubled, but to maintain the scan standard, only the first seven minutes of the experiment is used. Similar to the second data set, the first and last 10 scans are discarded to avoid stabilization errors.

4.1.4 Preprocessing

Data Sets 2 and 3 are preprocessed using the SPM12 software, as detailed in Section 1.3.4. Briefly, the volumes are realigned, time corrected, registered to a global space (MNI) and smoothed. Data Set 1 uses a preprocessed fMRI volume as a base.

4.2 Feature Extraction

The preprocessed volumes have a size of (53, 63, 52), which contains 173,628 voxels. Since each session has at least 120 captured volumes, the data grows close to 21 million points for each subject. The classification of such large data is unfeasible. Feature extraction reduces the amount of the data while preserving information and representing the data in a format that will be easier for a classifier to work with.

4.2.1 Activation Detection

The brain regions affected by the Alzheimer's disease were mentioned in section 2.4. Since the synaptic transmission in these regions are suppressed because of the disease, the activations in those areas should help the classifier to distinguish healthy subjects from the ones with the AD. However, the experiment should contain tasks that will target these regions.

For the data sets 1 and 2, activated voxels are used as a feature. The synthetic data set has different regions for subjects in different groups, and the motor task in data set 2 contains voxels close to the affected regions. It should be noted that the boundaries of the regions are not clear cut, nevertheless, activation detection is

expected to work better with the Ege University data set.

The activation detection is done by the Task Robust Regression Distance Method, which is detailed in Section 3.3.5. TRRD is chosen because it is an in-house method which performed better than other proposed and evaluated methods.

4.2.2 Subtractive Clustering

Activated voxels can be used as the representation of the subject. However, this data can be more characterized by finding the cluster centers of active voxels.

Clustering is an unsupervised pattern recognition algorithm where the data is grouped according to some similarity measure. Widely used clustering algorithms such as k-means or fuzzy c-means start with a fixed number of cluster centers. These centers are mostly randomly initialized. Since the number of cluster centers are manually set, and their initial values are randomly decided, the quality of the solution may vary at each run. With a poor choice of cluster centers, or initial values, the algorithm may fail to represent the data correctly. Additionally, with large data sets, it is not easy to check the quality of initial values, or guess the correct number of cluster centers.

To overcome this problem Chiu has proposed the subtractive clustering method to estimate the initial number of cluster centers and their values (Chiu, 1994). The algorithm is based on the Mountain Method by Yager and Filev (Yager and Filev, 1994).

The algorithm starts by considering every point in the data set as a potential cluster center. The potential for every cluster center is computed by the Equation 4.1,

$$P_i = \sum_{j=1}^{n} \exp(-\alpha \|x_i - x_j\|^2) \tag{4.1}$$

where P_i represents the potential for data point i, n is the number of points, and $\alpha = 1/r_a^2$ where r_a is the radius which defines a neighborhood for which the points outside will have less influence. As the equation shows, the potential is the inverse of the sum of distances to all other points in the data. For a data point that has many other points nearby, the potential will be high.

Once the potential for each point is computed, the one with the highest potential is chosen as the first cluster center, P_1. Then, remaining potential values are updated by subtracting an amount of the chosen potential value,

$$P_i \leftarrow P_i - P_1 exp(-\beta \|x_i - x_j\|^2) \tag{4.2}$$

where $\beta = 4/r_b^2$. The constant r_b is important in deciding the neighborhood radius that will have their potentials reduced greatly. The authors suggest a value of $r_b = 1.5r_a$, which helps avoid cluster centers being too close to each other.

After the potential reduction, the points around P_1 will have greatly reduced potential. Among these new potential values, the point with the highest is chosen as the second cluster center. The potentials are once again reduced, but this time according to their distance to this cluster center.

This process continues until one of the following stopping conditions are met. Chiu defines a lower and an upper threshold, denoted by $\underline{\varepsilon}$ and $\overline{\varepsilon}$ respectively. Let the current highest potential be denoted by P_k. If P_k is greater than $\overline{\varepsilon} \times P_1$ than the data point is accepted as a cluster center and the process continues. If it is not, then the process stops if P_k is less than $\underline{\varepsilon} \times P_1$.

If the potential falls between the gray area defined by these values, then the algorithm continues by checking if the data point is worth being accepted as a cluster center by defining a minimum distance, d_{min}, as the shortest of the distances between the data point and all other cluster centers. Chiu accepts the data point if $\frac{d_{\text{min}}}{r_a} + \frac{P_k}{P_1} \geq 1$, as he asserts that it is a good trade-off between having a sufficient potential and being far from other cluster centers. On the contrary result, the next highest potential is selected and test is repeated.

Although not a complete cure to the problem of initial number of clusters and cluster center initialization problem, the r_a value that the subtractive clustering depends on, is easier to estimate than estimating number of clusters required, if the nature of the data is well understood.

4.2.3 Connectivity Analysis

The resting state fMRI data does not contain any task-related activations, because it does not contain a task. Therefore, connectivity analysis can help to extract

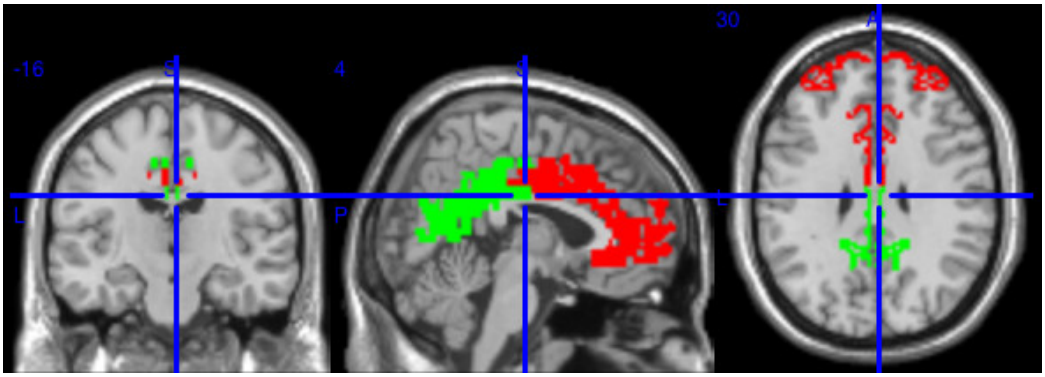

Figure 4.1. The mPFC and the PCC are shown in red and green, respectively. The masks are extracted by WFU Pickatlas (version 3.0) and overlayed to the MNI standard template.

information out of it.

Functional connectivity, as detailed earlier in Section 2.3, looks for temporal correlations in spatially remote regions of the brain. Although anatomically not directly connected, these regions work in harmony to handle specific tasks. This led Raichle et al. (2001) to discover the default mode network, which shows that brain is always active, even when the subject is at rest.

The most common approach to test for connectivity is the correlation method (Cao and Worsley, 1999). Following the studies that report on the regions for default mode network and AD, posterior cingulate cortex (PCC) and medial prefrontal cortex (mPFC) are chosen as regions of interest (ROI) (Raichle et al., 2001; Greicius et al., 2003; Buckner et al., 2008).

The selected ROI include the corresponding brain areas in Broadmann labeling, as shown in Table 2.2. In order to select only these voxels, binary masks have been created using the WFU Pickatlas (version 3.0) software, which uses Talairach Demon and includes atlases with Broadmann areas (Maldjian et al., 2003; Lancaster et al., 2000). The masked regions can be seen in Figure 4.1. The red region shows the mPFC and the green region shows the PCC.

Using the masks, only the voxel BOLD values in both of these regions are considered. The mean signal for each region has been computed and the correlation coefficient of this signal to all of the other voxels in the other region are computed, as detailed in Equation 2.4 in Section 2.3. The threshold value has been set as 0.7. The voxels that have a correlation coefficient greater than this threshold are accepted as “correlated”.

4.3 Classification Methods

The activation and functional connectivity data that belongs to three groups are classified using Learning Vector Quantization 3 (LVQ) and artificial neural networks (ANN).

4.3.1 Learning Vector Quantization 3

Kohonen introduced Learning Vector Quantization as a supervised pattern classification method (Kohonen, 1989). As in many other supervised pattern classification approaches, LVQ requires a set of correctly labeled training data, a set of reference or codebook vectors that represent a series of classes, and a disjoint set of test data that is used to evaluate the trained classifier.

If the training data is made up of n vectors, the LVQ architecture contains m number of nodes of the same vector size, each representing a class that is present in the training data. The vectors for the nodes are called weights, and are denoted with $w_{1...m}$, and the training vectors are denoted by $x_{1...n}$. The initialization of the weights can be done randomly, or can be selected and removed from the training data. Finally, let the correct class for the training data be denoted by t and the class represented by the weight be denoted by c.

Once the variables are set as defined above, the algorithm repeats the following steps for each training vector. The Euclidean distance between the training vector and every other weight is computed, and the closest weight, w_j, is determined. If the class of the training vector, t is the same as the class c_j that the weight belongs to, then the weight is updated to get closer to the training vector with a learning rate denoted by α, as shown in Equation 4.3. Otherwise, Equation 4.4 shows the update of the weight as it is pushed further away with the same rate.

$$w_j \leftarrow w_j + \alpha[\, x - w_j] \tag{4.3}$$

$$w_j \leftarrow w_j - \alpha[\, x - w_j] \tag{4.4}$$

When all of the training vectors are completed, the learning rate is reduced. Kohonen and other resources recommend a linear decreasing function (Kohonen, 1989; Fausett, 1994).

The algorithm stops either when a predefined number of iterations are completed, or when the learning rate reaches a small value.

Kohonen introduced LVQ versions 2 and 2.1 in his following study (Kohonen, 1990). Instead of updating only the closest weight, these versions also update the second-closest, also called the runner-up, too, albeit if several conditions are satisfied.

In LVQ2, both the winner and the runner-up are updated if the following three conditions are met. The first condition checks if the winner and the runner-up represent different classes. The second condition checks if the runner-up represents the same class as the training vector.

The third condition defines a window to check if the distance from the training vector to the winner and the runner-up are approximately the same. In order to formally define the window, let y_c show the weight closest to the training vector and y_r show the runner-up. Also, let d_c be the distance between the training vector and y_c, and d_r be the distance to y_r. If the conditions $\frac{d_c}{d_r} > (1-\epsilon)$ and $\frac{d_r}{d_c} > (1+\epsilon)$ hold, then the training vector is said to be approximately same distance from both y_c and y_r. Kohonen suggests a typical value of 0.35 for the ϵ variable.

If all of these conditions are met, then the weights, now denoted by y_c and y_r are updated as follows.

$$y_c \leftarrow y_c - \alpha[\, x - y_c] \tag{4.5}$$

$$y_r \leftarrow y_r + \alpha[x - y_r] \tag{4.6}$$

While LVQ2 differentiates between the winner and the runner-up weights if they belong to the correct class or not, Kohonen further improves the algorithm in the same study by allowing either of the two closest weights, now denoted by y_{c1} and y_{c2}, belong to the correct class (Kohonen, 1990). This modification, called as LVQ2.1, still checks if the training vector falls in the window defined earlier. However, the test becomes,

$$\min\left[\frac{d_{c1}}{d_{c2}}, \frac{d_{c2}}{d_{c1}}\right] > 1 - \epsilon \tag{4.7}$$

$$\max\left[\frac{d_{c1}}{d_{c2}}, \frac{d_{c2}}{d_{c1}}\right] < 1 + \epsilon \tag{4.8}$$

where, d_{c1} and d_{c2} represent the distance between the training vector and y_{c1} and y_{c2}, respectively.

Assuming that y_{c1} belongs to the same class as the training vector and y_{c2} does not, the weights are updated as follows.

$$y_{c1} \leftarrow y_{c1} + \alpha[x - y_{c1}] \tag{4.9}$$

$$y_{c2} \leftarrow y_{c2} - \alpha[x - y_{c2}] \tag{4.10}$$

Kohonen released a final improvement, named as LVQ3, where two closest weights are allowed to learn if they satisfy the window condition,

$$\min\left[\frac{d_{c1}}{d_{c2}}, \frac{d_{c2}}{d_{c1}}\right] > (1 - \epsilon)(1 + \epsilon) \tag{4.11}$$

where he suggest an ϵ value of 0.2 (Kohonen, 1992). The weight updates are the same as LVQ2.1 if one of the closest weights belong to the same class as the training vector, and the other does not. LVQ3 lets y_{c1} and y_{c2} to be updated if they both belong to the same class as the training vector. The update is done with the following equation,

$$y_c \leftarrow y_c + \alpha \times k \times [x - y_c] \tag{4.12}$$

where Kohonen suggests a range between 0.1 and 0.5 for the multiplier k. This final update ensures that weights continue to approximate the class definitions and do not stray away if the learning continues.

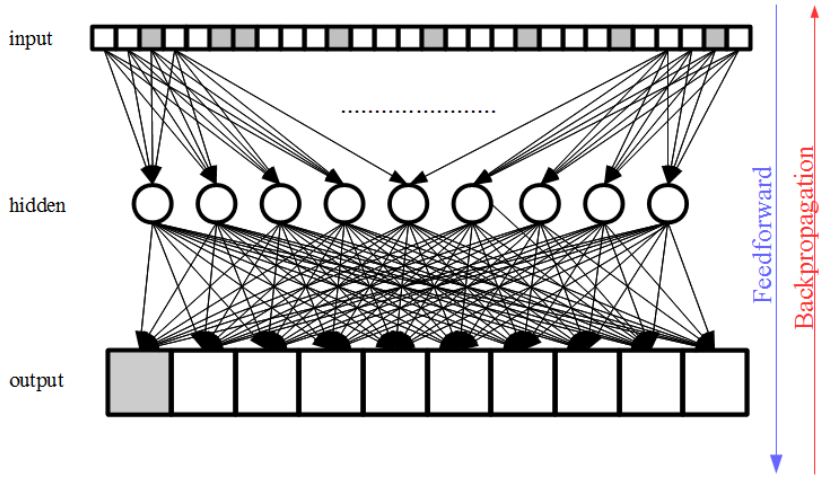

Figure 4.2. A multilayer, feedforward neural network trained by backpropagation. The training data is fed forward, as shown with a blue top-down direction on the right, where each layer sends its activation values to the next level. At the output layer, the outcome is compared to the target pattern, and an error is computed. This error is backpropagated to the previous levels, updating the connection weights, as shown with a red bottom-up direction on the right.

4.3.2 Artificial Neural Networks

Artificial neural networks work on the similar principles as the biological neurons to learn about problems, the same way a nervous system, such as a brain, does. Although it is interesting to use artificial neurons to distinguish the deficiencies present in biological neurons for this thesis, they do not work exactly the same way.

Figure 4.2 shows a typical multilayered ANN architecture made up of an input layer, a hidden layer and an output layer. The layers contains units, or perceptrons, a structure similar to a biological neuron which acts as the basic processing element (Rosenblatt, 1958). Each unit in a layer is connected by weighted edges to every unit in the following layer.

The likeness of perceptron to a biological neuron is that it receives signals from its inputs and sends a signal to its outputs. Every unit in the input layer starts by sending a signal, since it is the first layer. This first signal is the training data and it is received by every unit in the hidden layer.

A perceptron receives signals from all of its inputs and finds its activation value, y, as a weighted sum of these signals. Assuming that the perceptron has m connections, were each signal is denoted by s, and their weights are denoted by w, the weighted sum is given as follows,

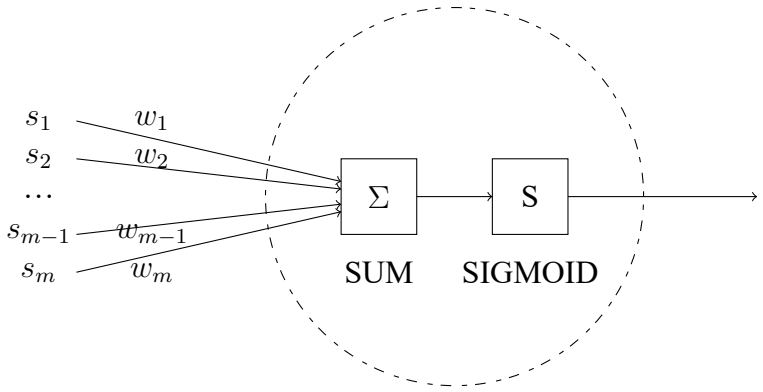

Figure 4.3. An artificial neuron receives input from its connections ($s_{1\ldots m}$), finds their weighted sums ($\sum_{i=1}^{m} s_i \times w_i + w_0$) and passes it to its activation function, mostly chosen as the sigmoid function. The figure is re-drawn to reflect the notation in the text from (Smith, 2003)

$$y = \sum_{i=1}^{m} w_i \times s_i + w_0 \tag{4.13}$$

where the w_0 represents the intercept value (Alpaydin, 2010).

When a biological neuron receives signals from its connections, it either fires, or it does not. The perceptron can be designed to behave similarly by applying a threshold value to the activation value. However, the backpropagation algorithm, which will be discussed shortly requires an activation function that is continuous, differentiable and monotonically non-decreasing (Fausett, 1994). Therefore, the activation function is mostly chosen as the sigmoid function, given in Equation 4.14, which has the derivative given in Equation 4.15. Figure 4.3 gives a more zoomed in view of the neuron, the weighted sum and the sigmoid function (Smith, 2003).

$$f_a(x) = \frac{1}{1 + exp(-x)} \tag{4.14}$$

$$f_a{}' = f_a(x)[1 - f_a(x)] \tag{4.15}$$

The activation value calculated with the weighted sum in Equation 4.13 is set as a parameter to the activation function f_a and its result becomes the input for the next layer. The hidden layer is the only layer in the architecture given in Figure 4.2 that both receives and sends a signal. The flow of data from the input layer to the

output layer is called feedforward.

When a unit in the output layer finds its activation value, $f_a(y)$ a variable defined as the error information term, denoted by δ is computed as follows,

$$\delta = (t - f_a(y)){f_a}'(y) \tag{4.16}$$

where t represents the target pattern corresponding to the training data. The unit then computes its weight correction term and its bias correction term. Both of these terms are updated after all of the units in all of the layers compute their own terms. The weight correction term is calculated by,

$$\Delta w = \alpha \delta z \tag{4.17}$$

where α is the learning rate, and z denotes the signal received from the associated weight. The bias correction term is very similar,

$$\Delta w_0 = \alpha \delta \tag{4.18}$$

since it is the bias weight for the unit, and does not have any signal value like the weights from the previous layer. The unit then sends the δ value to the previous layer, where each unit, this time, use this value like an activation value and compute the weighted sum of the error information term,

$$\delta = \sum_{k=1}^{m} \delta_k \times w_k \tag{4.19}$$

where it is assumed that the unit has m connections. Similar to feedforward process, the unit sends back its own error information term, until the input layer is reached. This process is called the backpropagation of error. Once it is complete, all of the weights, including the bias weights, are updated with the equation that follows.

$$w \leftarrow w + \Delta w \tag{4.20}$$

The training of ANN is done with two disjoint sets, one for training and one for validation. As the training continues, periodic tests are done to check the error rate of the ANN. If the error rate starts increasing, or a predefined number of epochs has been reached the training stops.

The underlying mathematical foundations of the backpropagation algorithm is the gradient descent optimization (Fausett, 1994). Other approaches to increase the learning speed has been proposed, such as the scaled conjugate gradient algorithm (Møller, 1993).

4.4 Training Sets And Methods

The three data sets defined earlier are used to create training sets with different properties.

The Data Set 1 is the synthetic data set and has activations in different regions of the brain for subjects in different groups. The activations has been detected by the TRRD method. Then, the cluster centers has been found using the subtractive clustering method. However, as mentioned earlier, the brain has 173,628 voxels and a feature vector of this size requires a similar size of training data. In order to reduce the number of voxels, the brain has been divided into cubic volumes and these volumes have been set as active, if they contain an active voxel. In order to find the best size, the brain has been partitioned into 4, 5 and 6 voxel-cubic volumes, reducing the feature vector size to 2912, 1573 and 891, respectively.

The same procedures has been applied to the Data Set 2; a real fMRI data set from National fMRI Data Center, submitted by (Buckner et al., 2000). The activations are found using TRRD method, and the same volumetric partitioning has been applied, yielding feature vectors of the same sizes, the data set has been registered to MNI space in preprocessing. Contrary to other data sets, Data Set 2 contains only two groups, the healthy and the demented, whereas the other groups have the healthy, MCI and AD subjects.

Since the Data Set 2 contains a simple sensory-motor task that does not disrupt the default mode network, it has been used in the functional connectivity of the default mode network as well (Greicius et al., 2004). The Data Set 3 contains the resting state data, which is best suitable for functional connectivity analysis, as well.

The regions mPFC and PCC has been defined as the most correlated regions

Table 4.3. Training data sets formed from Data Sets 1, 2 and 3. The activations are partitioned by volumes of size 4, 5 and 6, while the resting state data is reduced by only considering the voxels belonging to mPFC and PCC.

Training Set	Based On	Features	Feature Vector	Reduction
TS-1.4	Data Set 1	Activations	2912	4^3 volumes
TS-1.5	Data Set 1	Activations	1573	5^3 volumes
TS-1.6	Data Set 1	Activations	891	6^3 volumes
TS-2.4	Data Set 2	Activations	2912	4^3 volumes
TS-2.5	Data Set 2	Activations	1573	5^3 volumes
TS-2.6	Data Set 2	Activations	891	6^3 volumes
TS-2	Data Set 2	DMN Connectivity	1680	Masking
TS-3	Data Set 3	DMN Connectivity	1680	Masking

of the DMN (Raichle et al., 2001; Greicius et al., 2003; Buckner et al., 2008). For the Data Sets 2 and 3, these regions has been masked and their voxels have been extracted. Using the correlation coefficients for these two regions has reduced the feature vector size from 173,628 voxels to 1680, where mPFC contains 1206 voxels, and PCC contains 474.

Table 4.3 gives a brief list of the training set names, the data sets which they are based on, the features used, and the reductions performed.

The LVQ3 algorithm has been implemented in MATLAB (MATLAB Student version 2016a, http://www.mathworks.com). The results are cross-validated using a 10-fold data partitioning. The performance has been evaluated as the percentage of correctly identified test data. The average and the maximum values are saved for evaluation. The training vector selection has been randomized to remove any bias during training.

The MATLAB functions in the Neural Network Toolbox has been used to create and train a multilayer feedforward neural network, with a scaled conjugate gradient training algorithm. The number of hidden neurons can affect the performance of a network. The training sets are tested with 10, 20 and 30 number of hidden neurons.

The data partitioning is set as 80% for training, 10% for validation and 10% for testing with random selection. The training for each set has been repeated 10 times to compensate for any bias that can emerge. After each run the neural network has

Table 4.4. Training results for LVQ3 algorithm. The algorithm is cross-validated using 10-fold data partitioning. The average and maximum percent of correctly identified subjects are listed.

Training Set	Feature Vector	Unique Samples	Mean	Max
TS-1.4	2912	1500	84.93	88
TS-1.5	1573	1500	90.2	95.33
TS-1.6	891	1500	90.53	94
TS-2.4	2912	102	84.15	100
TS-2.5	1573	102	85.14	98.57
TS-2.6	891	102	89.43	98.57
TS-2	1680	103	86.7	87
TS-3	1680	439	86.86	88.1

been tested with the testing partition, and the percentage for the correctly identified data has been recorded. Similar to the LVQ3 results, the average and the maximum values are saved for evaluation.

4.5 Results

During the preprocessing and features extraction process some of the subjects or some of their sessions were left out. 44 of the ADNI sessions were discarded due to SPM having trouble structural data registration, leaving a set of 439 resting state fMRI scans. The TRRD method were not able to find any significant activation for one of the subjects in the second data set, and this session was also left out, leaving the second data set with 102 subjects with activations. The subject's resting state analysis is kept, so the same set has 103 for functional connectivity analysis.

The results for the LVQ3 algorithm are listed in Table 4.4. For the training sets that were partitioned with various sizes from the first data set, the average best score belongs to the partitioning with volumes of 6. An average score of 90.53 percent is also the best score on the table.

The training sets from the second data set also perform better with the volumes of 6, almost as good as the first set. The functional connectivity on the default mode network slightly underperformed when compared to activation analysis. However, they are not so far apart. On the DMN's defense, it can be said that it could have performed better if the experiment did not include any task.

The results for the ANN are given in Table 4.5. Appendix 10 lists the complete

Table 4.5. Training results for the ANN. The network has been trained 10 times with 10, 20 and 30 hidden units. The average and maximum percent of correctly identified subjects are listed.

Training Set	Feature Vector	Unique Samples	Hidden	Mean	Max
TS-1.4	2912	1500	30	92.2533	98.8667
TS-1.5	1573	1500	30	98.44	99.1333
TS-1.6	891	1500	20	97.88	98.9333
TS-2.4	2912	102	30	94.8039	100
TS-2.5	1573	102	30	98.2157	100
TS-2.6	891	102	10	98.2353	100
TS-2	1680	103	20	90.2913	90.2913
TS-3	1680	439	10	90.3417	91,344

results, including the results for tests with other hidden units. The results show that ANN performs better than the LVQ3 learning algorithm in all of the test configurations.

For activation features in Data Sets 1 and 2, the ANN performs best on average with 30 hidden units, and when the data is partitioned into volumes of size 5. This partitioning size keeps the most information while keeping the feature size very close to the number of samples.

The connectivity analysis for Data Sets 2 and 3 work best with 20 and 10 hidden units, respectively. The average score is above 90%. As with LVQ3, the functional connectivity features in the second data set failed to surpass the activation features.

Both of these results show that activations and functional connectivity provide valid features for classifying fMRI data. The second data set was the only one where it was possible to compare both features. The features extracted using activation analysis perform better; however this data set has only two groups, and the activations are not targeted on the regions that are affected by the AD.

5. EVALUATION AND CONCLUSION

This concluding chapter includes a broad review of the thesis, the novel contributions, discusses the results and explores possible future work.

5.1 Thesis Review

The thesis explores methods for classifying fMRI data in order to diagnose the Alzheimer's Disease which is one of the most common forms of dementia. As the world-wide research continues to probe for possible biomarkers to detect the disease as early as possible, this thesis humbly contributes with activation detection and classification techniques. The purpose of the thesis is to classify the data among subjects with Alzheimer's Disease, subjects with mild cognitive impairment and healthy subjects.

The AD is defined as a synaptic failure disease, which immediately brings forth the activation failure in affected brain regions. In this regard, an fMRI experiment is designed that will target activations on the affected regions of the brain.

The thesis first explores and evaluates the activation detection methods in the literature, including the popular tools that depend on the general linear model. Five novel methods have been proposed that can detect the activations in a more scrutinized way. The proposed methods are tested with three sets of data; a completely synthetic data at different noise levels (Approach 1), a set with real fMRI resting data with synthetic activations (Approach 2) and a set with real fMRI experiment data from the Ege University MR database. All of the data sets have the same structure; a block design experiment that contains two states; "no activity" or "resting" state, followed by an "activity" state. These blocks are repeated three times.

The applied hemodynamic response function is modeled as the difference of two gamma functions. A set of 10 HRFs are generated by different parameters, simulating different subjects and different areas within subjects.

The instantaneous methods, such as IAM, IAMP and IRRD, use the confidence intervals on the mean of the resting state block values to decide on the activation of voxels at each instance. Methods that use the complete experiment data, such as TAM and TRRD decide on the activation of voxels with a t-test on the values of two states. Finally, correlation method uses the canonical HRF to measure the similarity of the voxel to the expected block design.

IRRD and TRRD methods use a new distance metric that is not bound by the voxel intensities, while the instantaneous methods pave the way to analyze fMRI images in a new perspective.

The results for the methods are evaluated by receiver operating characteristic curves and PSNR values. They are also compared against the commonly used SPM method.

The ROC analyses show that the instantaneous methods are capable of finding the activations, but are not as good as other methods where the complete experiment data is used. However, instantaneous methods are good for locating activations to a stimulus at a specific instant, rather than the complete experiment. These activations, which may include relevant and important information may otherwise be statistically lost when the complete experiment is taken into account. The instantaneous methods provide the temporal flow of the activations which may yield more information. The relevant information extracted with the instantaneous methods will not be accessible to methods such as SPM, TAM and TRDD where the complete experiment data is used. Another contribution of these methods is to causally represent the active brain regions in consequent instances.

All of the methods are good at finding locations even at low SNR values. As the SNR value gets higher, the noise levels decrease and the methods perform better. It is also important to note that all of the methods are sensitive to the magnitude of the HRF. The instantaneous methods are sensitive to latency, since they try to find the activations at every instance of the active state and a late peak decreases their performance. The methods do as well as SPM on real data.

In order to classify the fMRI data, features should be extracted that will help differentiate the subjects in different groups. While the activation detection is one way to do it, the functional connectivity in the default mode network is also capable of distinguishing healthy subjects from the subjects with the AD (Greicius et al., 2004). The methods used for functional connectivity analysis are reviewed and correlation coefficient method is used to find correlations in the most functionally connected regions in the default mode network, mPFC and PCC. The mean BOLD signal that belongs to all of the voxels within a region is correlated with every voxel in the other region. The voxel correlation values are used as a feature vector for each subject.

The activation and functional connectivity features of the subjects are tested

with three data sets. The first data set is synthetic, which contains activations in different regions of the brain for subjects in different groups. The second data set comes from a sensory-motor experiment. This set is used with both activation detection features and the functional connectivity features, because the cognitive simplicity of the sensory-motor experiment is not expected to disrupt the default mode network. The final data set comes from the ADNI database which contains resting state fMRI scans of subjects for three different groups.

Before the classification, the subtractive clustering method is used to find the activation centers. Then the brain volumes are partitioned into volumes of size 4, 5 and 6. If a volume contains an active voxel, the volume is set active. After this operation, the input vector has been reduced to a smaller, more manageable size.

As classifiers, learning vector quantization (LVQ3) and a multilayer feedforward artificial neural network (ANN) are chosen. The results show that ANN performs better in classification process. Another important outcome shows that the second data set, which is analysed both for activation detection and functional connectivity, yielded better results in favor of activations.

The main outcome of the thesis is the novel contributions to the activation analysis of fMRI data. The classification is successfully performed using two different approaches with variations of three data sets. While one of the data sets is synthetic, the other two are real life fMRI data that are accessible online.

5.2 Future Work

The experiment described in detail in Section 1.4 is currently being executed on volunteering subjects. It is part of the TUBITAK 1001 project 214S029, titled "The comparison of neural components related with default mode, short-term memory store and recall of subjects diagnosed with mild cognitive impairment with early Alzheimer's Disease and their healthy siblings and controls." The scans are expected to be complete in one year. This data will be unique since it contains a task that targets affected brain regions and resting state data. The results from the different data sets where the activation and resting state features show that the combination of these features can yield better results. The future work will mostly contain the processing of this data, and learn more about Alzheimer's Disease as we will be able to compare a subject's DMN and activation maps.

The amount of data that results from a single subject is in the order of hundred

of megabytes. The storage, preprocessing and analysis of this data can also take a lot of time. One of the solutions to big data is to use parallel processing to analyze it. The quickest way to get parallel processing is to use the GPU that is available on almost every modern computer. The general processing on GPU is called GPGPU and researchers have been working on redesigning programs so that they could work in parallel (Eklund et al., 2012, 2013). Parallel computing can be applied to both activation detection and functional connectivity where each voxel is handled separately, without depending on others. The current trend topic, deep learning, can also be used to extract information from the data (Hatakeyama et al., 2014).

REFERENCES

Akhbari, M., Babaie-Zadeh, M., Fatemizadeh, E. and Jutten, C., 2010. An entropy based method for activation detection of functional MRI data using Independent Component Analysis. In 2010 IEEE International Conference on Acoustics Speech and Signal Processing (ICASSP). p. 2014–2017.

Alpaydin, E., 2010. Introduction to Machine Learning. MIT Press, Cambridge, Mass.

Ardekani, B., Kershaw, J., Kashikura, K. and Kanno, I., 1999. Activation detection in functional MRI using subspace modeling and maximum likelihood estimation. *IEEE Transactions on Medical Imaging*, 18(2):101–114.

Armananzas, R., Iglesias, M., Morales, D.A. and Alonso-Nanclares, L., 2016. Voxel-based diagnosis of Alzheimer's disease using classifier ensembles. *IEEE Journal of Biomedical and Health Informatics*, PP(99):1–1.

Ashburner, J., Barnes, G., Chen, C.C., Daunizeau, J., Friston, K., Kiebel, S., Kilner, J., Litvak, V., Moran, R., Penny, W., Stephan, K., Gitelman, D., Henson, R., Hutton, C., Mattout, V.G.J. and Phillips, C., 2014. SPM12 Manual. Functional Imaging Laboratory, Wellcome Trust Centre for Neuroimaging, Institute of Neurology, UCL, 12 Queen Square, London WC1N 3BG, UK.

Ashburner, J. and Friston, K.J., 2005. Unified segmentation. *NeuroImage*, 26(3):839 – 851.

Bandettini, P.A., Jesmanowicz, A., Wong, E.C. and Hyde, J.S., 1993. Processing strategies for time-course data sets in functional mri of the human brain. *Magnetic Resonance in Medicine*, 30(2):161–173.

Beckmann, C.F. and Smith, S.M., 2004. Probabilistic independent component analysis for functional magnetic resonance imaging. *IEEE Transactions on Medical Imaging*, 23(2):137–152.

Berg, L., McKeel, D.W.J., Miller, J.P., Storandt, M., Rubin, E.H., Morris, J.C., Baty, J., Coats, M., Norton, J., Goate, A.M., Price, J.L., Gearing, M., Mirra, S.S. and Saunders, A.M., 1998. Clinicopathologic studies in cognitively healthy aging and Alzheimer's disease: relation of histologic markers to dementia severity, age, sex, and apolipoprotein E genotype. *Archives of Neurology*, 55(3):326–335.

Brodmann, K., 1909. Vergleichende Lokalisationslehre der Grosshirnrinde : in ihren Prinzipien dargestellt auf Grund des Zellenbaues. Leipzig : Barth.

REFERENCES (continued)

Brown, R., Haacke, E., Cheng, Y., Thompson, M. and Venkatesan, R., 2014. Magnetic Resonance Imaging: Physical Principles and Sequence Design. Wiley.

Brück, A., Virta, J.R., Koivunen, J., Koikkalainen, J., Scheinin, N.M., Helenius, H., Någren, K., Helin, S., Parkkola, R., Viitanen, M. and Rinne, J.O., 2013. [11C]PIB, [18F]FDG and MR imaging in patients with mild cognitive impairment. *European Journal of Nuclear Medicine and Molecular Imaging*, 40(10):1567–1572.

Buckner, R.L., Andrews-Hanna, J.R. and Schacter, D.L., 2008. The Brain's Default Network. *Annals of the New York Academy of Sciences*, 1124(1):1–38.

Buckner, R.L., Snyder, A.Z., Sanders, A.L., Raichle, M.E. and Morris, J.C., 2000. Functional Brain Imaging of Young, Nondemented, and Demented Older Adults. *Journal of Cognitive Neuroscience*, 12(supplement 2):24–34.

Cao, J. and Worsley, K., 1999. The geometry of correlation fields with an application to functional connectivity of the brain. *Annals of Applied Probability*, 9(4):1021–1057.

Chiu, S.L., 1994. Fuzzy Model Identification Based on Cluster Estimation. *J. Intell. Fuzzy Syst.*, 2(3):267–278.

Collignon, A., Maes, F., Delaere, D., Vandermeulen, D., Suetens, P. and Marchal, G., 1995. Automated Multi-Modality Image Registration Based on Information Theory. In Proc. Information Processing in Medical Imaging, Y. Bizais, C. Barillot and R. Di Paola, eds.. Kluwer Academic Publishers, Dordrecht, The Netherlands, p. 263–274.

Constable, R., McCarthy, G., Allison, T., Anderson, A. and Gore, J., 1993. Functional brain imaging at 1.5 T using conventional gradient echo MR imaging techniques. *Magnetic Resonance Imaging*, 11(4):451 – 459.

Cordes, D., Haughton, V., Carew, J.D., Arfanakis, K. and Maravilla, K., 2002. Hierarchical clustering to measure connectivity in fMRI resting-state data. *Magnetic Resonance Imaging*, 20(4):305 – 317.

Cox, D.D. and Savoy, R.L., 2003. Functional magnetic resonance imaging (fMRI) "brain reading": detecting and classifying distributed patterns of fMRI activity in human visual cortex. *NeuroImage*, 19(2):261–270.

REFERENCES (continued)

Dale, A.M. and Buckner, R.L., 1997. Selective averaging of rapidly presented individual trials using fMRI. *Human Brain Mapping*, 5(5):329–340.

Deak, F., Freeman, W.M., Ungvari, Z., Csiszar, A. and Sonntag, W.E., 2016. Recent Developments in Understanding Brain Aging: Implications for Alzheimer's Disease and Vascular Cognitive Impairment. *The Journals of Gerontology Series A: Biological Sciences and Medical Sciences*, 71(1):13–20.

Deichmann, R., 2009. Principles of MRI and Functional MRI. In fMRI Techniques and Protocols, M. Filippi, ed., Humana Press, Totowa, NJ, volume 41, p. 3–29.

Descombes, X., Kruggel, F. and von Cramon, D., 1998. Spatio-temporal fMRI analysis using Markov random fields. *IEEE Transactions on Medical Imaging*, 17(6):1028–1039.

Deshmukh, A., Shivhare, V., Parihar, R., Gadre, V., Patkar, D., Shah, S. and Pungavkar, S., 2004. Functional MRI activation signal detection using the periodicity transform. In 2004 International Conference on Signal Processing and Communications, 2004. SPCOM '04. p. 121–125.

Douglas, P.K., Harris, S., Yuille, A. and Cohen, M.S., 2011. Performance comparison of machine learning algorithms and number of independent components used in fMRI decoding of belief vs. disbelief. *NeuroImage*, 56(2):544–553.

Ebner, N.C., Riediger, M. and Lindenberger, U., 2010. FACES—A database of facial expressions in young, middle-aged, and older women and men: Development and validation. *Behavior Research Methods*, 42(1):351–362.

Eklund, A., Andersson, M. and Knutsson, H., 2012. fMRI analysis on the GPU—Possibilities and challenges. *Computer Methods and Programs in Biomedicine*, 105(2):145–161. URL `http://www.sciencedirect.com/science/article/pii/S0169260711001957`.

Eklund, A., Dufort, P., Forsberg, D. and LaConte, S.M., 2013. Medical image processing on the GPU – Past, present and future. *Medical Image Analysis*, 17(8):1073–1094. URL `http://www.sciencedirect.com/science/article/pii/S1361841513000820`.

Evans, A.C., Collins, D.L., Mills, S.R., Brown, E.D., Kelly, R.L. and Peters, T.M., 1993. 3D statistical neuroanatomical models from 305 MRI volumes. In Nuclear Science Symposium and Medical Imaging Conference, 1993., 1993 IEEE Conference Record. p. 1813–1817 vol.3.

REFERENCES (continued)

Faisan, S., Thoraval, L., Armspach, J.P., Metz-Lutz, M.N. and Heitz, F., 2005. Unsupervised learning and mapping of active brain functional MRI signals based on hidden semi-Markov event sequence models. *Medical Imaging, IEEE Transactions on*, 24(2):263–276.

Fausett, L., 1994. Fundamentals of neural networks : architectures, algorithms, and applications. Prentice-Hall, Englewood Cliffs, NJ Delhi Dorling Kindersley.

Feilner, M., Blu, T. and Unser, M., 2000. Analysis of fMRI data using spline wavelets. In Signal Processing Conference, 2000 10th European. p. 1–4.

Friston, K., Frith, C., Frackowiak, R. and Turner, R., 1995a. Characterizing Dynamic Brain Responses with fMRI: A Multivariate Approach. *NeuroImage*, 2(2, Part A):166 – 172.

Friston, K., Holmes, A., Poline, J., Grasby, P.J., Williams, S.C.R., Frackowiak, R. and Turner, R., 1995b. Analysis of fMRI Time Series Revisited. *NeuroImage*, 2:45–53.

Friston, K.J., Frith, C.D., Liddle, P.F. and Frackowiak, R.S.J., 1993. Functional Connectivity: The Principal-Component Analysis of Large (PET) Data Sets. *Journal of Cerebral Blood Flow Metabolism*, 13(1):5–14.

Friston, K.J., Jezzard, P. and Turner, R., 1994. Analysis of functional MRI time-series. *Human Brain Mapping*, 1(2):153–171.

Fritsch, V., Varoquaux, G., Thyreau, B., Poline, J.B. and Thirion, B., 2012. Detecting outliers in high-dimensional neuroimaging datasets with robust covariance estimators. *Medical Image Analysis*, 16(7):1359 – 1370. Special Issue on the 2011 Conference on Medical Image Computing and Computer Assisted Intervention.

Glover, G.H., 1999. Deconvolution of Impulse Response in Event-Related {BOLD} fMRI1. *NeuroImage*, 9(4):416 – 429.

Golay, X., Kollias, S., Stoll, G., Meier, D., Valavanis, A. and Boesiger, P., 1998. A new correlation-based fuzzy logic clustering algorithm for FMRI. *Magnetic Resonance in Medicine*, 40(2):249–260.

Greicius, M.D., Krasnow, B., Reiss, A.L. and Menon, V., 2003. Functional connectivity in the resting brain: A network analysis of the default mode hypothesis. *Proceedings of the National Academy of Sciences*, 100(1):253–258.

REFERENCES (continued)

Greicius, M.D., Srivastava, G., Reiss, A.L. and Menon, V., 2004. Default-mode network activity distinguishes Alzheimer's disease from healthy aging: Evidence from functional MRI. *Proceedings of the National Academy of Sciences of the United States of America*, 101(13):4637–4642.

Handwerker, D.A., Ollinger, J.M. and D'Esposito, M., 2004. Variation of BOLD hemodynamic responses across subjects and brain regions and their effects on statistical analyses. *NeuroImage*, 21(4):1639 – 1651.

Hanson, S.J., Matsuka, T. and Haxby, J.V., 2004. Combinatorial codes in ventral temporal lobe for object recognition: Haxby (2001) revisited: is there a "face" area? *NeuroImage*, 23(1):156–166.

Hatakeyama, Y., Yoshida, S., Kataoka, H. and Okuhara, Y., 2014. Multi-Voxel Pattern Analysis of fMRI Based on Deep Learning Methods, Springer International Publishing, Cham, p. 29–38.

Haxby, J.V., Gobbini, M.I., Furey, M.L., Ishai, A., Schouten, J.L. and Pietrini, P., 2001. Distributed and Overlapping Representations of Faces and Objects in Ventral Temporal Cortex. *Science*, 293(5539):2425–2430.

Haynes, J.D. and Rees, G., 2005. Predicting the orientation of invisible stimuli from activity in human primary visual cortex. *Nature Neuroscience*, 8(5):686–691.

Haynes, J.D. and Rees, G., 2006. Decoding mental states from brain activity in humans. *Nature Reviews Neuroscience*, 7(7):523–534.

Hossein-Zadeh, G., Soltanian-Zadeh, H. and Ardekani, B., 2003. Multiresolution fMRI activation detection using translation invariant wavelet transform and statistical analysis based on resampling. *IEEE Transactions on Medical Imaging*, 22(3):302–314.

Hyvärinen, A. and Oja, E., 2000. Independent component analysis: algorithms and applications. *Neural Networks*, 13(4–5):411 – 430.

Janoutová, J., Šerý, O., Hosák, L. and Janout, V., 2015. Is Mild Cognitive Impairment a Precursor of Alzheimer's Disease? Short Review. *Central European Journal of Public Health*, 23(4):365–367.

Kamitani, Y. and Tong, F., 2005. Decoding the visual and subjective contents of the human brain. *Nature Neuroscience*, 8(5):679–685.

Kohonen, T., 1989. Self-organization and associative memory. Springer-Verlag, Berlin New York.

REFERENCES (continued)

Kohonen, T., 1990. Improved versions of learning vector quantization. In Neural Networks, 1990., 1990 IJCNN International Joint Conference on. p. 545–550 vol.1.

Kohonen, T., 1992. LVQ_PAK - The Learning Vector Quantization Program Package. Technical Report, Helsinki University of Technology.

Kuncheva, L.I. and Rodríguez, J.J., 2010. Classifier ensembles for fMRI data analysis: an experiment. *Magnetic Resonance Imaging*, 28(4):583–593.

Lancaster, J.L., Woldorff, M.G., Parsons, L.M., Liotti, M., Freitas, C.S., Rainey, L., Kochunov, P.V., Nickerson, D., Mikiten, S.A. and Fox, P.T., 2000. Automated Talairach atlas labels for functional brain mapping. *Human Brain Mapping*, 10(3):120–131.

Lasko, T.A., Bhagwat, J.G., Zou, K.H. and Ohno-Machado, L., 2005. The use of receiver operating characteristic curves in biomedical informatics. *Journal of Biomedical Informatics*, 38(5):404 – 415. Clinical Machine Learning.

Li, K., Guo, L., Nie, J., Li, G. and Liu, T., 2009. Review of methods for functional brain connectivity detection using fMRI. *Computerized Medical Imaging and Graphics*, 33(2):131–139.

Lian, Z., Lv, J., Xing, J., Li, X., Jiang, X., Zhu, D., Xu, J., Potenza, M.N., Liu, T. and Zhang, J., 2014. Generalized fMRI activation detection via Bayesian magnitude change point model. In 2014 IEEE 11th International Symposium on Biomedical Imaging (ISBI). p. 21–24.

Lindquist, M., 2014. Lecture notes in Statistical Methods in Functional MRI.

Liu, C., Fa, R., Abu-Jamous, B., Brattico, E. and Nandi, A., 2015. Scalable clustering based on enhanced-SMART for large-scale FMRI datasets. In 2015 IEEE International Conference on Acoustics, Speech and Signal Processing (ICASSP). p. 962–966.

Lukic, A., Wernick, M., Galatsanos, N., Yang, Y. and Strother, S., 2001. A signal-detection approach for analysis of functional neuroimages. In 2001 IEEE Nuclear Science Symposium Conference Record. volume 3, p. 1394–1398 vol.3.

Maldjian, J.A., Laurienti, P.J., Kraft, R.A. and Burdette, J.H., 2003. An automated method for neuroanatomic and cytoarchitectonic atlas-based interrogation of fMRI data sets. *NeuroImage*, 19(3):1233 – 1239.

REFERENCES (continued)

Mitchell, T.M., Hutchinson, R., Just, M.A., Niculescu, R.S., Pereira, F. and Wang, X., 2003. Classifying Instantaneous Cognitive States from fMRI Data. *AMIA Annual Symposium Proceedings*, 2003:465–469.

Møller, M.F., 1993. A scaled conjugate gradient algorithm for fast supervised learning. *Neural Networks*, 6(4):525–533.

Montgomery, D.C. and Runger, G.C., 2011. Applied statistics and probability for engineers. Wiley, Hoboken, NJ.

Morris, J.C., 1993. The Clinical Dementia Rating (CDR): current version and scoring rules. *Neurology*, 43(11):2412–2414.

Mourão-Miranda, J., Bokde, A.L.W., Born, C., Hampel, H. and Stetter, M., 2005. Classifying brain states and determining the discriminating activation patterns: Support Vector Machine on functional MRI data. *NeuroImage*, 28(4):980–995.

Noh, J. and Solo, V., 2006. A True Spatiotemporal Approach for Activation Detection in Functional MRI. In 2006 IEEE International Conference on Acoustics, Speech and Signal Processing, 2006. ICASSP 2006 Proceedings. volume 3, p. III–III.

Nüfus ve Vatandaşlık İşleri Genel Müdürlüğü, N., 2012. İstatistikler : 10'ar Yıllık En Çok Verilen İsimler İstatistikleri. URL `\url{http://www.nvi.gov.tr/Hizmetler/Istatistikler,Isim_Istatistigi_10ar_Yillik.html}`, [Online; accessed 8-May-2016].

Ogawa, S., Lee, T.M., Kay, A.R. and Tank, D.W., 1990. Brain magnetic resonance imaging with contrast dependent on blood oxygenation. *Proceedings of the National Academy of Sciences*, 87(24):9868–9872.

Ou, W., III, W.M.W. and Golland, P., 2010. Combining spatial priors and anatomical information for fMRI detection. *Medical Image Analysis*, 14(3):318 – 331.

Parrish, T.B., Gitelman, D.R., LaBar, K.S. and Mesulam, M.M., 2000. Impact of signal-to-noise on functional MRI. *Magnetic Resonance in Medicine*, 44(6):925–932.

REFERENCES (continued)

Pereira, F., Just, M. and Mitchell, T., 2001. Distinguishing Natural Language Processes on the Basis of fMRI-Measured Brain Activation. In Principles of Data Mining and Knowledge Discovery, L.D. Raedt and A. Siebes, eds., Springer Berlin Heidelberg, number 2168 in Lecture Notes in Computer Science, p. 374–385. DOI: 10.1007/3-540-44794-6_31.

Prince, M., Wimo, A., Guerchet, M., Ali, G.C., Wu, Y.T. and Prina, M., 2015. World Alzheimer Report 2015, The Global Impact of Dementia, An Analysis of Prevalence, Incidence, Cost and Trends.

Querfurth, H.W. and LaFerla, F.M., 2010. Alzheimer's Disease. *New England Journal of Medicine*, 362(4):329–344.

Raichle, M.E., MacLeod, A.M., Snyder, A.Z., Powers, W.J., Gusnard, D.A. and Shulman, G.L., 2001. A default mode of brain function. *Proceedings of the National Academy of Sciences*, 98(2):676–682.

Ren, T., Zeng, W., Wang, N., Chen, L. and Wang, C., 2014. A novel approach for fMRI data analysis based on the combination of sparse approximation and affinity propagation clustering. *Magnetic Resonance Imaging*, 32(6):736 – 746.

Roche, A., Lahaye, P.J. and Poline, J.B., 2004. Incremental activation detection in fMRI series using Kalman filtering. In IEEE International Symposium on Biomedical Imaging: Nano to Macro, 2004. p. 376–379 Vol. 1.

Rombouts, S.A.R.B., Barkhof, F., Goekoop, R., Stam, C.J. and Scheltens, P., 2005. Altered resting state networks in mild cognitive impairment and mild Alzheimer's disease: an fMRI study. *Human Brain Mapping*, 26(4):231–239.

Rosenblatt, F., 1958. The perceptron: a probabilistic model for information storage and organization in the brain. *Psychological Review*, 65(6):386–408.

Sanguineti, V., Parodi, C., Perissinotto, S., Frisone, F., Vitali, P., Morasso, P. and Rodriguez, G., 2000. Analysis of fMRI time series with mixtures of Gaussians. In IJCNN 2000, Proceedings of the IEEE-INNS-ENNS International Joint Conference on Neural Networks, 2000. volume 1, p. 331–334 vol.1.

Scheff, S.W., Price, D.A., Schmitt, F.A., DeKosky, S.T. and Mufson, E.J., 2007. Synaptic alterations in CA1 in mild Alzheimer disease and mild cognitive impairment. *Neurology*, 68(18):1501–1508.

REFERENCES (continued)

Selkoe, D.J., 2002. Alzheimer's Disease Is a Synaptic Failure. *Science*, 298(5594):789–791.

Singh, M., Kim, T. and Colletti, P., 1999. Cross-correlation technique to identify activated pixels in a three-condition fMRI task. *IEEE Transactions on Nuclear Science*, 46(3):520–526.

Smith, S., 2003. Digital signal processing : a practical guide for engineers and scientists. Newnes, Amsterdam Boston.

Sorg, C., Riedl, V., Mühlau, M., Calhoun, V.D., Eichele, T., Läer, L., Drzezga, A., Förstl, H., Kurz, A., Zimmer, C. and Wohlschläger, A.M., 2007. Selective changes of resting-state networks in individuals at risk for Alzheimer's disease. *Proceedings of the National Academy of Sciences*, 104(47):18760–18765.

Sun, F.T., Miller, L.M. and D'Esposito, M., 2004. Measuring interregional functional connectivity using coherence and partial coherence analyses of fMRI data. *NeuroImage*, 21(2):647 – 658.

Talairach, J. and Tournoux, P., 1988. Co-planar Stereotaxic Atlas of the Human Brain: 3-dimensional Proportional System : an Approach to Cerebral Imaging. Thieme classics. G. Thieme.

Tang, X., Zeng, W., Wang, N. and Yang, J., 2015. An adaptive {RV} measure based fuzzy weighting subspace clustering (ARV-FWSC) for fMRI data analysis. *Biomedical Signal Processing and Control*, 22:146 – 154.

Teipel, S., Drzezga, A., Grothe, M.J., Barthel, H., Chételat, G., Schuff, N., Skudlarski, P., Cavedo, E., Frisoni, G.B., Hoffmann, W., Thyrian, J.R., Fox, C., Minoshima, S., Sabri, O. and Fellgiebel, A., 2015. Multimodal imaging in Alzheimer's disease: validity and usefulness for early detection. *The Lancet Neurology*, 14(10):1037–1053.

Thirion, B., Duchesnay, E., Hubbard, E., Dubois, J., Poline, J.B., Lebihan, D. and Dehaene, S., 2006. Inverse retinotopy: Inferring the visual content of images from brain activation patterns. *NeuroImage*, 33(4):1104–1116.

Thirion, B. and Faugeras, O., 2001. Revisiting non-parametric activation detection on fMRI time series. In IEEE Workshop on Mathematical Methods in Biomedical Image Analysis, 2001. MMBIA 2001. p. 121–128.

REFERENCES (continued)

Thompson, E., Holland, S. and Schmithorst, V., 2002. Detecting cortical activities from fMRI data using the STAP algorithm. In 2002 International Conference on Image Processing. 2002. Proceedings. volume 3, p. 1001–1004 vol.3.

Tripoliti, E.E., Fotiadis, D.I. and Argyropoulou, M., 2008. A supervised method to assist the diagnosis and classification of the status of Alzheimer's disease using data from an fMRI experiment. In 2008 30th Annual International Conference of the IEEE Engineering in Medicine and Biology Society. p. 4419–4422.

Tzikas, D.G., Likas, A., Galatsanos, N.P., Lukic, A.S. and Wernick, M.N., 2004. Bayesian regression of functional neuroimages. In Signal Processing Conference, 2004 12th European. p. 801–804.

von Tscharner, V. and Thulborn, K., 2001. Specified-resolution wavelet analysis of activation patterns from BOLD contrast fMRI. *IEEE Transactions on Medical Imaging*, 20(8):704–714.

Wang, K., Liang, M., Wang, L., Tian, L., Zhang, X., Li, K. and Jiang, T., 2007. Altered functional connectivity in early Alzheimer's disease: A resting-state fMRI study. *Human Brain Mapping*, 28(10):967–978.

Wang, N., Zeng, W. and Chen, L., 2013. SACICA: A sparse approximation coefficient-based {ICA} model for functional magnetic resonance imaging data analysis. *Journal of Neuroscience Methods*, 216(1):49 – 61.

Weiner, M., Veitch, D., Aisen, P., Beckett, L., Cairns, N., Green, R., Harvey, D., Jack, C., Jagust, W., Liu, E., Morris, J., Petersen, R., Saykin, A., Schmidt, M., Shaw, L., Shen, L., Siuciak, J., Soares, H., Toga, A. and Trojanowski, J., 2013. The Alzheimer's Disease Neuroimaging Initiative: A review of papers published since its inception. *Alzheimer's and Dementia*, 9(5):e111–e194.

Weiner, M.W., Veitch, D.P., Aisen, P.S., Beckett, L.A., Cairns, N.J., Cedarbaum, J., Green, R.C., Harvey, D., Jack, C.R., Jagust, W., Luthman, J., Morris, J.C., Petersen, R.C., Saykin, A.J., Shaw, L., Shen, L., Schwarz, A., Toga, A.W. and Trojanowski, J.Q., 2015. 2014 Update of the Alzheimer's Disease Neuroimaging Initiative: A review of papers published since its inception. *Alzheimer's & Dementia*, 11(6):e1–e120.

Welvaert, M. and Rosseel, Y., 2013. On the Definition of Signal-To-Noise Ratio and Contrast-To-Noise Ratio for fMRI Data. *PLoS ONE*, 8(11):e77089.

REFERENCES (continued)

Welvaert, M. and Rosseel, Y., 2014. A Review of fMRI Simulation Studies. *PLoS ONE*, 9(7):e101953.

Wenk, G.L., 2006. Neuropathologic changes in Alzheimer's disease: potential targets for treatment. *The Journal of Clinical Psychiatry*, 67 Suppl 3:3–7; quiz 23.

Woolrich, M.W., Beckmann, C.F., Nichols, T.E. and Smith, S.M., 2009. fMRI Techniques and Protocols, Humana Press, Totowa, NJ, chapter Statistical Analysis of fMRI Data, p. 179–236.

Xiong, J., Gao, J.H., Lancaster, J.L. and Fox, P.T., 1996. Assessment and optimization of functional MRI analyses. *Human Brain Mapping*, 4(3):153–167.

Yager, R.R. and Filev, D.P., 1994. Approximate clustering via the mountain method. *IEEE Transactions on Systems, Man, and Cybernetics*, 24(8):1279–1284.

Yu, Z., Li, L., Liu, J. and Han, G., 2015. Hybrid Adaptive Classifier Ensemble. *IEEE Transactions on Cybernetics*, 45(2):177–190.

Zou, K.H., O'Malley, A.J. and Mauri, L., 2007. Receiver-Operating Characteristic Analysis for Evaluating Diagnostic Tests and Predictive Models. *Circulation*, 115(5):654–657.

CURRICULUM VITAE

Kaya OĞUZ

Address: International Computer Institute, Izmir/TURKEY
Mobile: (+90) 555 285 49 00
E-mail:kaya@oguz.name.tr

Personal Information
Nationality: Turkish
Birth Place and Date: Izmir, 21.01.1980

Education
M.Sc. (with distinction): 2007-2009, University of Abertay Dundee, School of Computing and Creative Technologies, Computer Games Technology
B.Sc.: 2003-2007, Izmir University of Economics, Software Engineering

Foreign Languages
Turkish : First Language
English : Advanced (TOEFL: 103)
Italian: Beginner

Programming Languages
C/C++, C#, Java, Matlab

Projects
2015: Hafif Bilişsel Bozukluk Tanısı Alan Bireylerin Default Mode, Kısa Süreli Bellek Kayıt ve Geri Çağırma ile İlişkili Nöral Bileşenlerinin Erken Alzheimer Hastaları ile Onların Sağlıklı Kardeşleri ve Kontroller ile Karşılaştırılması. (TÜBİTAK: 214S029)

Publications

Biyik, U., Keskin, D., Oguz, K., Akdeniz, F. and Gonul, A.S., 2015. Facial emotion recognition in remitted depressed women. *Asian Journal of Psychiatry*, 17:111–113.

Dagdeviren, Z.A., Oguz, K. and Cinsdikici, M., 2015. Automatic registration of structural brain MR images to MNI image space. in Signal Processing and Communications Applications Conference (SIU), 2015 23th. p. 359–362.

Dagdeviren, Z.A., Oguz, K. and Cinsdikici, M.G., 2014. Three techniques for automatic extraction of corpus callosum in structural midsagittal brain MR images: Valley Matching, Evolutionary Corpus Callosum Detection and Hybrid method. *Engineering Applications of Artificial Intelligence*, 31:101–115.

Kitis, O., Ozalay, O., Zengin, E.B., Haznedaroglu, D., Eker, M.C., Yalvac, D., Oguz, K., Coburn, K. and Gonul, A.S., 2012. Reduced left uncinate fasciculus fractional anisotropy in deficit schizophrenia but not in non-deficit schizophrenia. *Psychiatry and Clinical Neurosciences*, 66(1):34–43.

Simsek, F., Oguz, K., Akan, S., Haznedaroglu Isman, D., Acikel, D., Kitis, O., Cetinkalp, S., Eker, M., Coburn, K. and Gonul, A., 2013. P.2.b.032 Neural correlates of emotion regulation response to negative stimuli in young women at high risk for depression. *European Neuropsychopharmacology*, 23, Supplement 2:S337–S338.

Oğuz, K., 2010. Bilgisayar Oyunlarında Kalabalıkların Hızlı Çizimi. *Anadolu Üniversitesi Bilim ve Teknoloji Dergisi-A, Uygulamalı Bilimler ve Mühendislik*, 11(1):23–33.

Unluturk, M.S., Oguz, K. and Atay, C., 2009a. A comparison of neural networks for real-time emotion recognition from speech signals. *WSEAS Trans. Sig. Proc.*, 5(3):116–125.

Unluturk, M.S., Oguz, K. and Atay, C., 2009b. Emotion recognition using neural networks. in Proceedings of the 10th WSEAS international conference on Neural networks. World Scientific and Engineering Academy and Society (WSEAS), Stevens Point, Wisconsin, USA, NN'09, p. 82–85.

APPENDIX

Appendix 1 Generated HRFs sampled at different rates

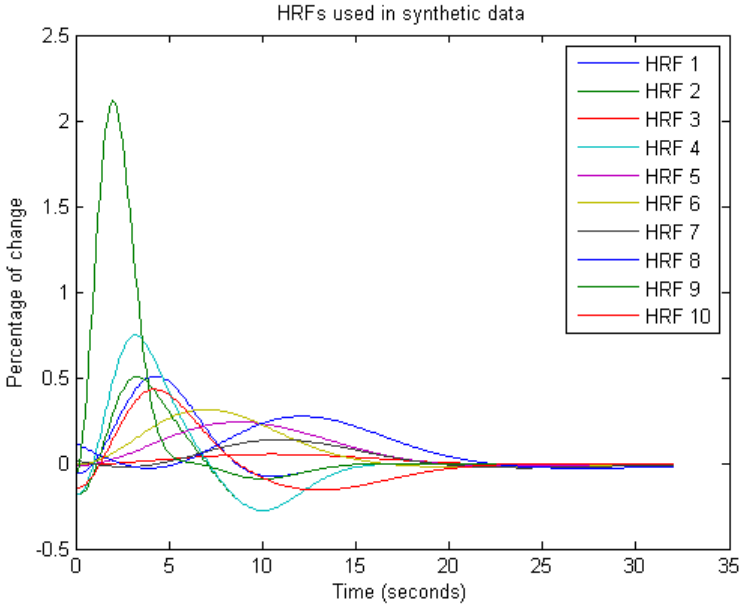

HRFs with a 0.1 seconds sampling rate.

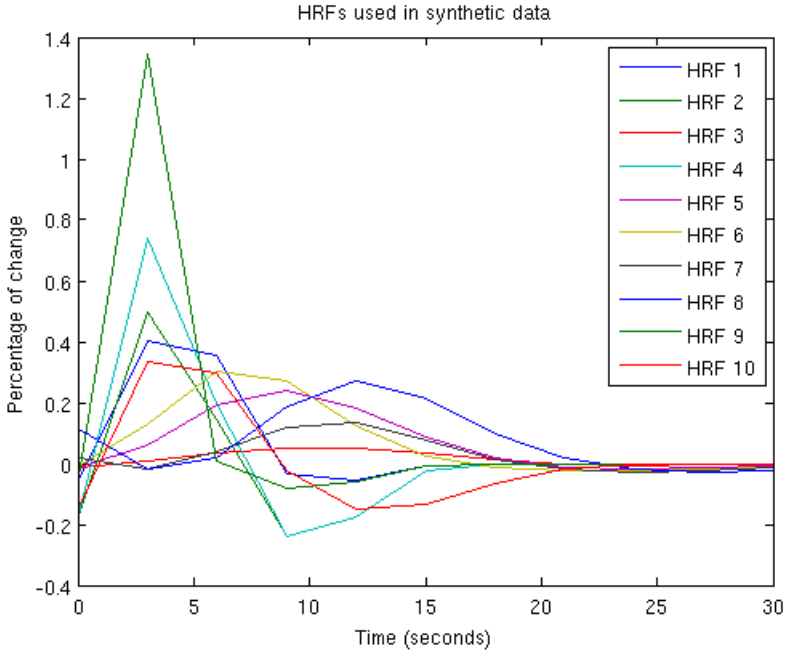

HRFs with a 3 seconds sampling rate.

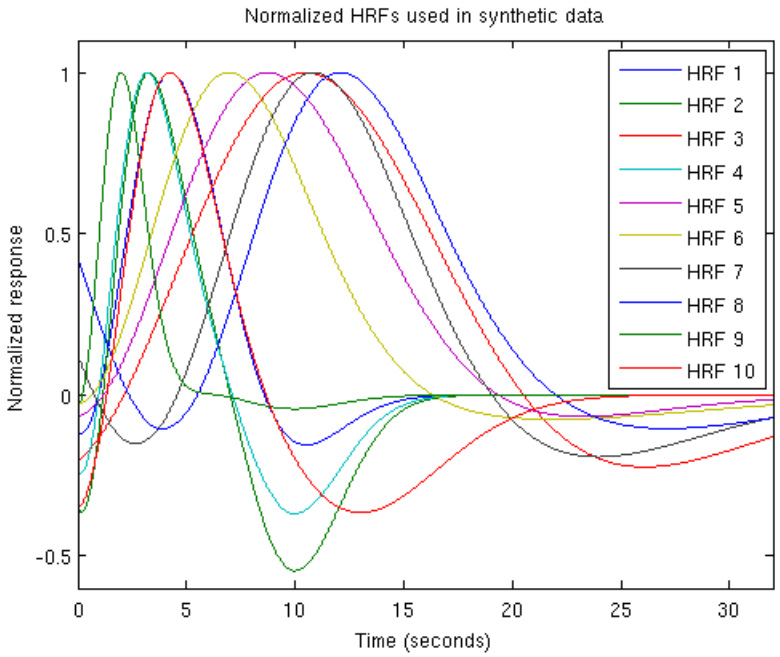

The normalized HRFs with a 0.1 seconds sampling rate.

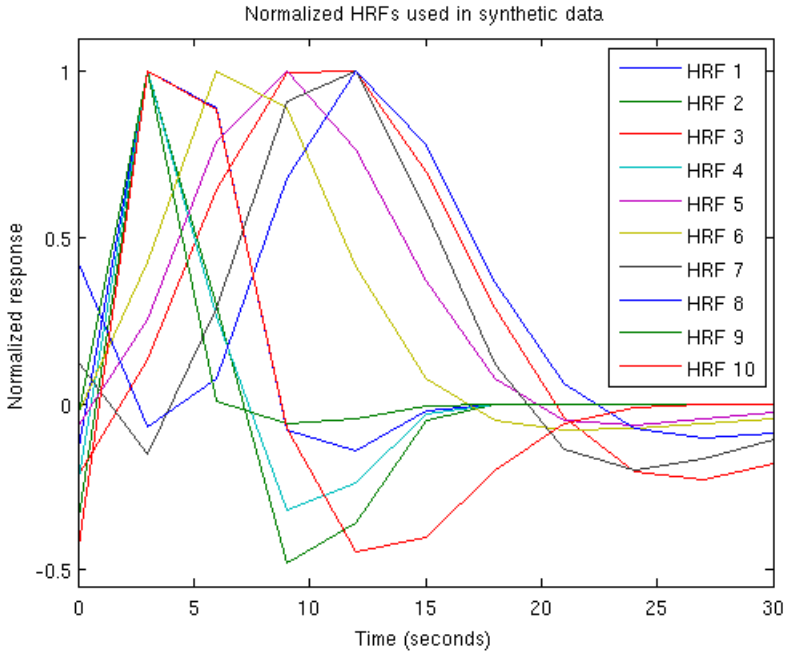

The normalized HRFs with a 3 seconds sampling rate.

Appendix 2 Area under the curve for synthetic data created by Approach 1

Method	SNR	HRF 1	HRF 2	HRF 3	HRF 4	HRF 5	HRF 6	HRF 7	HRF 8	HRF 9	HRF 10
	SNR 3	0,651	0,5341	0,5569	0,6074	0,6326	0,6563	0,5622	0,6506	0,7223	0,5499
	SNR 5	0,6673	0,5505	0,5375	0,6304	0,6742	0,6828	0,5874	0,674	0,7648	0,5704
IAM(*)	SNR 10	0,7636	0,5794	0,572	0,7222	0,7469	0,7719	0,653	0,7368	0,8499	0,6209
	SNR 15	0,8501	0,6088	0,6299	0,7967	0,8126	0,8369	0,7291	0,8012	**0,8717**	0,6764
	SNR 20	**0,8652**	**0,6421**	**0,7233**	**0,8451**	**0,8301**	**0,8502**	**0,7927**	**0,8526**	0,8646	**0,754**
	SNR 3	0,6341	0,5628	0,5355	0,595	0,5997	0,6169	0,536	0,5981	0,7003	0,5845
	SNR 5	0,6463	0,5606	0,5403	0,632	0,6125	0,645	0,5707	0,6039	0,7254	0,591
IAMP(*)	SNR 10	0,7341	0,5935	0,5713	0,7058	0,6695	0,7216	0,6131	0,6604	0,7989	0,6526
	SNR 15	0,7862	0,6274	0,5992	0,7635	0,7144	0,7549	0,6718	**0,6831**	**0,8019**	0,708
	SNR 20	**0,7972**	**0,6684**	**0,6482**	**0,7912**	**0,716**	**0,7576**	**0,7012**	0,681	**0,8019**	**0,7568**
	SNR 3	0,8459	0,584	0,5335	0,748	0,7331	0,8103	0,5301	0,7231	0,9531	0,6717
	SNR 5	0,892	0,6362	0,5237	0,8668	0,7911	0,9059	0,6321	0,7942	0,9662	0,7217
TAM	SNR 10	0,9626	0,7616	0,5887	0,9619	0,9312	0,9642	0,8083	0,9262	0,9662	0,921
	SNR 15	**0,9678**	0,9145	0,7535	0,9668	**0,9674**	0,9665	0,9411	0,9638	0,9665	0,9632
	SNR 20	0,9659	**0,9603**	**0,918**	**0,9671**	0,9662	**0,9674**	**0,966**	**0,9658**	**0,9668**	**0,9662**
	SNR 3	0,6433	0,535	0,5537	0,5966	0,6256	0,6495	0,5593	0,641	0,7154	0,5524
	SNR 5	0,66	0,5454	0,5341	0,6275	0,6661	0,6786	0,5887	0,6669	0,7535	0,5676
IRRD(*)	SNR 10	0,7493	0,5797	0,5691	0,7144	0,7425	0,7634	0,6484	0,7253	0,8402	0,6196
	SNR 15	0,8381	0,6073	0,6268	0,7867	0,7957	0,8325	0,7165	0,7968	**0,8643**	0,6687
	SNR 20	**0,8566**	**0,6383**	**0,7129**	**0,8332**	**0,8202**	**0,8387**	**0,7859**	**0,8402**	0,858	**0,7432**
	SNR 3	0,8457	0,5835	0,5324	0,7487	0,7331	0,8104	0,5301	0,7243	0,9531	0,6716
	SNR 5	0,8914	0,6366	0,5238	0,8669	0,7915	0,9055	0,6313	0,7946	0,9663	0,7222
TRRD	SNR 10	0,9629	0,762	0,5881	0,9617	0,9323	0,9639	0,8078	0,9269	0,9662	0,9216
	SNR 15	**0,9674**	0,9143	0,7533	**0,9671**	**0,9671**	0,9665	0,9406	0,9643	0,9665	0,9631
	SNR 20	0,9653	**0,9605**	**0,9177**	**0,9671**	0,9659	**0,9674**	**0,9666**	**0,9655**	**0,9668**	**0,9659**
	SNR 3	0,9379	0,7259	0,6745	0,906	0,8991	0,9322	0,726	0,8747	0,9673	0,8668
	SNR 5	0,9604	0,7833	0,6535	0,9384	0,9411	0,963	0,8064	0,9031	0,9689	0,9063
Correlation(**)	SNR 10	**0,969**	0,894	0,7956	0,9686	0,9683	**0,969**	0,9382	0,9641	**0,969**	0,9664
	SNR 15	**0,969**	0,9608	0,9075	**0,969**	**0,969**	**0,969**	0,9677	0,9689	**0,969**	**0,969**
	SNR 20	**0,969**	**0,9686**	**0,9671**	**0,969**	**0,969**	**0,969**	**0,969**	**0,969**	**0,969**	**0,969**

(*) Please refer to Section 3.4.2 for details on instantaneous methods.
(**) Please refer to Section 3.4.3 for details on Correlation method.

Appendix 3 PSNR values for synthetic data created by Approach 1

Method	SNR	HRF 1	HRF 2	HRF 3	HRF 4	HRF 5	HRF 6	HRF 7	HRF 8	HRF 9	HRF 10
	SNR 3	8,8024	8,9517	8,9635	9,0602	8,9608	8,9795	8,9573	8,9153	8,8299	8,8763
	SNR 5	8,9381	9,2495	9,1919	8,9987	9,0558	9,0987	9,2618	9,1437	8,8103	9,3248
IAM	SNR 10	9,6329	10,0942	9,9901	9,7071	9,8548	9,7099	9,8597	9,6335	9,8257	9,7518
	SNR 15	10,0131	10,3771	10,2268	**10,3876**	10,2934	10,0662	10,2527	10,1919	9,939	10,4898
	SNR 20	**10,4427**	**10,7901**	**10,6859**	10,3371	**10,7499**	**10,5565**	**10,5887**	**10,6056**	**10,2727**	**10,9001**
	SNR 3	6,663	6,7803	6,6654	6,7381	6,78	6,6779	6,5362	6,5771	6,2977	6,7078
	SNR 5	6,8195	6,8649	6,9257	6,6367	6,7186	6,699	6,8612	7,0826	6,4029	7,1059
IAMP	SNR 10	7,249	7,5313	7,5791	7,3832	7,2179	7,3832	7,6857	7,2889	6,9747	7,477
	SNR 15	7,5856	8,0072	7,9573	7,7826	7,7793	7,4406	7,8642	7,8135	7,6625	8,0799
	SNR 20	**8,3437**	**8,4065**	**8,2479**	**8,2111**	**8,2585**	**8,4467**	**8,2443**	**8,3771**	**8,0355**	**8,3595**
	SNR 3	19,3306	18,2557	18,1475	18,8742	19,3936	19,0451	19,7026	20,2711	16,2557	19,2469
	SNR 5	18,6808	19,7288	19,2461	19,5929	19,8041	18,3966	19,5384	20,6321	16,5101	19,8698
TAM	SNR 10	18,2857	21,1519	20,9292	19,2201	20,2486	19,0681	20,2636	20,4491	18,696	20,1667
	SNR 15	22,6052	22,3548	21,0669	22,1118	21,9918	22,5038	21,223	21,4712	21,7609	21,2438
	SNR 20	**25,2065**	**23,4661**	**22,1031**	**26,1041**	**25,3674**	**25,6927**	**23,667**	**25,1948**	**25,608**	**25,6503**
	SNR 3	8,3528	8,5924	8,5139	8,5233	8,3113	8,6138	8,5515	8,5571	8,5406	8,4937
	SNR 5	8,6438	8,8208	8,7955	8,7208	8,5275	8,5204	8,7724	8,6353	8,2536	8,9916
IRRD	SNR 10	9,0321	9,7219	9,5781	9,3181	9,5423	9,0023	9,3327	9,1014	9,0419	9,3753
	SNR 15	9,3799	9,7385	9,9476	**10,1508**	9,7793	9,2745	9,979	9,5163	9,3601	9,7526
	SNR 20	**9,8569**	**10,0123**	**10,3229**	9,9783	**10,2481**	**9,8183**	**10,3337**	**9,7942**	**9,5839**	**10,5852**
	SNR 3	19,1594	18,4102	18,0083	18,9124	19,4755	18,9009	19,7865	20,3509	16,2186	19,352
	SNR 5	18,6808	19,6854	19,1654	19,7322	19,8039	18,5386	19,6074	20,4853	16,4289	19,8698
TRRD	SNR 10	18,3794	21,1899	20,9452	19,2197	20,182	19,0118	20,408	20,4092	18,696	20,3295
	SNR 15	22,5349	22,3264	20,911	22,2249	21,8931	22,5038	21,0685	21,5491	21,6547	21,2435
	SNR 20	**25,0406**	**23,5017**	**22,1115**	**26,1041**	**25,1538**	**25,6927**	**24,2475**	**24,8038**	**25,608**	**25,5152**
	SNR 3	22,1795	19,4476	18,893	20,3277	20,5613	21,2438	21,2358	22,2639	23,627	19,9105
	SNR 5	21,8715	20,0505	20,2155	21,3949	22,5954	22,215	20,0933	22,9526	23,9077	20,7872
Correlation(*)	SNR 10	24,2544	22,0926	22,3572	23,0287	23,8744	24,7284	21,5907	23,794	26,3964	23,0971
	SNR 15	26,5008	24,2312	22,4369	26,0648	27,1828	26,948	24,4087	27,4991	28,1658	25,103
	SNR 20	**28,5769**	**26,0696**	**24,4759**	**28,9629**	**29,0058**	**29,5034**	**27,7418**	**29,9985**	**30,0472**	**28,0499**

(*) Please refer to Section 3.4.3 for details on Correlation method.

Appendix 4 ROC curves for instantaneous methods, Approach 1

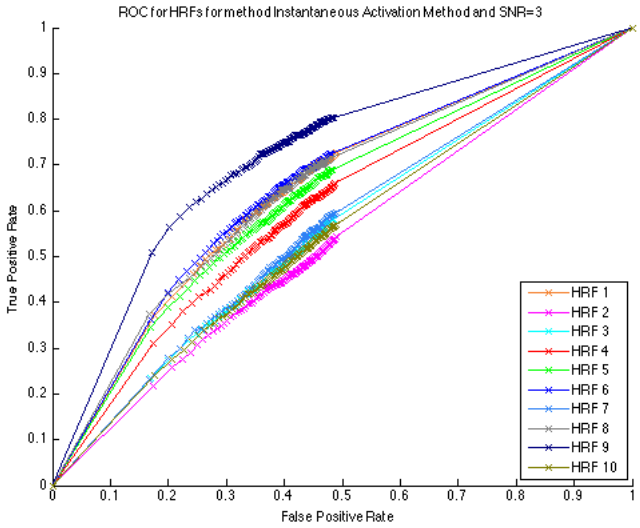

ROC Curves of IAM for all HRFs at SNR=3.

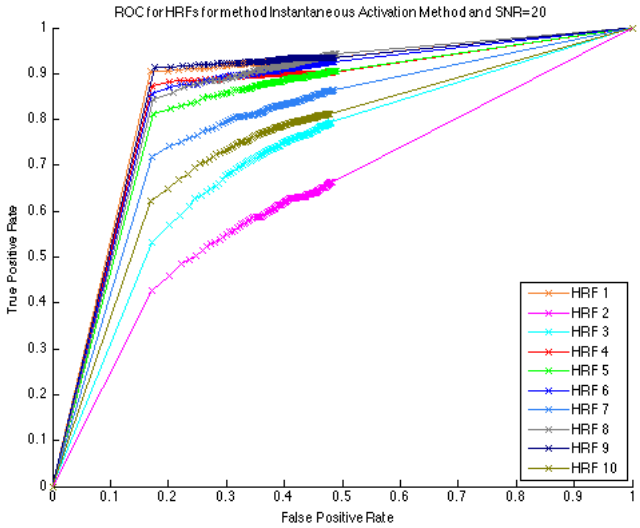

ROC Curves of IAM for all HRFs at SNR=20.

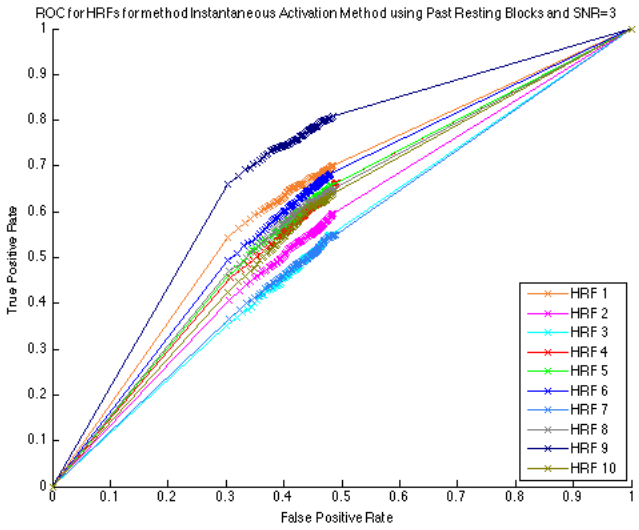

ROC Curves of IAMP for all HRFs at SNR=3.

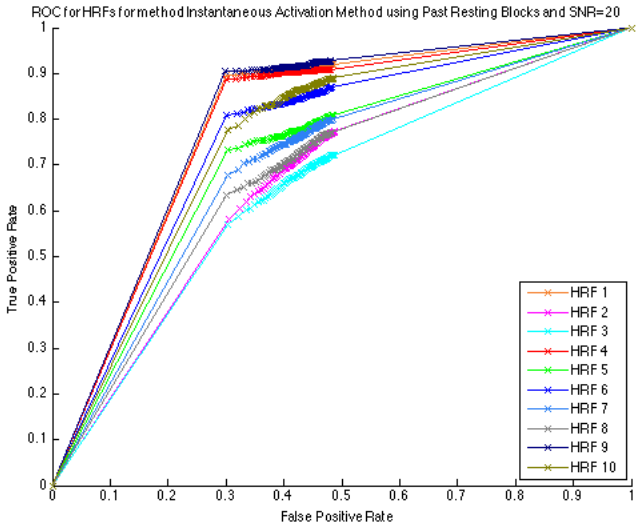

ROC Curves of IAMP for all HRFs at SNR=20.

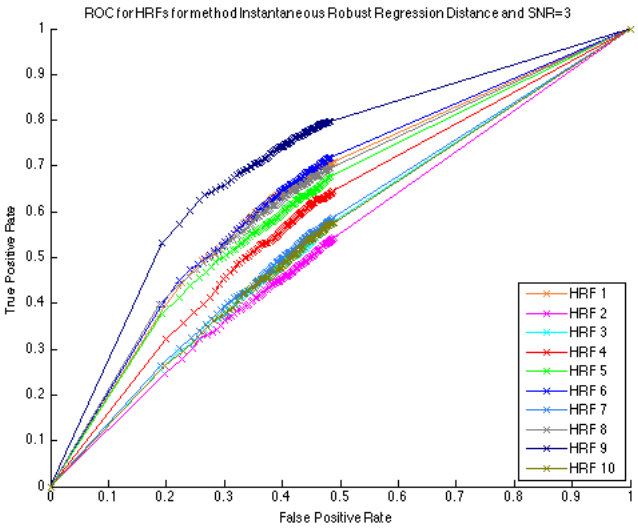

ROC Curves of IRRD for all HRFs at SNR=3.

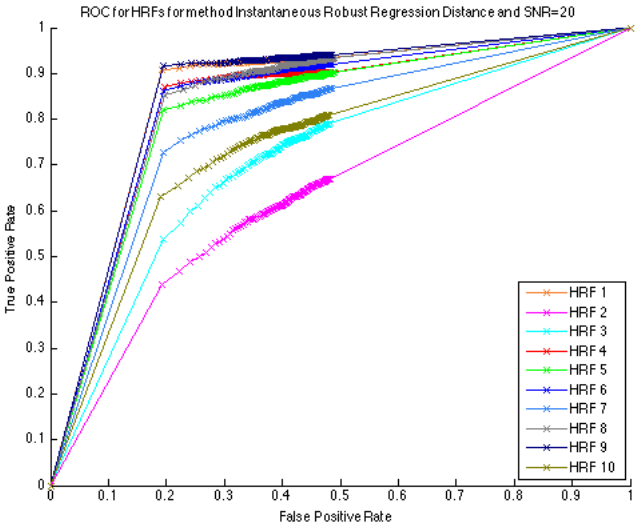

ROC Curves of IRRD for all HRFs at SNR=20.

Appendix 5 ROC curves for task based methods, Approach 1

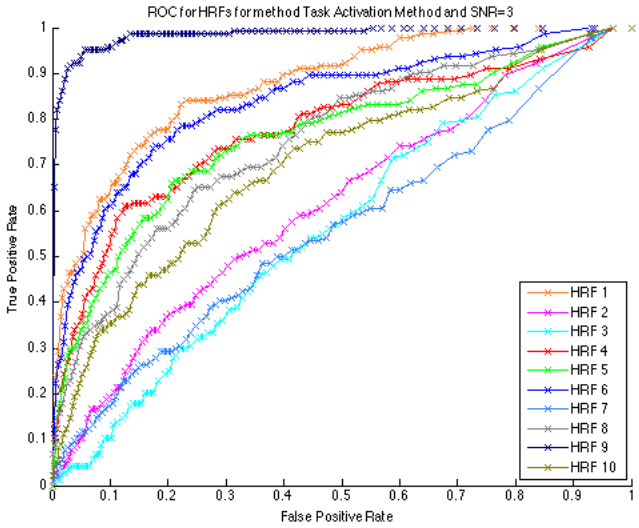

ROC Curves of TAM for all HRFs at SNR=3.

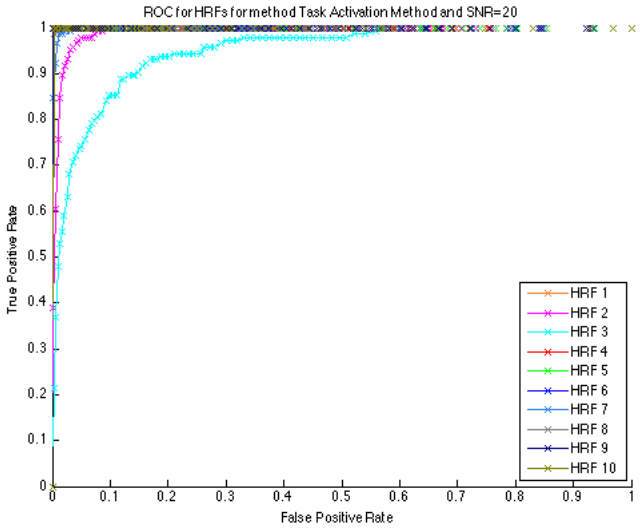

ROC Curves of TAM for all HRFs at SNR=20.

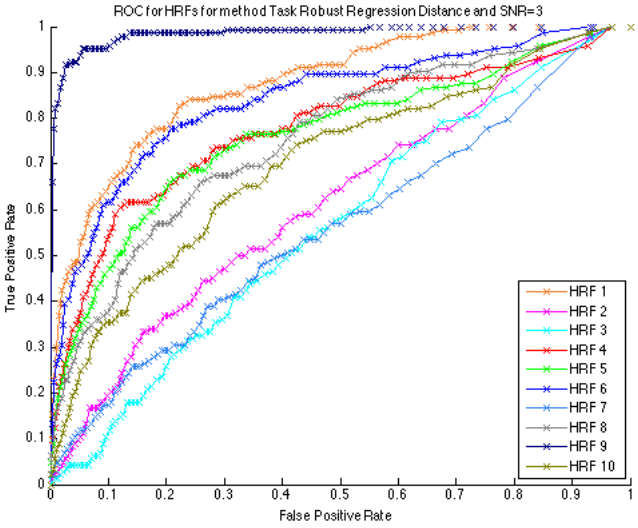

ROC Curves of TRRD for all HRFs at SNR=3.

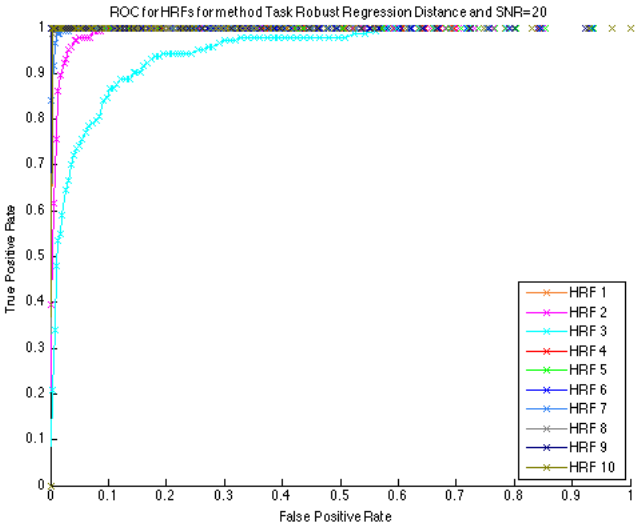

ROC Curves of TRRD for all HRFs at SNR=20.

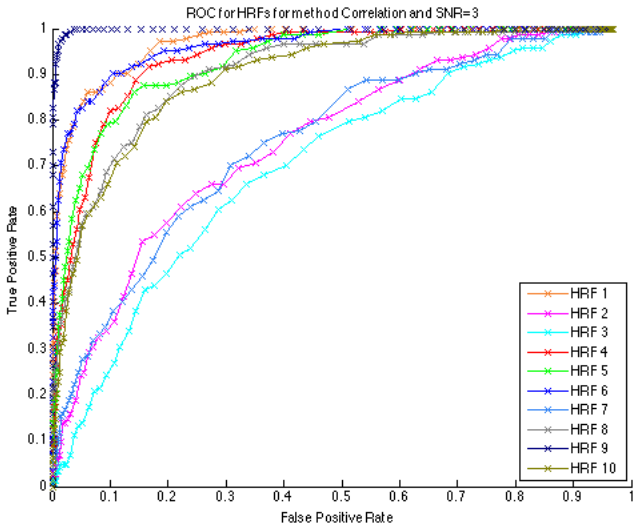

ROC Curves of Correlation for all HRFs at SNR=3.

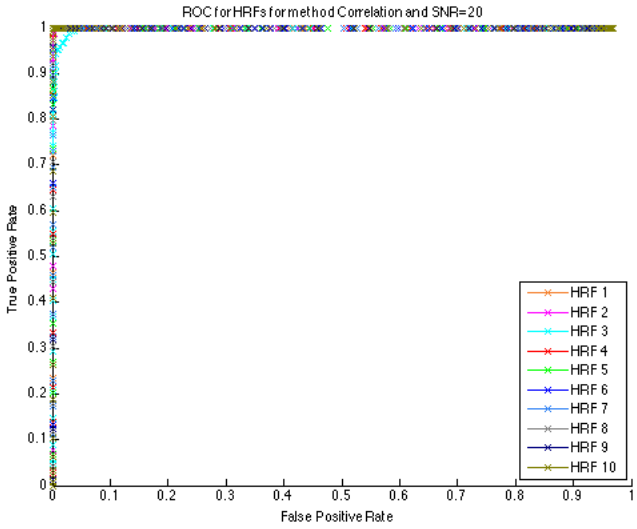

ROC Curves of Correlation for all HRFs at SNR=20.

Appendix 6 Area under the curve for synthetic data created by Approach 2

Method	Subject	HRF 1	HRF 2	HRF 3	HRF 4	HRF 5	HRF 6	HRF 7	HRF 8	HRF 9	HRF 10
IAM(*)	Subject 1	**0,8516**	**0,7997**	**0,811**	**0,8514**	**0,8576**	**0,8656**	**0,855**	**0,9149**	**0,8516**	**0,8513**
	Subject 2	0,8078	0,7407	0,7787	0,8078	0,8141	0,8239	0,8145	0,8707	0,8078	0,8059
	Subject 3	0,8315	0,7377	0,8012	0,8313	0,8424	0,853	0,8359	0,8975	0,8315	0,8295
	Subject 4	0,8366	0,7875	0,7992	0,8366	0,8418	0,8546	0,8411	0,9031	0,8366	0,8359
IAMP(*)	Subject 1	**0,7839**	**0,7262**	**0,6904**	**0,7839**	**0,7075**	**0,7541**	**0,6758**	**0,6491**	**0,7839**	**0,7839**
	Subject 2	0,7544	0,6898	0,6468	0,7544	0,6722	0,7175	0,6411	0,616	0,7544	0,754
	Subject 3	0,7685	0,6985	0,6582	0,7685	0,6843	0,7339	0,6522	0,6275	0,7685	0,7684
	Subject 4	0,7364	0,6569	0,6351	0,736	0,6531	0,6994	0,6283	0,5982	0,7363	0,7367
TAM	Subject 1	0,928	0,928	0,928	0,928	0,928	0,928	0,928	0,928	0,928	0,928
	Subject 2	**0,9637**	**0,9637**	**0,9636**	**0,9637**	**0,9637**	**0,9637**	**0,9637**	**0,9637**	**0,9637**	**0,9637**
	Subject 3	0,9186	0,9186	0,9186	0,9186	0,9186	0,9186	0,9186	0,9186	0,9186	0,9186
	Subject 4	0,9449	0,9449	0,9449	0,9449	0,9449	0,9449	0,9449	0,9449	0,9449	0,9449
IRRD(*)	Subject 1	**0,8354**	**0,7925**	**0,7949**	**0,8349**	**0,8424**	**0,85**	**0,8308**	**0,8968**	**0,8354**	**0,8349**
	Subject 2	0,7961	0,7278	0,7717	0,7961	0,8039	0,815	0,8059	0,8573	0,7961	0,7938
	Subject 3	0,8194	0,7344	0,7834	0,8191	0,8288	0,8388	0,816	0,8838	0,8194	0,8178
	Subject 4	0,8179	0,7739	0,7801	0,8175	0,8246	0,8358	0,8158	0,882	0,8179	0,8158
TRRD	Subject 1	0,9117	0,9117	0,9117	0,9117	0,9117	0,9117	0,9117	0,9117	0,9117	0,9117
	Subject 2	**0,9596**	**0,9596**	**0,9596**	**0,9596**	**0,9596**	**0,9596**	**0,9596**	**0,9596**	**0,9596**	**0,9596**
	Subject 3	0,9189	0,9189	0,9189	0,9189	0,9189	0,9189	0,9189	0,9189	0,9189	0,9189
	Subject 4	0,9302	0,9302	0,9302	0,9302	0,9302	0,9302	0,9302	0,9302	0,9302	0,9302
Correlation(**)	Subject 1	0,9684	0,9628	0,9684	0,9684	0,9684	0,9684	0,9684	0,9676	0,9684	0,9684
	Subject 2	**0,9947**	**0,9907**	**0,9946**	**0,9947**	**0,9947**	**0,9947**	**0,9947**	**0,9938**	**0,9947**	**0,9947**
	Subject 3	0,9941	0,975	0,9913	0,9937	0,9933	0,9941	0,9921	0,9873	0,9941	0,9937
	Subject 4	0,9881	0,9721	0,985	0,9875	0,9872	0,9881	0,9852	0,9808	0,9881	0,9875

(*) Please refer to Section 3.4.2 for details on instantaneous methods.
(**) Please refer to Section 3.4.3 for details on Correlation methods.

Appendix 7 PSNR values for synthetic data created by Approach 2

Method	Subject	HRF 1	HRF 2	HRF 3	HRF 4	HRF 5	HRF 6	HRF 7	HRF 8	HRF 9	HRF 10
IAM	Subject 1	**11.1494**	**12.2153**	**11.8742**	**11.4571**	**11.2281**	**11.2592**	**11.5808**	**11.6923**	**11.1494**	**11.703**
	Subject 2	10.6265	10.4898	10.738	10.4898	10.7081	10.7512	10.9901	11.2592	10.6265	10.5217
	Subject 3	10.3366	10.8785	11.185	10.9942	10.9185	11.0128	10.6921	11.0037	9.5884	11.1828
	Subject 4	10.978	10.8307	11.0743	10.8307	11.0592	11.0859	11.3538	11.6401	10.978	10.9903
IAMP	Subject 1	8.1377	**9.2266**	8.9732	**8.6349**	**8.7023**	8.2699	**8.6935**	8.4723	8.1377	**9.1331**
	Subject 2	**8.4901**	8.9144	**9.1034**	8.4061	8.6384	**8.6827**	8.6076	**8.6704**	**8.4901**	9.1034
	Subject 3	8.2974	8.7494	8.8611	8.5786	8.3246	8.3291	8.6717	8.4019	8.2974	8.8611
	Subject 4	8.1205	8.1548	8.1677	8.0436	8.1462	8.1504	8.1785	8.218	8.1205	8.3399
TAM	Subject 1	**17.5874**	**17.6564**	**17.5874**	**17.5874**	**17.5874**	**17.5874**	**17.5874**	**17.3669**	**17.5874**	**17.5874**
	Subject 2	16.9539	16.9539	16.9279	16.9539	16.9539	16.9539	16.9539	16.9539	16.9539	16.9539
	Subject 3	14.5624	14.8913	15.0163	14.6339	15.0163	14.9649	15.0163	15.0163	14.5624	14.9111
	Subject 4	15.9465	16.0504	16.0132	15.9465	15.9465	15.9465	15.9465	15.9465	15.9465	16.0504
IRRD	Subject 1	**10.543**	**11.8617**	**11.4282**	**11.0056**	10.3326	10.2178	**10.9294**	10.3082	**9.8995**	**11.2678**
	Subject 2	9.7475	10.0139	10.0585	9.6355	9.8584	9.8649	10.064	10.2571	9.7475	10.0493
	Subject 3	9.9039	10.5837	10.8389	10.6389	**10.4203**	**10.4533**	10.3058	**10.4505**	9.0923	10.8368
	Subject 4	9.5336	10.2672	10.3805	9.9655	9.6391	9.686	10.0099	9.9373	9.4169	10.3291
TRRD	Subject 1	15.7672	15.8434	15.7672	15.7672	15.7672	15.7672	15.7672	15.5383	15.7672	15.7672
	Subject 2	**16.9105**	**16.9105**	**16.9105**	**16.9105**	**16.9105**	**16.9105**	**16.9105**	**16.9105**	**16.9105**	**16.9105**
	Subject 3	14.5764	14.9046	15.0295	14.6477	15.0295	14.9784	15.0295	15.0295	14.5764	14.9246
	Subject 4	15.0163	15.136	15.1006	15.0163	15.0163	15.0163	15.0163	15.0163	15.0163	15.136
Correlation(*)	Subject 1	**26.4425**	**24.1656**	**25.3328**	**26.8508**	**26.9312**	**27.2751**	**25.5495**	**27.4428**	**27.4815**	**25.6615**
	Subject 2	20.4457	18.9714	19	20.8244	21.1285	21.7334	19.4853	21.7513	23.0022	19.8727
	Subject 3	20.9872	19.2168	18.8965	21.3673	21.3387	21.5637	19.3998	22.1477	23.2397	20.1532
	Subject 4	21.0079	19.4141	18.3107	21.3398	21.2799	21.6586	18.9088	21.9645	22.869	19.5437
(*)	Please refer to Section 3.4.3 for details on Correlation method.										

Appendix 8 ROC curves of HRFs for all methods, Approach 2

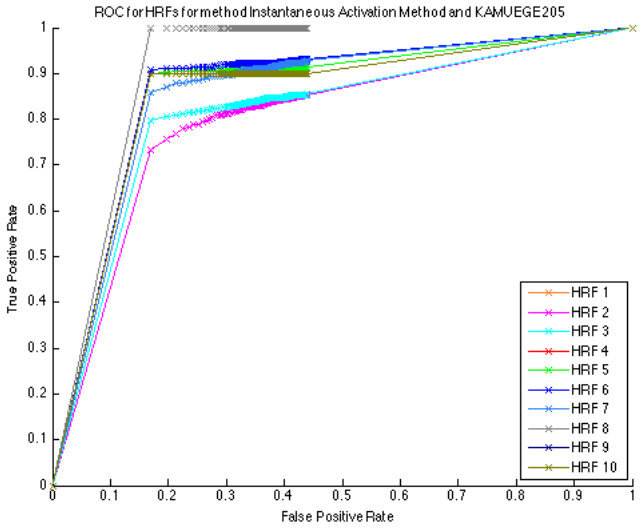

ROC Curves of IAM for all HRFs for Subject KAMUEGE205.

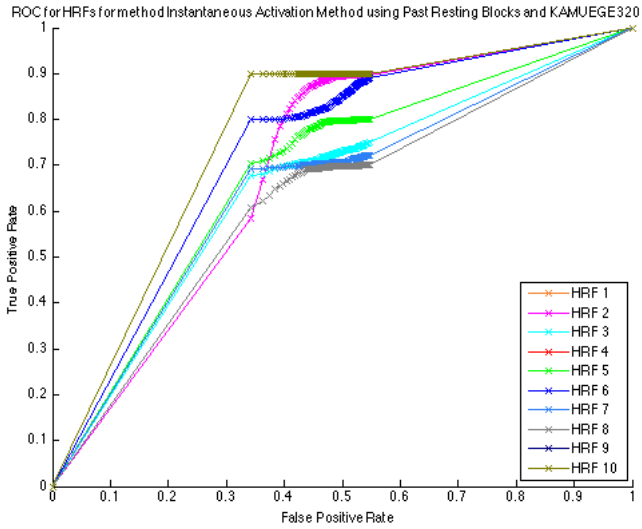

ROC Curves of IAMP for all HRFs for Subject KAMUEGE320.

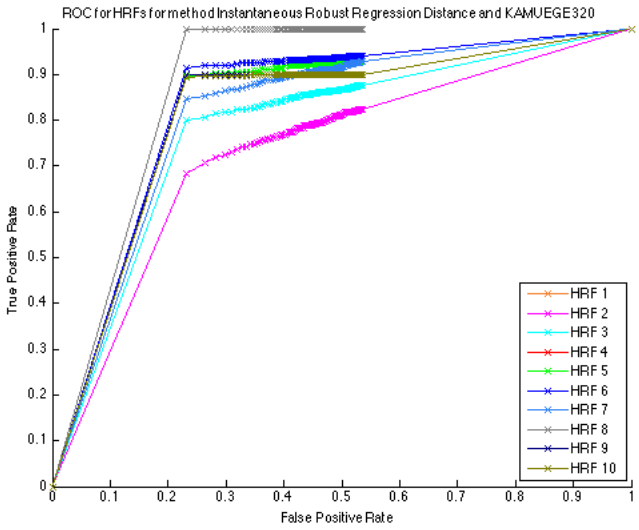

ROC Curves of IRRD for all HRFs for Subject KAMUEGE320.

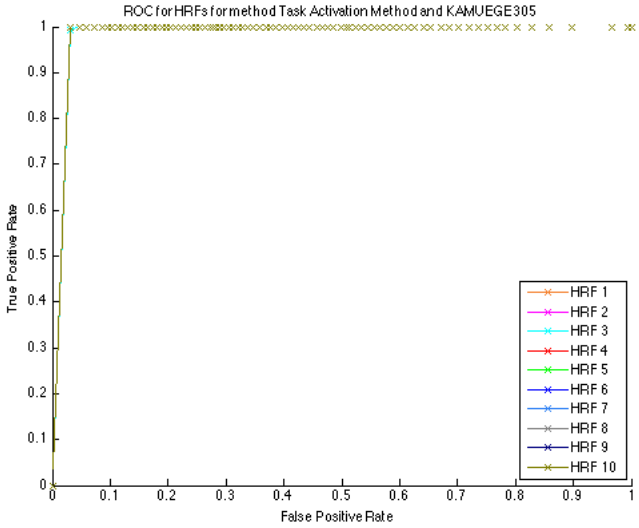

ROC Curves of TAM for all HRFs for Subject KAMUEGE305.

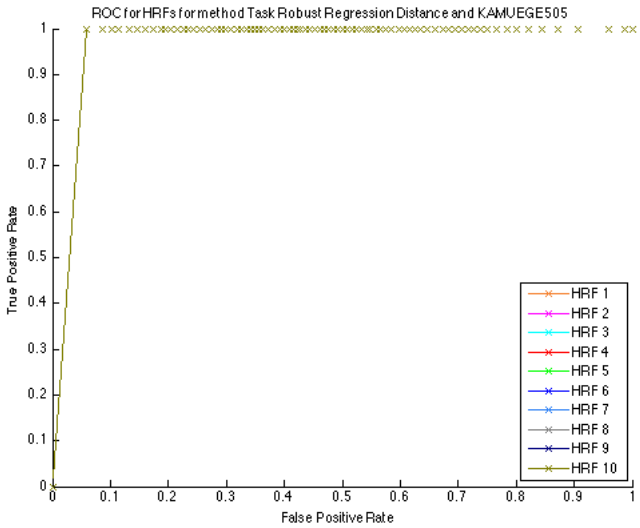

ROC Curves of TRRD for all HRFs for Subject KAMUEGE505.

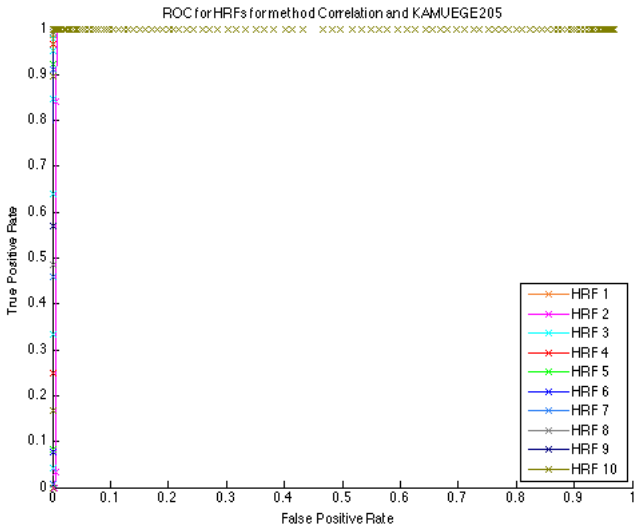

ROC Curves of Correlation for all HRFs for Subject KAMUEGE320.

Appendix 9 Results for subject KAMUEGE305

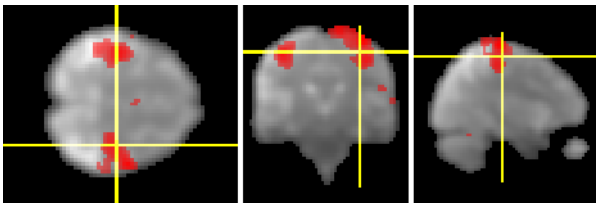

Results for SPM with a FWE corrected $p = 0.05$.

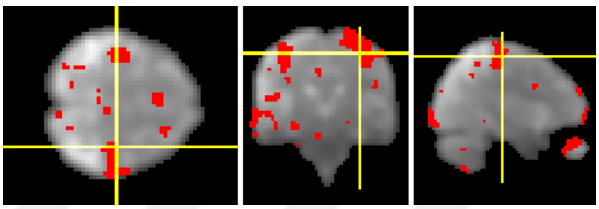

Results for IAM with a FWE corrected $p = 0.05$.

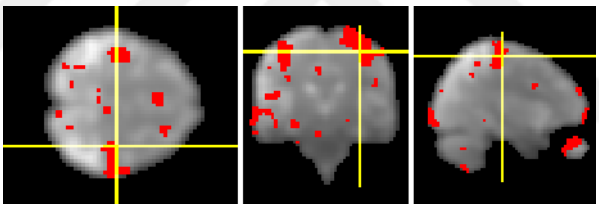

Results for IAMP with a FWE corrected $p = 0.05$.

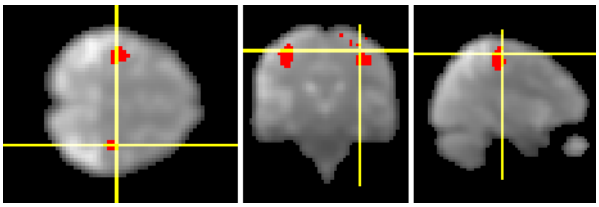

Results for TAM with a FWE corrected $p = 0.05$.

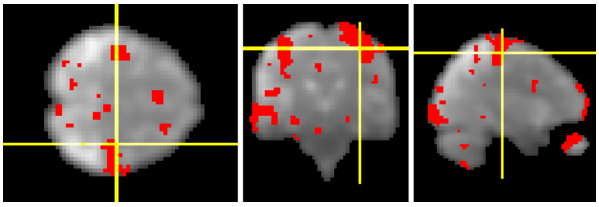

Results for IRRD with a FWE corrected $p = 0.05$.

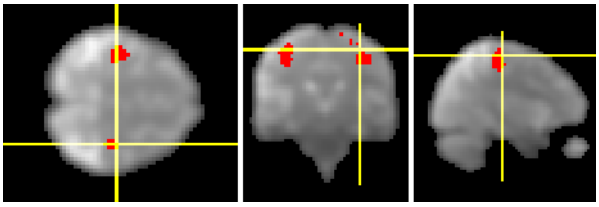

Results for TRRD with a FWE corrected $p = 0.05$

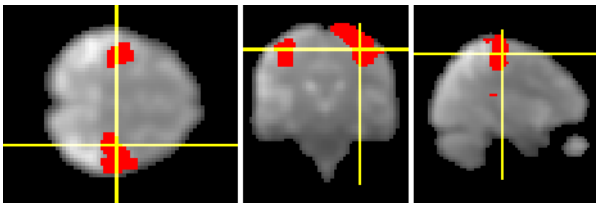

Results for Correlation method with $c = 0.7$

.

Appendix 10 Training results for the ANN

Training Set	Feature Vector	Unique Samples	Hidden	Mean	Max
TS-1.4	2912	1500	10	72.9667	98,8
			20	91.4267	98,9333
			30	**92.2533**	98,8667
TS-1.5	1573	1500	10	88.6133	99,0667
			20	94.5067	99,0667
			30	**98.44**	99,1333
TS-1.6	891	1500	10	96.8933	98,8667
			20	**97.88**	98,9333
			30	96.66	98,8
TS-2.4	2912	102	10	83.3333	100
			20	83.9216	100
			30	**94.8039**	100
TS-2.5	1573	102	10	86.4706	100
			20	90.2941	100
			30	**98.2157**	100
TS-2.6	891	102	10	**98.2353**	100
			20	83.1373	100
			30	90.6863	100
TS-2	1680	103	10	89.9029	90,2913
			20	**90.2913**	90,2913
			30	89.7087	90,2913
TS-3	1680	439	10	**90.3417**	91,344
			20	89.5444	91,344
			30	86.1276	91,344